NOAA Scientific Publications Report

MARCH 1, 2013

HIGHLIGHTED ARTICLE

Radiocesium in Pacific bluefin tuna *Thunnus orientalis* in 2012 validates new tracer technique

Increased toxicity of *Karenia brevis* during phosphate limited growth: ecological and evolutionary implications

Assessing the risk of ships striking large whales in marine spatial planning

ADDITIONAL ARTICLES

A harmonic approach for calculating daily temperature normals constrained by homogenized monthly temperature normals

The *Vibrio harveyi* bioassay routinely used to detect AI-2 quorum sensing inhibition is confounded by inconsistent normalization across marine matrices

Sensitivity of tropospheric oxidants to wildfires: implications for radiative forcing

Size distribution and concentrations of heavy metals in atmospheric aerosols originating from industrial emissions as predicted by the HYSPLIT model

Body condition reference ranges for wild bottlenose dolphins (Tursiops truncatus)

Comparative toxicity of pyrethroid insecticides to two estuarine crustacean species, *Americamysis bahia* and *Palaemonetes pugio*

Influence of terrestrial inputs on continental shelf carbon dioxide

Cloud tuning in a coupled climate model: impact on 20th century warming

Bioavailability and intravenous toxicokinetic parameters for Pacific ciguatoxin P-CTX-1 in rats

Brevetoxin in blood, biological fluids, and tissues of sea turtles naturally exposed to *Karenia brevis blooms* in central west Florida

Controls of global snow under climate change

OTHER REPORTS, BOOK CHAPTERS, & INTERNAL PUBLICATIONS

Probability of taking a western North Pacific gray whale during the proposed Makah hunt

Small scale experimental systems for coral research: considerations, planning, and recommendations

Seabird protection network: your guide to starting a chapter

Deepwater Horizon Oil Spill: assessment of potential impacts on the deep soft-bottom benthos

HIGHLIGHTED ARTICLE

AUTHORS

D. J. Madigan, Z. Baumann, **O. E. Snodgrass (NMFS/SWFSC)**, H. A. Ergül, **H. Dewar (NMFS/SWFSC),** and N. S. Fisher

PUBLICATION DATE

Expected late February 2013

TITLE

Radiocesium in Pacific Bluefin Tuna Thunnus orientalis in 2012 validates new tracer technique

JOURNAL

Environmental Science & Technology

SIGNIFICANCE

- Fukushima-derived radionuclides were detected in Pacific bluefin tuna (PBFT) tissue, and used to track the movement of tuna migrating across the North Pacific Ocean basin and into the California Current Large Marine Ecosystem (CCLME).
- Differences in Cs isotope concentrations in migrant v. resident PBFT tissues suggested that this radiotracer can be used to distinguish these populations of tuna in the CCLME (especially 134Cs).
- Radiocesium concentrations in 2012 PBFT were less than half those from 2011 and well below safety guidelines for public health.

Bluefin Tuna

SUMMARY

The detection of Fukushima-derived radionuclides in Pacific bluefin tuna (PBFT) that crossed the Pacific Ocean to the California Current Large Marine Ecosystem (CCLME) in 2011 presented the potential to use radiocesium as a tracer in highly migratory species. This tracer requires that all western Pacific Ocean emigrants acquire the 134Cs signal, a radioisotope undetectable in Pacific biota prior to the Fukushima accident in 2011. We tested the efficacy of the radiocesium tracer by measuring 134Cs and 137Cs in PBFT (n = 50) caught in the CCLME in 2012, more than a year after the Fukushima accident. All small PBFT (n = 28; recent migrants from Japan) had 134Cs (0.7 ± 0.2 Bq kg–1) and elevated 137Cs (2.0 ± 0.5 Bq kg–1) in their white muscle tissue. Most larger, older fish (n = 22) had no 134Cs and only background levels of 137Cs, showing that one year in the CCLME is sufficient for 134Cs and 137Cs values in PBFT to reach pre-Fukushima levels. Radiocesium concentrations in 2012 PBFT were less than half those from 2011 and well below safety guidelines for public health. Detection of 134Cs in all recent migrant PBFT supports the radiocesium tracer in migratory animals in 2012.

VISIT THE SCIENTIFIC PUBLICATIONS REPORT ARCHIVE

HIGHLIGHTED ARTICLE

AUTHORS

D. R. Hardison, W. G. Sunda, D. Shea, **R. W. Litaker**
(NOS/NCCOS)

PUBLICATION DATE

Expected March 2013

TITLE

Increased toxicity of Karenia brevis *during phosphate limited growth: ecological and evolutionary implications*

JOURNAL

PLoS ONE

SIGNIFICANCE

- Concentrations of the potent neurotoxins in the Florida red tide dinoflagellate *Karenia brevis* vary among genetic strains and increase two- to three-fold with nutrient limitation of growth rate.
- The increase in neurotoxins per cell under nutrient limitation of growth rate will increase the toxicity of a red tide bloom of *Karenia brevis* for a given bloom biomass.
- Phosphorous limited blooms will be more toxic than nitrogen limited blooms at a given *K. brevis* cell concentration, which is of significance to environmental managers because the concentration of *Karenia* cells is currently used to gauge the potential toxicity and adverse impact of *Karenia* blooms in coastal waters of the Gulf of Mexico.

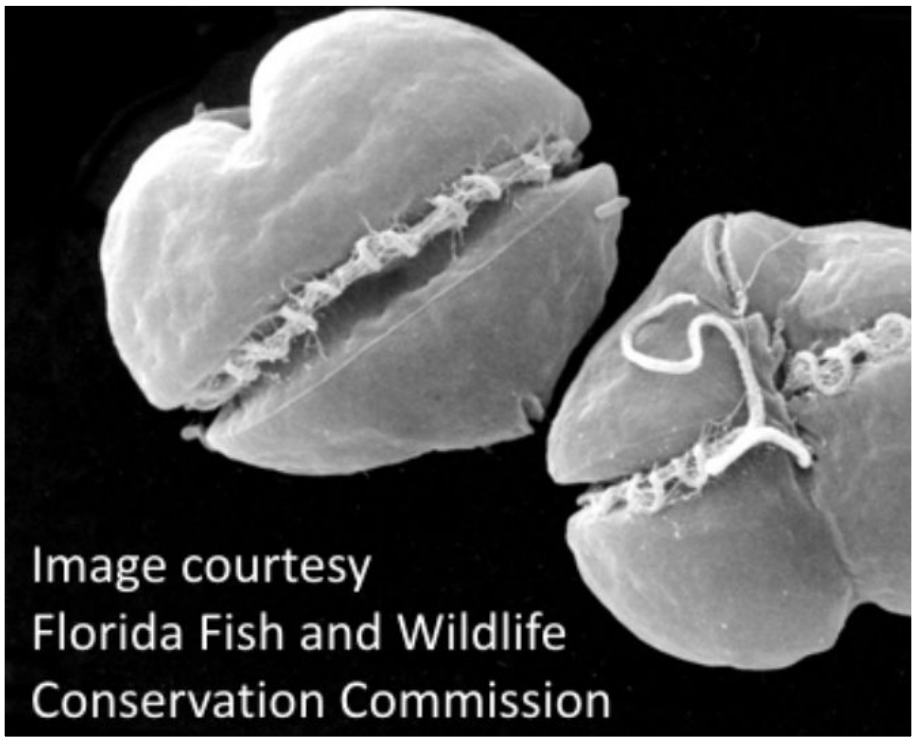

Karenia Brevis (Red Tide)

SUMMARY

Karenia brevis is the dominant toxic red tide algal species in the Gulf of Mexico. It produces potent neurotoxins (brevetoxins [PbTxs]), which negatively impact human and animal health, local economies, and ecosystem function. Field measurements have shown that cellular brevetoxin contents vary from 1-68 pg/cell but the source of this variability is uncertain. Increases in cellular toxicity caused by nutrient-limitation and inter-strain differences have been observed in many algal species. This study examined the effect of P-limitation of growth rate on cellular toxin concentrations in five *Karenia brevis* strains from different geographic locations. Phosphorous was selected because of evidence for P-limitation of algal growth in some regions of the Gulf of Mexico. Depending on the isolate, P-limited cells had 2.3- to 7.3-fold higher PbTx per cell than P-replete cells. The percent of cellular carbon associated with brevetoxins (%C- PbTx) was ~ 0.7 to 2.1% in P-replete cells, but increased to 1.6-5% under P-limitation. Because PbTxs are potent anti-grazing compounds, this increased investment in PbTxs should enhance cellular survival during periods of nutrient-limited growth. The %C-PbTx was inversely related to the specific growth rate in both the nutrient-replete and P-limited cultures of all strains. This inverse relationship is consistent with an evolutionary tradeoff between carbon investment in PbTxs and other grazing defenses, and C investment in growth and reproduction. In aquatic environments where nutrient supply and grazing pressure often vary on different temporal and spatial scales, this tradeoff would be selectively advantageous as it would result in increased net population growth rates. The variation in PbTx/cell values observed in this study can account for the range of values observed in the field, including the highest values, which are not observed under N-limitation. These results suggest P-limitation is an important factor regulating cellular toxicity and adverse impacts during at least some *K. brevis* blooms.

VISIT THE SCIENTIFIC PUBLICATIONS REPORT ARCHIVE

HIGHLIGHTED ARTICLE

AUTHORS

J. V. Redfern (NMFS/SWFSC), M. F. McKenna, T. J. Moore (NMFS/SWFSC), J. Calambokidis, M. L. DeAngelis (NMFS/SWRO), E. A. Becker (NMFS/SWFSC), J. Barlow (NMFS/SWFSC), K. A. Forney (NMFS/SWFSC), P. C. Fiedler (NMFS/SWFSC), S. J. Chivers (NMFS/SWFSC)

PUBLICATION DATE

Expected February or March 2013

TITLE

Assessing the risk of ships striking large whales in marine spatial planning

JOURNAL

Conservation Biology

SIGNIFICANCE

- Risk of ship strike to humpbacks and fin whales may be ameliorated by creating a new route south of the northern Channel Islands, this area contains military training ranges.
- This paper also suggests that changing shipping routes will not have the same impact on ship strike numbers for blue whales because of their broader geographic distribution and that ship strikes may exceed levels established in U.S. law.
- The analytical tools presented in this paper could be used at stakeholder meetings to discuss alternative shipping routes and used to incorporate marine mammal distributions in marine planning. The authors admit that their results are potentially controversial.

Right Whale After Ship Strike

SUMMARY

Marine spatial planning provides a comprehensive framework for managing multiple uses of the marine environment and has the potential to minimize environmental impacts and reduce conflicts among users. Spatially explicit assessments of the risks to key marine species from human activities are a requirement of marine spatial planning. The authors assessed the risk of ships striking humpback, blue, and fin whales in alternative shipping routes derived from patterns of shipping traffic off Southern California. For this study the authors utilized whale-habitat use models, alternative shipping routes, whether the ships traveled multiple routes, overlap of shipping routes with protected areas, and if the route was used by multiple sectors (i.e. commerce and military) to determine possible ship strike risk. The route with the lowest risk for humpback whales had the highest risk for fin whales and vice versa. Risk to both species may be ameliorated by creating a new route south of the northern Channel Islands and spreading traffic between this new route and the existing route in the Santa Barbara Channel. Creating a longer route may reduce the overlap between shipping and other uses by concentrating shipping traffic. Blue whales are distributed more evenly across our study area than humpback and fin whales; thus, risk could not be ameliorated by concentrating shipping traffic in any of the routes we considered. Alternative measures for reducing ship-strike risk for blue whales may be necessary because our assessment of the potential number of strikes suggests that they are likely to exceed allowable levels of anthropogenic impacts established under U.S. laws.

VISIT THE SCIENTIFIC PUBLICATIONS REPORT ARCHIVE

ADDITIONAL ARTICLE

AUTHORS

A. Arguez and **S. Applequist (NESDIS/NCDC)**

PUBLICATION DATE

Expected September 2013

TITLE

A harmonic approach for calculating daily temperature normals constrained by homogenized monthly temperature normals

JOURNAL

Journal of Atmospheric and Oceanic Technology

SIGNIFICANCE

- This study offers a constrained harmonic technique that forces daily temperature normals to be consistent with monthly temperature normals.
- This approach effectively passes the homogenization applied at the monthly scale down to the daily scale, resulting in a smooth annual cycle devoid of day-to-day sampling variability and inter-month discontinuities.

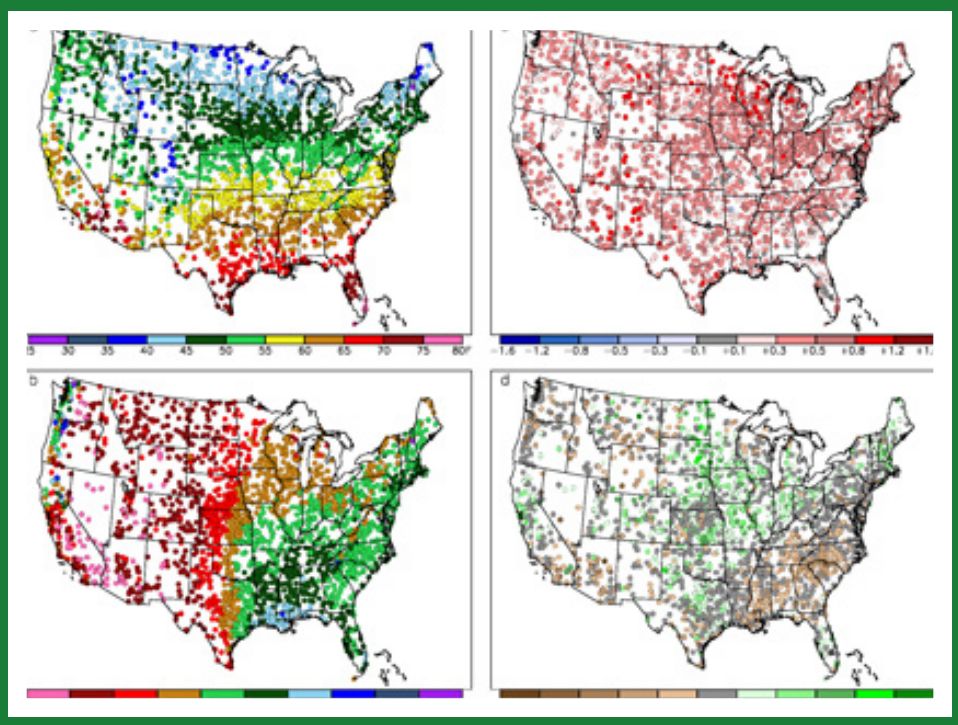

Climate normals

SUMMARY

NOAA released the new 1981-2010 climate normals in July 2011. These included monthly and daily normals of minimum and maximum temperature. Monthly normals were computed from monthly temperature values that were corrected for biases (i.e., homogenized) due to changes in observing practices over the course of the normals period (station moves, changes in observation time, and changes in instrumentation). Daily temperature observations, however, are not homogenized, which could lead to inconsistencies between the daily and monthly normals. Here, we offer a constrained harmonic technique that forces the daily temperature normals to be consistent with the monthly temperature normals. This approach replaces the cubic spline interpolation of monthly temperature normals that was used to compute earlier versions of NOAA's daily temperature normals. This new method represents a change in computation of a commonly used NOAA product and can be used in other applications.

VISIT THE SCIENTIFIC PUBLICATIONS REPORT ARCHIVE

ADDITIONAL ARTICLE

AUTHORS

W. M. Blair and **G. J. Doucette (NOS/NCCOS)**

PUBLICATION DATE

Expected February 2013

TITLE

The Vibrio harveyi *bioassay routinely used to detect AI-2 quorum sensing inhibition is confounded by inconsistent normalization across marine matrices*

JOURNAL

Journal of Microbiological Methods

SIGNIFICANCE

- The results identify important limitations of the currently available and commonly used methodology for detecting inhibition in quorum sensing (intercellular communication among microbes) in the marine environment.
- Quorum sensing may play a role in regulating the dynamics of harmful algal blooms, and the authors are currently investigating this possibility.

SUMMARY

The *Vibrio harveyi* autoinducer-2 (AI-2) bioassay is used routinely to screen for inhibition of the AI-2 quorum sensing system. This study utilizes three well-described bacterial strains to demonstrate that inconsistent normalization across matrices undermines the use of this assay in screening marine samples for AI-2 inhibition.

VISIT THE SCIENTIFIC PUBLICATIONS REPORT ARCHIVE

ADDITIONAL ARTICLE

AUTHORS

J. Mao, **L. W. Horowitz,** V. Naik, **S. Fan,** J. Liu, and A. M. Fiore **(OAR/GFDL)**

PUBLICATION DATE

Expected April 2013

TITLE

Sensitivity of tropospheric oxidants to wildfires: implications for radiative forcing

JOURNAL

Geophysical Research Letters

SIGNIFICANCE

- Wildfires are one of the largest uncontrollable sources of trace gases and aerosols, and have profound influence on tropospheric oxidants and radiative forcing.
- At present-day emission levels, biomass burning produces a negative net radiative forcing, but increasing emissions to over 5 times present levels would result in a positive net forcing.

SUMMARY

The goal of this research was to better understand the impact of wildfires on tropospheric oxidants and radiative forcing. There are large uncertainties in current estimates of direct radiative forcing from biomass burning aerosols. Despite this, using a coupled chemistry-climate model, we show that the warming resulting from CH_4 and CH_4-induced changes in O_3 and stratospheric H_2O (which can be considered as an indirect chemical forcing) is comparable to the cooling from biomass burning aerosols with direct and indirect effect taken into account. We find that gas and aerosol emissions combine to increase CH_4 lifetime non-linearly. Heterogeneous processes are partly responsible for the observed lower ozone production efficiency in northern high latitudes compared to tropical regions. The radiative forcing from biomass burning is shown to vary non-linearly with biomass burning strength. At present-day emission levels, biomass burning produces a net radiative forcing of –0.21 W/m^2 (-0.29 from gas and aerosol emissions, 0.08 from CH_4 and CH_4-induced changes in O_3 and stratospheric H_2O), but increasing emissions to over 5 times present levels would result in a positive net forcing.

ADDITIONAL ARTICLE

AUTHORS

B. Chen, **A. F. Stein (OAR/ARL),** P. G. Maldonado, A. M. Sanchez de la Campa, Y. Gonzalez-Castanedo, N. Castell, J. D. de la Rosa

PUBLICATION DATE

Expected April 2013

TITLE

Size distribution and concentrations of heavy metals in atmospheric aerosols originating from industrial emissions as predicted by the HYSPLIT model

JOURNAL

Atmospheric Environment

SIGNIFICANCE

- HYSPLIT has been used to model the transport and dispersion of heavy metals in aerosols in an industrial area in Southern Europe.
- In this study, HYSPLIT runs underestimated the intensity of metal pollution surrounding industrial areas due to low resolution meteorological data.
- Additionally, HYSPLIT runs overestimated aerosol loading at regional to global scales due to intense vertical dispersion.

SUMMARY

This study presents a description of the emission, transport, dispersion, and deposition of heavy metals contained in atmospheric aerosols emitted from a large industrial complex in southern Spain using the HYSPLIT model coupled with high- (MM5) and low-resolution (GDAS) meteorological simulations. The dispersion model was configured to simulate eight size fractions (<0.33, 0.66, 1.3, 2.5, 5, 14, 17, and >17 μm) of six major metals (Cr, Co, Ni, La, Zn, and Mo) based on direct measurements taken at twelve industrial emission stacks in four plants. The stacks showed considerable differences for both emission fluxes and size ranges of metals. The HYSPLIT predictions show that modeled industrial emissions produce an enrichment of heavy metals by a factor of 2-5 for local receptor sites when compared to urban and rural background areas in Spain, and based on meteorological fields from MM5 show reasonable consistency with the temporal evolution of concentrations of Cr, Co, and Ni observed at three sites downwind of the industrial area. The magnitude of concentrations of metals at two receptors was underestimated for both MM5 (by a factor of 2-3) and GDAS (by a factor of 4-5) meteorological runs. The model prediction shows that heavy metal pollution from industrial emissions in this area is dominated by the ultra-fine (<0.66 μm) and fine (<2.5 μm) size fractions.

VISIT THE SCIENTIFIC PUBLICATIONS REPORT ARCHIVE

ADDITIONAL ARTICLE

AUTHORS

L. B. Hart, R. S. Wells, and **L. H. Schwacke (NOS/NCCOS)**

PUBLICATION DATE

Acceptance January 10, 2013

TITLE

Body condition reference ranges for wild bottlenose dolphins (Tursiops truncatus)

JOURNAL

Aquatic Biology

SIGNIFICANCE

- This paper establishes male and female estuarine bottlenose dolphin baseline reference ranges for indices of body condition including body mass index and the relationships between mass and length, as well as girth and length.
- Bottlenose dolphin capture-release projects have increased in number and geographic range in recent years; therefore, these reference ranges can be used to identify individuals or stocks with compromised health conditions that may be related to or reflected by changes in body condition (in response to acute or chronic exposure to environmental or anthropogenic stressors).

Bottlenose dolphins

SUMMARY

Marine mammal body condition, as evaluated by a combination of mass, length and/or girth measurements, has often been considered an indicator of nutritional status. As such, measurements of total mass, total length, and maximum girth from long-term bottlenose dolphin (*Tursiops truncatus*) capture-release research conducted in Sarasota, Bay, FL, USA, (1987-2009) was used to develop 95th percentile reference ranges for two body condition models relating these metrics: 1) total mass vs. total length; and 2) maximum girth vs. total length. Nonlinear and linear quantile regression methods were used to estimate the parameters for the reference ranges and develop predictive models to examine body condition among individual dolphins. The flexibility of these models and reliance upon commonly acquired morphometrics allows for broad application among researchers lacking data on mass or age. Ultimately these reference ranges can be used to evaluate and compare the body condition of individual animals and provide an additional metric for evaluating the general health of coastal populations.

VISIT THE SCIENTIFIC PUBLICATIONS REPORT ARCHIVE

ADDITIONAL ARTICLE

AUTHORS

M. E. DeLorenzo, P. B. Key, K. W. Chung, Y. Sapozhnikova, M. H. Fulton (NOS/NCCOS)

PUBLICATION DATE

Expected January 2013 (online)

TITLE

Comparative toxicity of pyrethroid insecticides to two estuarine crustacean species, Americamysis bahia *and* Palaemonetes pugio

JOURNAL

Environmental Toxicology

SIGNIFICANCE

- Acute toxicity to estuarine crustaceans occurred at low nanogram per liter concentrations of some pyrethroids, illustrating the need for careful regulation of the use of pyrethroid compounds in the coastal zone.

SUMMARY

Pyrethroid insecticides are widely used on agricultural crops, as well as for nurseries, golf courses, urban structural and landscaping sites, residential home and garden pest control, and mosquito abatement. Evaluation of sensitive marine and estuarine species is essential for the development of toxicity testing and risk assessment protocols. Two estuarine crustacean species, *Americamysis bahia* (mysids) and *Palaemonetes pugio* (grass shrimp), were tested with the commonly used pyrethroid compounds, lambda-cyhalothrin, permethrin, cypermethrin, deltamethrin, and phenothrin. Sensitivities of adult and larval grass shrimp and 7d old mysids were compared using standard 96h LC50 bioassay protocols. Adult and larval grass shrimp were more sensitive than the mysids to all the pyrethroids tested. Larval grass shrimp were approximately eighteen fold more sensitive to lambda-cyhalothrin than the mysids. Larval grass shrimp were similar in sensitivity to adult grass shrimp for cypermethrin, deltamethrin, and phenothrin, but larvae were approximately twice as sensitive to lambda-cyhalothrin and permethrin as adult shrimp.

ADDITIONAL ARTICLE

AUTHORS

L. -Q. Jiang, W. -J. Cai, Y. Wang, J. E. Bauer **(NESDIS/NODC)**

PUBLICATION DATE

February 7, 2013

TITLE

Influence of terrestrial inputs on continental shelf carbon dioxide

JOURNAL

Biogeosciences

SIGNIFICANCE

- Analyses of dissolved inorganic carbon, dissolved organic carbon, and partial pressure of carbon dioxide (pCO_2) in the South Atlantic Bight (SAB) demonstrate how temperature, air-sea gas exchange, and terrestrial inputs control sea surface pCO_2 on the continental shelf.
- Terrestrial sources increase the nearshore pCO_2 by direct input of inorganic carbon from rivers and salt marshes, and indirectly by input of organic carbon that is later remineralized in the SAB.
- This mechanism is the most likely explanation for findings of the inner continental shelf of the SAB being a source of atmospheric carbon dioxide, and the middle and outer shelf of the SAB being a sink.

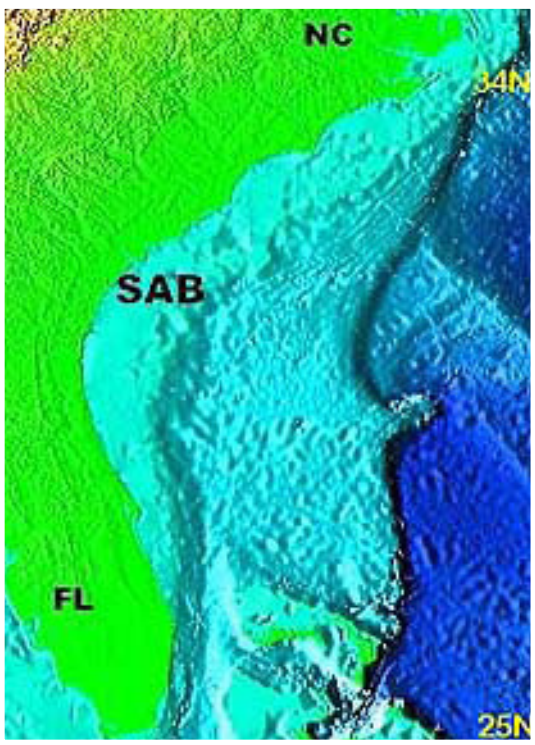

South Atlantic blight

SUMMARY

The U.S. South Atlantic Bight (SAB) is a low latitude shallow continental shelf bordered landward by abundant salt marshes and rivers. Based on previously published data on sea surface partial pressure of carbon dioxide (pCO2) and new dissolved inorganic carbon (DIC) and dissolved organic carbon (DOC) data, a model analysis is presented to identify and quantify the contributions of various terrestrial carbon inputs on SAB sea surface pCO_2. Our findings demonstrate that although additions of CO_2 from within shelf waters were the greatest of the three components and underwent the largest seasonal changes, pCO_2 from shelf waters showed smaller onshore–offshore gradients than rivers and marshes. In contrast, CO_2 contributions from river and salt marsh components were greatest closest to the coast and decreased with distance offshore. In addition, the magnitude of pCO_2 contributions from salt marsh was about three-fold greater than pCO_2 from rivers. Our findings also revealed that decomposition of terrestrial organic carbon was an important factor regulating the seasonal pattern of pCO_2 on the inner shelf. Despite large uncertainties, this study demonstrates the importance of terrestrial inputs, in particular those from coastal wetlands, on coastal ocean CO_2 distributions.

ADDITIONAL ARTICLE

AUTHORS

J. -C. Golaz, L. W. Horowitz, and H. Levy II (OAR/GFDL)

PUBLICATION DATE

Expected April 2013

TITLE

Cloud tuning in a coupled climate model: impact on 20th century warming

JOURNAL

Geophysical Research Letters

SIGNIFICANCE

- Clouds remain one of the largest sources of uncertainties in predictions from climate models and can have considerable impact on the simulated climate.
- The present-day climate (1981-2000) is nearly indistinguishable between the two cloud configurations. However, the magnitude of the aerosol indirect effects varies substantially from one configuration to another.
- As a result, the degree of warming over the 20th century is very different in the warmest configuration (CM3w) and compares the best with observations.

Ice and open water in the Beaufort Sea north of Alaska

SUMMARY

We investigate the impact of uncertainties in cloud tuning in GFDL's CM3 coupled climate model by constructing two alternate configurations (CM3w, CM3c). They achieve the observed radiation balance using different, but plausible, combinations of parameters. The present-day climate is nearly indistinguishable among all configurations. However, the magnitude of the indirect effects differs by as much as 1.2 Wm–2 , resulting in significantly different temperature evolution over the 20th century (Figure below). CM3 predicts a warming of 0.22 °C. CM3w, with weaker indirect effects, warms by 0.57 °C, whereas CM3c, with stronger indirect effects, shows essentially no warming.

VISIT THE SCIENTIFIC PUBLICATIONS REPORT ARCHIVE

ADDITIONAL ARTICLE

AUTHORS

A. Ledreux and J. S. Ramsdell (NOS/NCCOS)

PUBLICATION DATE

January 11, 2013 (online)

TITLE

Bioavailability and intravenous toxicokinetic parameters for Pacific ciguatoxin P-CTX-1 in rats

JOURNAL

Toxicon

SIGNIFICANCE

- This research provides parameters to model ciguatoxin poisoning in humans and the endangered Hawaiian monk seal.
- Because of difficulty in human and monk seal testing, assessment of the risk of ciguatera poisoning will need to rely upon computer or "in silico" modeling. NCCOS scientists have now determined key internal parameters that are required to simulate the entry, fate and effects of the toxin.

SUMMARY

Ciguatoxins are sodium channel activator toxins responsible for ciguatera fish poisoning. In this study, the authors determined the toxicokinetic parameters of the Pacific ciguatoxin P-CTX-1 in rats after an intravenous dose of 0.13 ng P-CTX-1 per g of body weight. The ciguatoxin activity was assessed over time in blood using the sensitive functional Neuro2a assay. The data were analyzed with a two-compartmental model. After exposure, the ciguatoxin activity exhibited a rapid (alpha half-life of 6 min) and extensive distribution into tissues (apparent steady state volume of distribution of 7.8 L). Ciguatoxin elimination from blood was slower with a beta half-life estimated at 35.5 h. The toxicokinetic parameters determined from this study were compared to data previously obtained after oral and intraperitoneal exposure of rats to 0.26 ng P-CTX-1 per g of body weight. Maximal bioavailability was determined by the area under the concentration curve, and was used to calculate the absolute P-CTX-1 bioavailabilities for oral and intraperitoneal routes of exposures of 39% and 75%, respectively.

VISIT THE SCIENTIFIC PUBLICATIONS REPORT ARCHIVE

ADDITIONAL ARTICLE

AUTHORS

D. A. Fauquier (NMFS/OPR), L. J. Flewelling, **J. Maucher (NOS/NCCOS),** C. A. Manire, V. Socha, M. J. Kinsel, B. A. Stacy, M. Henry, J. Gannon, **J. S. Ramsdell (NOS/NCCOS),** J. H. Landsberg

PUBLICATION DATE

TBD

TITLE

Brevetoxin in blood, biological fluids, and tissues of sea turtles naturally exposed to Karenia brevis *blooms in central west Florida*

JOURNAL

Journal of Zoo and Wildlife Medicine

SIGNIFICANCE

- In depth analyses of tissues and blood from sea turtles during two large red tide events in 2005 and 2006 showed that brevetoxicosis was largely responsible for the strandings and mortalities of sea turtles along the west coast of Florida during that time.
- Although all species of sea turtles in United States waters are listed on the Endangered Species Act of 1973 as endangered or threatened, limited data has been previously available linking brevetoxin exposure to sea turtle morbidity and mortality.

Red tide

SUMMARY

In 2005 and 2006, the central west Florida coast experienced two intense *Karenia brevis* red tide events lasting from February 2005 through December 2005 and August 2006 through December 2006. Strandings of sea turtles were increased in the study area with 318 turtles (n=174, 2005; n=144, 2006) stranding between January 1st 2005 and December 31st, 2006 compared to the 12-year average of 43 ± 23 turtles. Live turtles (n=61) admitted for rehabilitation showed clinical signs including unresponsiveness paresis, and circling. Testing of biological fluids and tissues for the presence of brevetoxin activity by enzyme-linked immunosorbent assay found toxin present in 93% of live stranded sea turtles, and 98% of dead stranded sea turtles tested. Serial plasma samples were taken from several live sea turtles during rehabilitation and toxin was cleared from the blood within 5-80 days post-admit depending upon the species tested. Among dead animals the highest brevetoxin levels were found in feces, stomach contents, and liver. The lack of significant pathological findings in the majority of animals necropsied supports toxin-related mortality.

VISIT THE SCIENTIFIC PUBLICATIONS REPORT ARCHIVE

ADDITIONAL ARTICLE

AUTHORS

S. Kapnick and **T. Delworth (OAR/GFDL)**

PUBLICATION DATE

Expected April 2013

TITLE

Controls of global snow under climate change

JOURNAL

Journal of Climate

SIGNIFICANCE

- This paper furthers the model development for CM2.5 by validating the model and showing its ability to capture hydroclimate variability.
- Understanding snowfall variability is key to understanding future water supply in snow-melt-dominated regions, like the western US.

SUMMARY

The goals of this research were to validate the CM2.5 and CM2.1 models for snowfall and to explore changes in snowfall in an idealized future climate run to determine if resolution differences influence snowfall signals. The new high-resolution global climate model, CM2.5, better represents snowfall and snow-related variables than CM2.1 in the present climate. CM2.5 is unique in that its high resolution allows it to resolve complex orography, leading to a change in sign in snowfall projections over high mountains, in particular over (1) the Himalayas, (2) the highest peak in SW Yukon, and (3) the Andes. In the first two locations, literature supports such trends in the present climate, implying that they are a continuation.

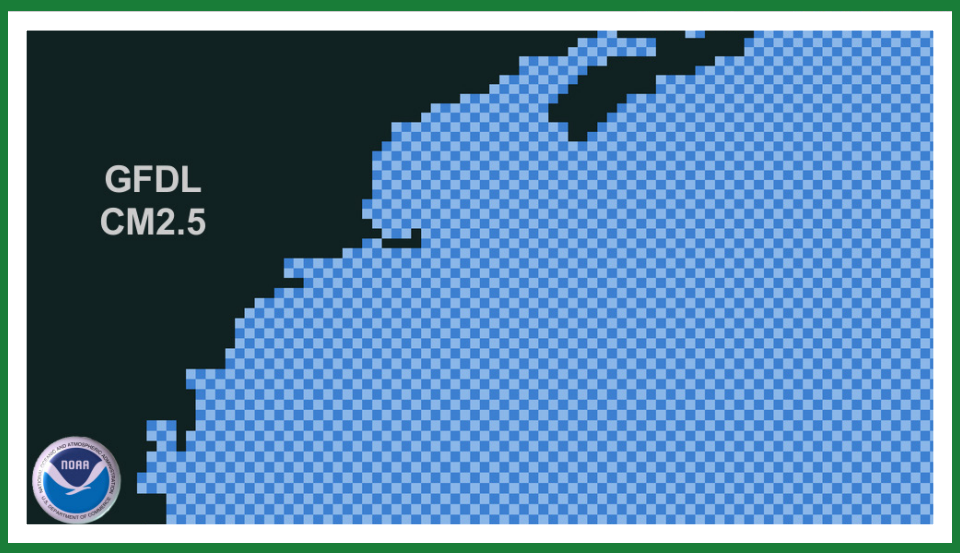

In the newer, eddy-permitting GFDL CM2.5 model, we see ocean grid cell sizes that are ~21 kilometers (13 miles) on a side at the latitude of New York City.

VISIT THE SCIENTIFIC PUBLICATIONS REPORT ARCHIVE

AUTHORS

J. Moore and D. Weller (NMFS/SWFSC)

PUBLICATION DATE

January 2013

TITLE

Probability of taking a western North Pacific gray whale during the proposed Makah hunt

JOURNAL

NOAA Technical Memorandum

SIGNIFICANCE

- The results show a low probability that at least one western North Pacific gray whale would be struck within a 5-year period corresponding to the proposed gray whale hunt by the Makah tribe.

North Pacific Gray Whale

SUMMARY

Recent observations of gray whales (*Eschrichtius robustus*) in the western North Pacific (WNP) migrating to areas off the coast of North America (Alaska to Mexico) raise concern about the possibility of the small western population being subjected to the gray whale hunt proposed by the Makah Indian Tribe in northern Washington, USA. To address this concern, we estimated the probability of striking (i.e. killing or seriously injuring) a WNP whale during the Makah hunt using six models from 4 model sets that varied based on the assumptions and types of data used for estimation. Model set 1 used WNP and ENP abundance estimates. Model set 2 used these abundance estimates, as well as sightings data from the proposed hunt area. Model sets 3 and 4 used only the sightings data. Within model sets 1 and 2, two models (A and B) differed based upon whether migrating ENP and WNP whales were assumed to be equally available to the hunt per capita (A) or whether this assumption is relaxed (B). We consider Model 2B the most plausible of all models because model set 2 makes use of all available information and 2B contains fewer assumptions than 2A. Based on model 2B, the probability of striking ≥1 WNP whale in a single season ranges from 0.007 to 0.036, depending on if the median or upper 95th percentile estimate is used and on which maximum is used for the total number of whales struck. The probability of striking ≥1 WNP whale out of 5 seasons ranges from 0.036 to 0.170 across the same scenarios. The expected number to be struck in a single year ranges from 0.01 to 0.04 and from 0.04 to 0.19 across 5 years. For context, these strike estimates were compared to different possible values of Potential Biological Removal (PBR). We also summarized analogous estimates for the number of WNP whales that would be "taken" non-lethally, in terms of the number of attempted but unsuccessful strikes as well as the number of animals approached and pursued during the hunt.

AUTHORS

T. C. Bartlett (NOS/NCCOS)

PUBLICATION DATE

TBD

TITLE

Small scale experimental systems for coral research: considerations, planning, and recommendations

JOURNAL

NOAA Technical Memorandum

SIGNIFICANCE

- Techniques and procedures are presented to assist researchers in developing small experimental systems for coral and attempts to identify possible confounding factors to consider when setting up laboratory experiments with coral.

SUMMARY

Only a few decades ago, keeping coral alive and healthy in closed, captive systems proved to be challenging. In the short time since, there has been a surge of interest, knowledge, and technological advances with significant contributions from marine science, the aquarium industry, and aquarium hobbyists. Likewise, the difficulty in keeping coral in captivity has limited their use in well controlled laboratory experimentation. Much of the research on coral health and disease has been observational, and until recently, experimentation has been performed in a field setting which is subject to many uncontrolled variables, some measurable and some not. Furthermore, experimentation with infectious agents of coral diseases and toxicant effectors in the wild carries the risk of harming natural populations and raises ethical dilemmas. As a result of these issues, we and others are working to create laboratory life support systems for corals that can be used for experimentation under well controlled and monitored parameters. In the following technical memorandum, techniques and procedures are presented to assist researchers in developing small experimental systems for coral and attempts to identify possible confounding factors to consider when setting up laboratory experiments with coral. The system features presented here are intended for relatively simple experiments when funding, space, and time are limiting.

AUTHORS

S. Tezak, M. Maheigan, K. Reyna, M. Brown, G. McChesney, J. Boyce, C. Plaisted **(NOS/ONMS)**

PUBLICATION DATE

TBD

TITLE

Seabird protection network: your guide to starting a chapter

JOURNAL

ONMS Condition Report Series

SIGNIFICANCE

- The goal of the Seabird Protection Network is to minimize levels of human disturbance to breeding and roosting seabird colonies along the California coast. This report provides background information on the Network and a pathway to successfully develop additional Chapters throughout California.

Red-footed Boobies

SUMMARY

In California, oil spill restoration funds have been used for long-term seabird protection. Seabird biologists have shown that healthy and thriving seabird populations are more capable of withstanding a catastrophic oil spill, and the best way to support seabird populations is to protect breeding and roosting sites from human disturbance. The overarching vision of the Seabird Protection Network (Network) is resilient seabird populations flourishing throughout the coastal and near-shore waters of California. The Network works to help seabirds thrive by informing coastal and ocean users how activities, like low-flying aircraft and close-approaching boats can cause nesting seabirds to flee from their nests, leaving eggs or chicks vulnerable to predators. These efforts are accomplished through an organized outreach and education program combined with management actions and enforcement of wildlife disturbance regulations. The structure of the Network is modeled on the Audubon Society that uses Chapters to function in designated geographic areas. By establishing Network Chapters, different projects throughout the state participate in a framework that facilitates collaboration and sharing of information, lessons learned and outreach materials. This framework provides leverage, builds greater support for the Network, and creates an identity that can be recognized state-wide, thus furthering the goal of minimizing disturbance to marine wildlife. Gulf of the Farallones National Marine Sanctuary, who manages the founding Chapter, facilitates program expansion and incorporates additional Chapters throughout the coastal and near-shore waters of California as they develop.

AUTHORS

P. A. Montagna, **J. G. Baguley, C. Cooksey, and J. L. Hyland (NOS/NCCOS)**

PUBLICATION DATE

Available Online: February 2013

TITLE

Deepwater Horizon *oil spill: assessment of potential impacts on the deep soft-bottom benthos*

JOURNAL

NOAA Technical Memorandum

SIGNIFICANCE

- This report provides an increased understanding of the impacts of the *Deepwater Horizon* oil spill on natural resources, such as deep-sea benthos and sediment quality, in deepwater areas of the Gulf of Mexico.

Deepwater Horizon incident

SUMMARY

A study was initiated in May 2011, under the direction of the *Deepwater Horizon* (DWH) Natural Resource Damage Assessment (NRDA) Deepwater Benthic Communities Technical Working Group, to assess potential impacts of the DWH oil spill on sediments and resident benthic fauna in deepwater (> 200 meters) areas of the Gulf. Key objectives of the study were to complete the analysis of samples from 65 priority stations sampled in September-October 2010 on two DWH Response cruises and from 38 long-term monitoring sites (including a subset of 35 of the original 65) sampled on a follow-up NRDA cruise in May-June 2011. The present progress report provides a brief summary of results from the initial processing of samples from fall 2010 priority sites (plus three additional historical sites). Data on key macrofaunal, meiofaunal, and abiotic environmental variables are presented for each of these samples and additional maps are included to depict spatial patterns in these variables throughout the study region. The near-field zone within about 3 km of the wellhead, where many of the stations showed evidence of impaired benthic condition (e.g. low taxa richness, high nematode/harpacticoid- copepod ratios), also is an area that contained some of the highest concentrations of total petroleum hydrocarbons, total polycyclic aromatic hydrocarbons, and barium in sediments (as possible indicators of DWH discharges). There were similar co-occurrences at other sites outside this zone, especially to the southwest of the wellhead out to about 15 km. However, there also were exceptions to this pattern, for example at several farther-field sites in deeper-slope and canyon locations where there was low benthic species richness but no evidence of exposure to DWH discharges. Such cases are consistent with historical patterns of benthic distributions in relation to natural controlling factors such as depth, position within canyons, and availability of organic matter derived from surface-water primary production.

A Harmonic Approach for Calculating Daily Temperature Normals Constrained by Homogenized Monthly Temperature Normals

Anthony Arguez and Scott Applequist

National Oceanic and Atmospheric Administration's

National Climatic Data Center

Accepted February 6, 2013

Submitted to the Journal of Atmospheric and Oceanic Technology (JTECH)

as an Expedited Contribution

Author Contact Information:

Anthony Arguez

NOAA/NCDC Room 506

151 Patton Avenue

Asheville, NC 28801

Phone: (828) 271-4338

Email: Anthony.Arguez@noaa.gov

VISIT THE SCIENTIFIC PUBLICATIONS REPORT ARCHIVE

ABSTRACT

NOAA released the new 1981-2010 climate normals in July 2011. These included monthly and daily normals of minimum and maximum temperature. Monthly normals were computed from monthly temperature values that were corrected for biases (i.e., homogenized) due to changes in observing practices over the course of the normals period (station moves, changes in observation time, and changes in instrumentation). Daily temperature observations, however, are not homogenized, which could lead to inconsistencies between the daily and monthly normals. Here, we offer a constrained harmonic technique that forces the daily temperature normals to be consistent with the monthly temperature normals. This approach replaces the cubic spline interpolation of monthly temperature normals that was used to compute earlier versions of NOAA's daily temperature normals. It effectively passes the homogenization applied at the monthly scale down to the daily scale, resulting in a smooth annual cycle devoid of day-to-day sampling variability and inter-month discontinuities.

VISIT THE SCIENTIFIC PUBLICATIONS REPORT ARCHIVE

1. Introduction

It is well known that daily temperature normals computed by simply averaging the 30 values for each day of the year (i.e., "raw daily normals") constitute a fairly noisy time series due to sampling variability (see Fig. 1). This effect is exacerbated if missing values are present in the data record. There are numerous ways to calculate daily temperature normals such that high frequency noise is suppressed, yielding a smooth representation of the annual cycle[1]. Two common approaches are time series filtering and interpolation. The filtering approach applies a low pass filter to the raw daily normals. The interpolation approach fits a curve through the 12 monthly normals. This method is extremely useful in situations where the underlying daily data are not available, which is not uncommon when dealing with international data as nations are more likely to make their monthly data freely available rather than their daily data (Thomas Peterson, personal communication).

A factor complicating the computation of daily temperature normals is the need to homogenize temperature time series. The U.S. surface temperature record is known to contain inhomogeneities due to station moves, instrumentation changes, and other changes in observing practices (Menne et al. 2010). For example, the transition from manual observations to Automated Surface Observing System by the National Weather Service in the 1990s is known to have introduced inhomogeneities into those stations' time series (Guttman and Baker 1996). Homogenization is essential for ensuring that climate normals are as representative of the current observing practices as possible at the time of computation. Currently, the U.S. surface temperature record is only homogenized at the monthly (and annual) scale (Menne and Williams

[1] The term "annual cycle" is often used to refer to a single cosine, sine, or harmonic even though the annual march of temperatures for some locations can be highly asymmetric. Here, we refer to an "annual cycle" as the annual march of temperatures whose morphology can vary from station to station.

VISIT THE SCIENTIFIC PUBLICATIONS REPORT ARCHIVE

2009; Menne et al. 2009), whereas daily temperature values from the Global Historical Climatology Network – Daily (GHCN-Daily) are not (Menne et al. 2012), even though the mean monthly temperatures are derived from daily observations. Figure 1 illustrates this difference. The raw daily normals for minimum temperature at the Reno, NV station are ~2°F (~1.1°C) cooler than the homogenized monthly normals for each month of the year. As articulated by Menne et al. (2009), this station's minimum temperature time series was homogenized to account for an apparent urbanization signal, resulting in warmer temperature values over 1981-2010 and a substantially reduced upward trend over the last three decades that is more in line with the trends at neighboring stations (see their Figure 8 for more information).

Thus we developed a technique for computing daily normals with the following properties:

1. Day-to-day sampling variability is removed.
2. The monthly average of the daily temperatures exactly equals the corresponding monthly normal for each month, thereby "passing through" the monthly homogeneity adjustments to the daily scale.
3. There are no inter-month discontinuities (which can be evident in other methods when monthly-varying homogeneity adjustments are applied).
4. The shape of the annual cycle is influenced by the daily data.

Prior to the release of the 1981-2010 climate normals, daily climate normals computed at the National Oceanic and Atmospheric Administration's (NOAA's) National Climatic Data Center (NCDC) were not computed directly from daily data values. The 1971-2000 monthly normals were homogenized following the procedures outlined by Peterson and Easterling (1994) and

VISIT THE SCIENTIFIC PUBLICATIONS REPORT ARCHIVE

Easterling and Peterson (1995). Next, the daily temperature normals were interpolated using a cubic spline through the 12 homogenized monthly normals. Endpoint issues were addressed by applying the spline to a once-repeating 24-point July-June series (Owen and Whitehurst 2002). The monthly means anchored the middle of the month; e.g., the July 16th value is set to the July normal value. Finally, an ad hoc post-spline correction was utilized in an attempt to make the monthly and daily normals consistent, as well as to make the temperature normals consistent with the heating and cooling degree day normals. However, this ad hoc approach could not guarantee consistency for all stations (Richard Heim, Jr., personal communication). Therefore, this cubic spline approach does not satisfy property number 2 listed above, or number 4 as we show in Section 4.

A method that satisfies all four properties is an approach we call the constrained harmonic fit, which was utilized to compute NOAA's 1981-2010 daily temperature normals (Arguez et al. 2012). Harmonic analysis (without constraints) has been shown to be a useful tool for estimating an annual cycle (see Examples 8.8-8.11 in Wilks 2006). By incorporating constraints, we can ensure that the average of the resulting daily temperature normals for each month exactly equals the corresponding monthly temperature normal. The constrained harmonic fit approach is described in greater detail in Section 2. Examples are shown in Section 3, followed by a summary in Section 4.

2. Data and Methodology

Daily maximum temperatures (tmax) and minimum temperatures (tmin) were extracted from GHCN-Daily for 2,041 U.S. stations. The data values in GHCN-Daily have undergone

VISIT THE SCIENTIFIC PUBLICATIONS REPORT ARCHIVE

extensive quality control as described by Durre et al. 2010, resulting in some values that are flagged as erroneous. Each station has at least 25 non-flagged values available for each Julian day (t), for both tmax and tmin, over the 1981-2010 time period. The raw daily normals, $y(t)$, are calculated as the simple arithmetic mean of the valid values for each Julian day. The homogenized monthly normals of tmin and tmax are also used. The generalized approach presented here does not depend on the manner in which monthly temperature normals are calculated. For the purposes of this study, we assume that accurate monthly temperature normals have been computed a priori for use in calculating daily temperature normals.

We can model the daily temperature normals function as a linear combination of harmonics. As described by Wilks (2006), a single harmonic can sometimes provide a reasonable representation of the annual cycle, but additional harmonics are needed in order to account for features that deviate from a single sinusoidal shape, such as asymmetries between summer and winter, or between transition seasons. The equation for the harmonic fit, $h(t)$, takes the familiar form:

$$h(t) = A_0 + \sum_{k=1}^{M} [A_k \cos(\omega_k t) + B_k sin(\omega_k t)] \qquad (1)$$

where t ranges from 1 to N=365, ω_k=2πk/N, and M is the number of harmonics used. If M=$N/2$, then $h(t)$=$y(t)$; the curve $y(t)$ has been reconstructed exactly via the superposition of sines and cosines. If $M << N/2$ then $h(t)$ represents a heavily smoothed version of $y(t)$, equivalent to a low pass filter. If no constraints are applied, we can solve for the coefficient vectors $\vec{A}$ and $\vec{B}$ in (1) via least squares minimization of the following cost function:

VISIT THE SCIENTIFIC PUBLICATIONS REPORT ARCHIVE

$$J_u(\vec{A},\vec{B}) = \sum_{t=1}^{N}\left[y(t) - A_0 - \sum_{k=1}^{M}[A_k\cos(\omega_k t) + B_k sin(\omega_k t)]\right]^2 \qquad (2)$$

This system of linear equations (2*M*+1 equations and 2*M*+1 unknowns) can be solved fairly easily using singular value decomposition (SVD). For this unconstrained case, the coefficient vectors $\vec{A}$ and $\vec{B}$ are more commonly calculated using a Fourier transform.

However, we need to constrain the coefficient values such that the means of the daily normals for a particular month are consistent with the monthly normal. For example, we need to guarantee that the average of the 31 daily tmax normals in January will equal the monthly tmax normal for January. The cost function with 12 monthly constraints is:

$$J_c(\vec{A},\vec{B},\vec{\lambda}) = \sum_{t=1}^{N}[y(t) - h(t)]^2 + \lambda_{jan}\left[T_{jan} - \frac{1}{31}\sum_{t=1}^{31}h(t)\right] \qquad (3)$$

$$+\lambda_{feb}\left[T_{feb} - \frac{1}{28}\sum_{t=32}^{59}h(t)\right] \ldots + \lambda_{dec}\left[T_{dec} - \frac{1}{31}\sum_{t=335}^{365}h(t)\right]$$

T_{jan} is the monthly temperature normal for January, T_{feb} is the monthly temperature normal for February, etc. The λ terms are Lagrange multipliers that impose the constraints. The above formulation follows the "earlier tradition" or the "Lagrangian function approach" described by Kalman (2009). Once again, we can solve this linear system of equations using SVD.

If the number of harmonics, *M*, is greater than or equal to 6, the constraints may be met exactly. Otherwise, the linear system is over-determined and, though SVD can yield a solution

VISIT THE SCIENTIFIC PUBLICATIONS REPORT ARCHIVE

for the coefficients, the constraints will not be met, as we will illustrate in the next section. After experimenting with $M \geq 6$ and visually inspecting the smoothing provided on several samples, we chose to set M equal to 6 for this exercise, although $M>6$ can be a viable alternative for other applications so long as the potential for over-fitting is accounted for. The constrained harmonic fit was calculated for tmax and tmin for all 2,041 stations.

3. Results

The raw daily tmax normal curve for Salinas, CA (Fig. 2a) clearly demonstrates an annual cycle that deviates from a classic sinusoidal curve. In fact, using a single harmonic (M=1), the constrained harmonic fit would place the annual peak in early August, whereas the daily data indicate the warmest time of year in Salinas is September/early October. Salinas is representative of many stations in the western U.S. that have a steeper transition during fall and a more gradual transition during spring. Both the cubic spline interpolation and the constrained harmonic fit (M=6) do a respectable job of capturing the annual cycle in Salinas (the maximum absolute difference between the two is ~0.5°F [~0.3°C]), although the cubic spline interpolation is incapable of resolving intra-month fluctuations (Fig. 2b). For example, the raw daily normals clearly indicate the presence of a local minimum in late July, a feature that is captured by the constrained harmonic fit, yet the cubic spline interpolation increases monotonically from June through August.

The raw daily tmax normal curve for Beaver City, NE (Fig. 3) exhibits strong continentality, in sharp contrast to the much narrower annual range of tmax in coastal California as seen in Salinas. The raw daily normals are noticeably warmer (~2.5°F; ~1.4°C) than the cubic

VISIT THE SCIENTIFIC PUBLICATIONS REPORT ARCHIVE

spline interpolation or the constrained harmonic fit, as the monthly homogenization procedure had the net effect of lowering the monthly tmax values for Beaver City (in contrast to Reno tmin; Fig. 1). The constrained harmonic fit is shifted toward cooler tmax values to accommodate this, whereas the cubic spline interpolation is simply fit through the cooler homogenized normals. The two methods result in daily temperature normals that differ by as much as +/-1.5°F (+/-0.8°C) for specific days, particularly in the warmest and coldest months, although the annual means differ by less than 0.1°F (0.06°C).

Consider how the cubic spline interpolation performs in December for Beaver City tmax. The December tmax normal is 40.8°F (4.9°C), and the average of the constrained harmonic fit values for December is also 40.8°F (4.9°C) given the hard constraint. The cubic spline interpolation is anchored at 40.8°F (4.9°C) on December 16th (the middle of the month), but early December values range from 41-46°F (5.0-7.8°C) whereas late December values bottom out near 40°F (4.4°C). As a result, the mean of the cubic spline interpolation for December is over 0.7°F (0.4°C) warmer than the December normal (see inset in Fig. 3). This highlights the inability of the cubic spline interpolation to preserve the homogenized monthly mean. This leads the cubic spline interpolation to underestimate peaks in summer and overestimate minima in winter, resulting in a slight underestimation of total variance with respect to the raw daily normals as well as the constrained harmonic fit approach, which does not result in lowered total variance (not shown).

Overall, the mean differences between the constrained harmonic fit and the cubic spline interpolation results for the 2,041 stations considered is essentially zero for both tmax and tmin. However, individual values can vary to some degree, as seen in Figs. 2 and 3. The average absolute difference between the two approaches is 0.3°F (0.2°C) for both tmax and tmin. In

VISIT THE SCIENTIFIC PUBLICATIONS REPORT ARCHIVE

terms of maintaining consistency between the monthly temperature normals and the resulting daily temperature normals, the constrained harmonic fit approach with (M=6) has zero discrepancy, by design, for all station-months. For both tmax and tmin, the spline fit interpolation is typically off by 0.2°F (0.1°C) in an absolute sense from maintaining consistency, and the discrepancy can be as high as 1.0°F (0.6°C). As intimated by Fig. 3, the largest inconsistencies tend to occur in summer and winter months near the maxima and minima for the year.

An alternative to these methods is to apply a low-pass filter to the raw daily normals, such as successive passes of the 1-2-1 filter (see von Storch and Zwiers 1999). However, this simple approach cannot guarantee preservation of the mean. Further, low-pass filtering typically results in reduced variance (e.g., see Arguez et al. 2008), which can lead to severe underestimation and overestimation of highs and lows, respectively.

Other potential options involve a multi-step approach. For example, one could pass the monthly adjustments down to either the daily data or to the raw daily normals series (e.g., Vincent et al. 2002). Then, an unconstrained harmonic fit could be used to derive the daily temperature normals. Again, this method does not guarantee preservation of the monthly normals. Another approach is to compute the unconstrained harmonic fit of the raw daily normals, and then adjust the values in each month up or down to match the corresponding monthly normal. However, this introduces inter-month discontinuities, as seen when it is applied to the raw daily tmin normals for Hartford, CT (Fig. 4).

As stated earlier, the constrained harmonic fit does not preserve the mean monthly normals when less than 6 harmonics are used. Table 1 shows the root mean square errors (RMSEs) between the homogenized monthly normals and the monthly averages of the

VISIT THE SCIENTIFIC PUBLICATIONS REPORT ARCHIVE

constrained harmonic fit values for the four time series considered in this investigation, as a function of M, the number of harmonics used. For example, the M=1 case for Salinas tmax, which was displayed graphically in Fig. 2a, has an RMSE value of 1.69°F (0.9°C). The constraints in (3) ensure that RMSE will equal 0 for every month when $M \geq 6$, which is reflected in Table 1.

4. Summary

The constrained harmonic fit effectively smooths the raw daily normals without introducing discontinuities, and ensures preservation of the mean monthly normals. The cubic spline interpolation approach results in a smooth and continuous daily temperature normals curve. However, it does not always capture intra-seasonal fluctuations as seen in Fig. 2a, and it does not guarantee preservation of the mean monthly normals as documented in Fig. 3.

The constrained harmonic fit described here offers a one-step approach for computing daily temperature normals satisfying the four properties listed in the introduction. It is particularly useful when monthly temperatures are homogenized but the underlying daily data values are not. However, it also accommodates inherent inconsistencies between monthly and daily data caused by other factors, such as separate quality control of monthly and daily temperatures or the manner in which monthly temperature normals are computed. We recommend the constrained harmonic fit approach for computation of daily temperature normals when the underlying daily data are available and monthly temperature data are deemed to be of superior quality versus the daily data.

VISIT THE SCIENTIFIC PUBLICATIONS REPORT ARCHIVE

Acknowledgments

The authors kindly acknowledge I. Durre, R. Vose, M. Squires, X. Yin, J. Nielsen-Gammon, J. Christy, and J. Curtis for providing feedback on this approach. We also thank three anonymous reviewers for providing actionable feedback that helped strengthen the manuscript.

VISIT THE SCIENTIFIC PUBLICATIONS REPORT ARCHIVE

References

Arguez, A., P. Yu, and J. J. O'Brien, 2008: A new method for time series filtering near endpoints. Journal of Atmospheric and Oceanic Technology, 25, 534-546.

Arguez, A., I. Durre, S. Applequist, R. S. Vose, M. F. Squires, X. Yin, R. R. Heim, Jr., and T. W. Owen, 2012: NOAA's 1981-2010 U.S. Climate Normals: An Overview. In press, *Bulletin of the American Meteorological Society*.

Durre, I., M. J. Menne, B. E. Gleason, T. G. Houston, and R. S. Vose, 2010: Comprehensive automated quality assurance of daily surface observations. *Journal of Applied Meteorology and Climatology*, **8**, 1615-1633.

Easterling, D. R., and T. C. Peterson, 1995: A new method for detecting and adjusting for undocumented discontinuities in climatological time series. *International Journal of Climatology*, **15**, 369-377.

Guttman, N. B., and C. B. Baker, 1996: Exploratory analysis of the difference between temperature observations recorded by ASOS and conventional methods. *Bull. Amer. Meteor. Soc*., **77**, 2865–2873.

Kalman, D., 2009: Leveling with Lagrange: An Alternative View of Constrained Optimization. *Mathematics Magazine*, **82**, 186-196.

Menne, M. J., and C. N. Williams, Jr., 2009: Homogenization of Temperature Series via Pairwise Comparisons. *J. Clim*., **22,** 1700-1717.

Menne, M. J., C. N. Williams, Jr., and R. S. Vose, 2009: The United States Historical Climatology Network Monthly Temperature Data Version 2. *Bull. Amer. Meteor. Soc*., **90**, 993-1007.

VISIT THE SCIENTIFIC PUBLICATIONS REPORT ARCHIVE

Menne, M. J., Williams, C. N. Jr., and Palecki M. A., 2010: On the reliability of the U.S. surface temperature record. *J. Geophys. Res. Atmos.*, **115**, no. D11108, doi: 10.1029.

Menne, M. J., I. Durre, R. S. Vose, B. E. Gleason, and T. G. Houston, 2012: An overview of the Global Historical Climatology Network-Daily Database. *Journal of Atmospheric and Oceanic Technology*, **29**, 897-910.

Owen, T. W. and T. Whitehurst, 2002: United States climate normals for the 1971-2000 period: product descriptions and applications. *Preprints, Third Symposium on Environmental Applications: facilitating the use of environmental information, 13-17 January, Orlando, FL*, American Meteorological Society, Boston, MA, J27-J28.

Peterson, T. C., and D. R. Easterling, 1994: Creation of homogeneous composite climatological reference series. *International Journal of Climatology*, **14**, 671-679.

Vincent, L. A., X. Zhang, B. R. Bonsal, W.D. Hogg, 2002: Homogenization of daily temperatures over Canada. *Journal of Climate*, **15**, 1322-1334.

von Storch, H. and F. W. Zwiers, 1999: Statistical Analysis in Climate Research. Cambridge University Press, 484 pp.

Wilks, D.S., 2006. Statistical Methods in the Atmospheric Sciences, 2nd Ed. International Geophysics Series, Vol. 59, Academic Press, 627 pp.

VISIT THE SCIENTIFIC PUBLICATIONS REPORT ARCHIVE

Figure Captions

Figure 1. Raw daily averages of minimum temperatures for Reno, NV (light gray curve). Monthly averages computed from the raw daily averages are indicated by light gray squares. Homogenized monthly normals are indicated by black circles.

Figure 2. (a) Raw daily averages of maximum temperatures for Salinas, CA (light gray time series). The constrained harmonic fit for this time series is shown as a bold black curve. The dashed gray curve shows the cubic spline interpolation. The dotted black line indicates the (unconstrained) harmonic fit using only one harmonic. (b) As in (a) but for the June-August period. The black circles indicate the homogenized monthly normals.

Figure 3. As in Fig. 2 but for maximum temperatures in Beaver City, NE. December values are highlighted in the inset. The gray square indicates the average of the December values of the cubic spline interpolation, while the black circle indicates the homogenized December normal.

Figure 4. Raw daily averages of tmin for Hartford, CT for the October-December period (light gray time series). The constrained harmonic fit for this time series is shown as a solid black curve. The dark gray circles indicate an unconstrained harmonic fit (M=6) subsequently adjusted such that the average of the daily values in a month matches the corresponding, homogenized monthly normal.

VISIT THE SCIENTIFIC PUBLICATIONS REPORT ARCHIVE

Table 1. Root mean square errors (°F; °C) between the homogenized monthly normal and the average of the daily normals (per month) calculated using the constrained harmonic fit, as a function of *M*.

	M=1	M=2	M=3	M=4	M=5	M=6+
Reno, NV tmin	1.73 (0.96°C)	0.45 (0.25°C)	0.32 (0.18°C)	0.27 (0.15°C)	0.23 (0.13°C)	0.00
Salinas, CA tmax	1.69 (0.94°C)	0.71 (0.39°C)	0.27 (0.15°C)	0.14 (0.08°C)	0.02 (0.01°C)	0.00
Beaver City, NE tmax	2.03 (1.13°C)	0.82 (0.46°C)	0.58 (0.32°C)	0.41 (0.23°C)	0.19 (0.11°C)	0.00
Hartford, CT tmin	1.11 (0.62°C)	1.09 (0.61°C)	0.57 (0.32°C)	0.42 (0.23°C)	0.07 (0.04°C)	0.00

VISIT THE SCIENTIFIC PUBLICATIONS REPORT ARCHIVE

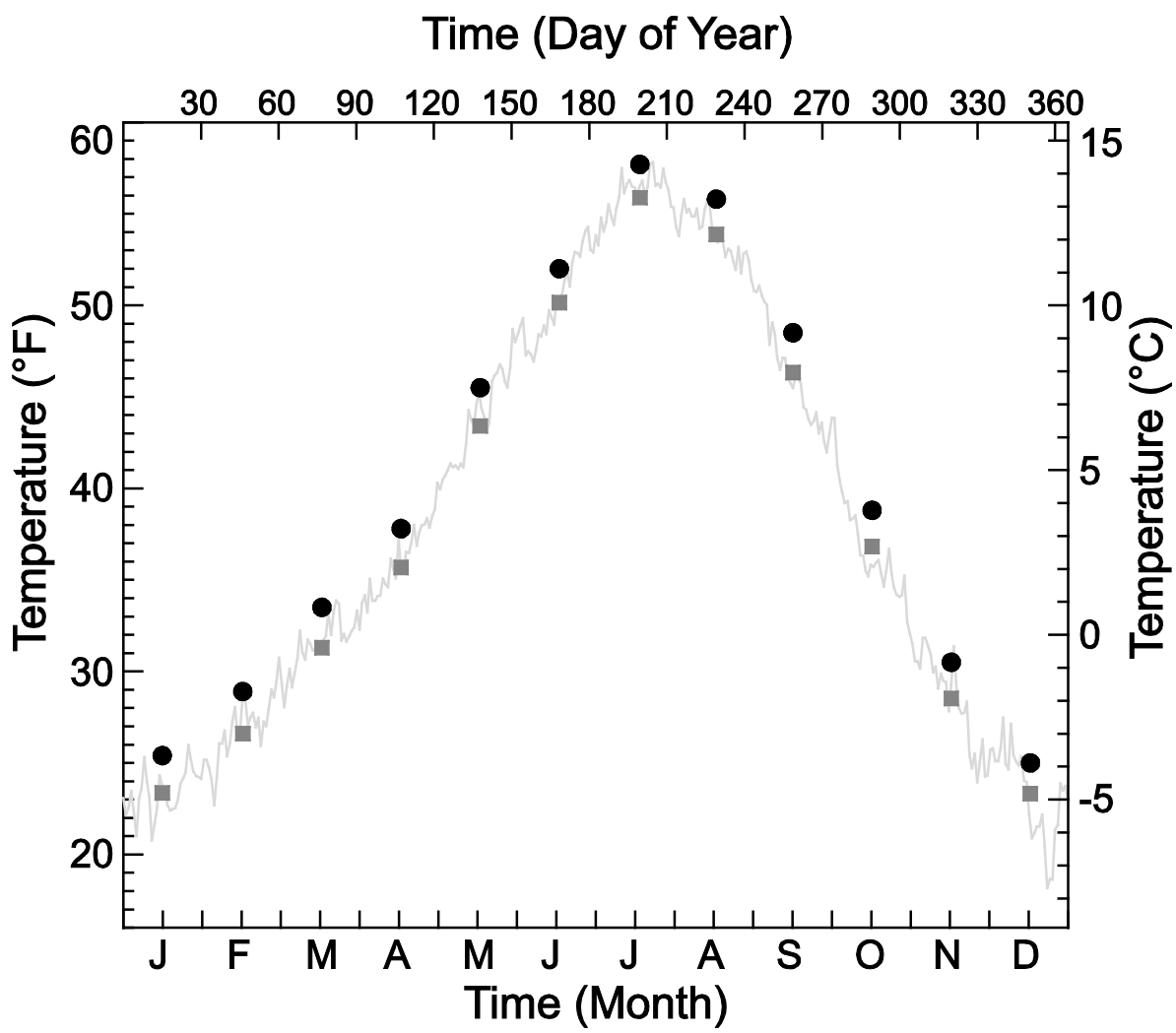

Figure 1. Raw daily averages of minimum temperatures for Reno, NV (light gray curve). Monthly averages computed from the raw daily averages are indicated by light gray squares. Homogenized monthly normals are indicated by black circles.

VISIT THE SCIENTIFIC PUBLICATIONS REPORT ARCHIVE

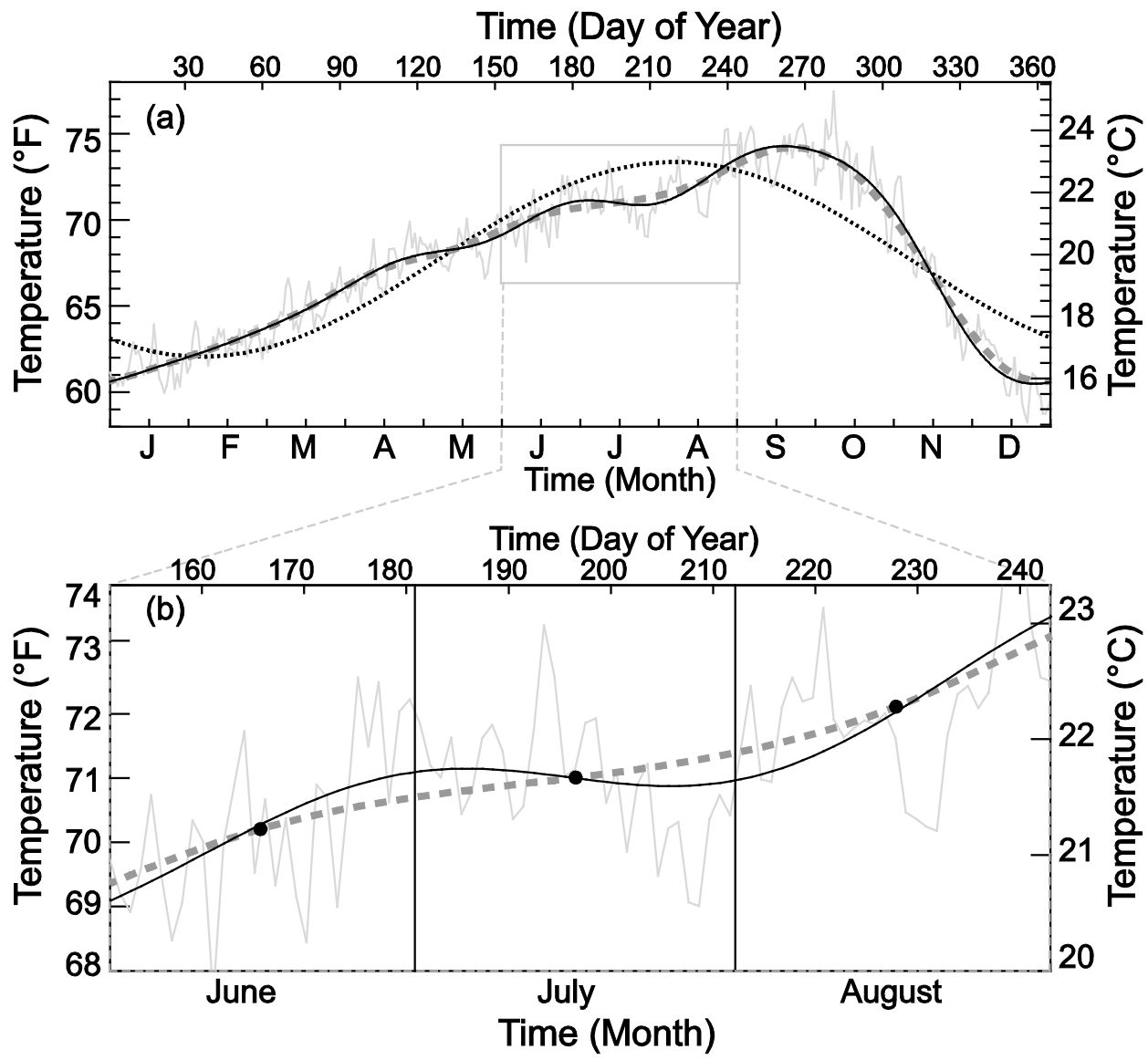

Figure 2. (a) Raw daily averages of maximum temperatures for Salinas, CA (light gray time series). The constrained harmonic fit for this time series is shown as a bold black curve. The dashed gray curve shows the cubic spline interpolation. The dotted black line indicates the (unconstrained) harmonic fit using only one harmonic. (b) As in (a) but for the June-August period. The black circles indicate the homogenized monthly normals.

VISIT THE SCIENTIFIC PUBLICATIONS REPORT ARCHIVE

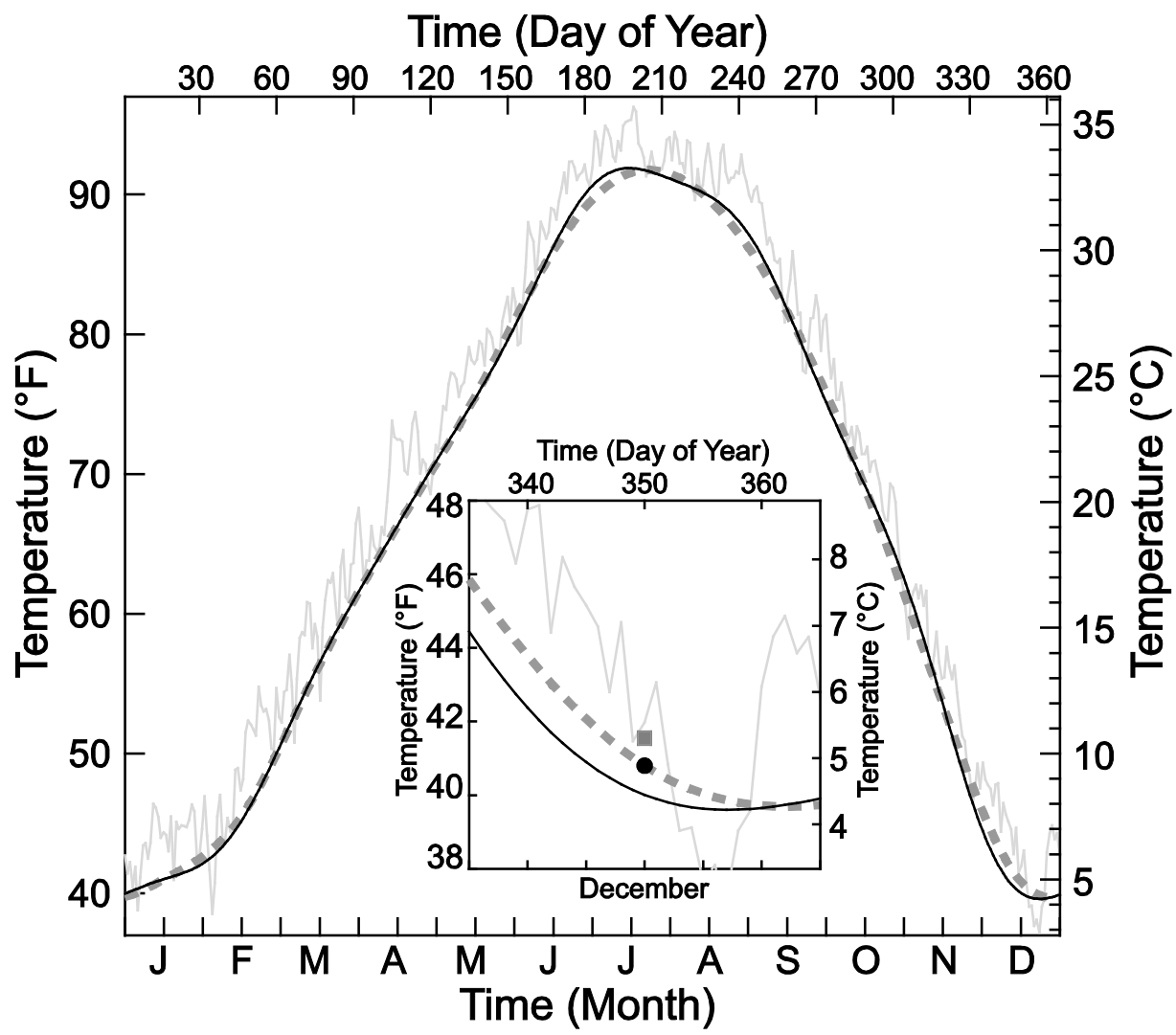

Figure 3. As in Fig. 2 but for maximum temperatures in Beaver City, NE. December values are highlighted in the inset. The gray square indicates the average of the December values of the cubic spline interpolation, while the black circle indicates the homogenized December normal.

VISIT THE SCIENTIFIC PUBLICATIONS REPORT ARCHIVE

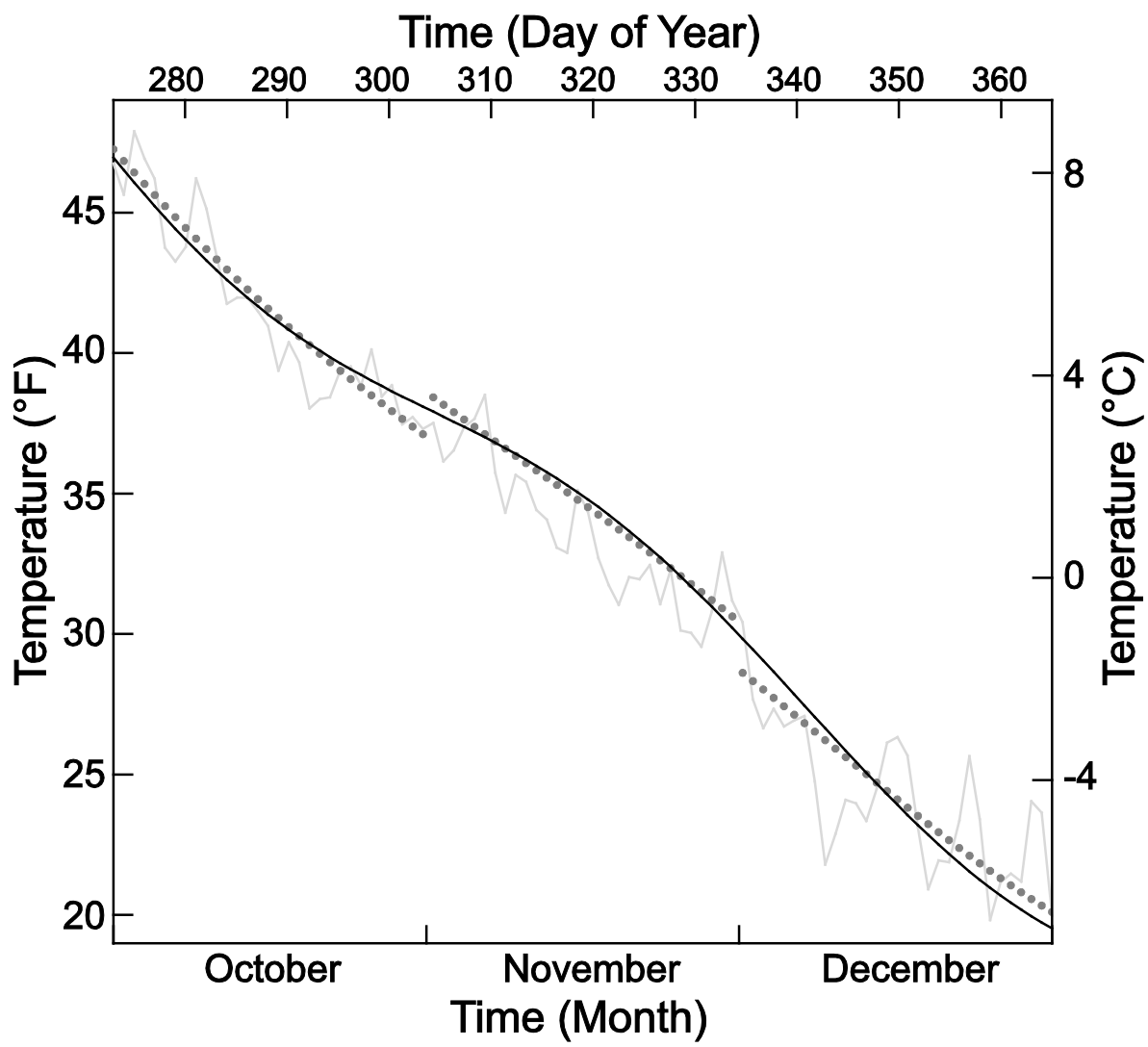

Figure 4. Raw daily averages of tmin for Hartford, CT for the October-December period (light gray time series). The constrained harmonic fit for this time series is shown as a solid black curve. The dark gray circles indicate an unconstrained harmonic fit (M=6) subsequently adjusted such that the average of the daily values in a month matches the corresponding, homogenized monthly normal.

VISIT THE SCIENTIFIC PUBLICATIONS REPORT ARCHIVE

Biogeosciences, 10, 839–849, 2013
www.biogeosciences.net/10/839/2013/
doi:10.5194/bg-10-839-2013
© Author(s) 2013. CC Attribution 3.0 License.

Biogeosciences
Open Access

Influence of terrestrial inputs on continental shelf carbon dioxide

L.-Q. Jiang[1,*], W.-J. Cai[1,], Y. Wang[1], and J. E. Bauer[2]**

[1]Department of Marine Sciences, The University of Georgia, Athens, Georgia 30602, USA
[2]Department of Evolution, Ecology, and Organismal Biology, The Ohio State University, Columbus, Ohio 43212, USA
[*]Present address: Cooperative Institute for Climate and Satellites, Earth System Science Interdisciplinary Center, University of Maryland, College Park, Maryland 20740, USA
[**]Present address: School of Marine Science and Policy, University of Delaware, Newark, Delaware 19716, USA

Correspondence to: W.-J. Cai (wcai@udel.edu)

Received: 2 July 2012 – Published in Biogeosciences Discuss.: 27 July 2012
Revised: 6 December 2012 – Accepted: 19 December 2012 – Published: 7 February 2013

Abstract. The US South Atlantic Bight (SAB) is a low-latitude shallow continental shelf bordered landward by abundant salt marshes and rivers. Based on previously published data on sea surface partial pressure of carbon dioxide (pCO_2) and new dissolved inorganic carbon (DIC) and dissolved organic carbon (DOC) data, a model analysis is presented to identify and quantify the contributions of various terrestrial carbon inputs on SAB sea surface pCO_2. After removal of pCO_2 variations due to annual temperature variability and air–sea gas exchange from the in situ pCO_2, the temperature- and gas-exchange-corrected pCO_2 (TG-corrected pCO_2) is derived. Contributions from rivers, salt marshes, and the continental shelf to the TG-corrected pCO_2 are then calculated. Our findings demonstrate that although additions of CO_2 from within shelf waters (i.e., ΔpCO_2(shelf)) were the greatest of the three components and underwent the largest seasonal changes, ΔpCO_2(shelf) showed smaller onshore–offshore gradients than rivers and marshes. In contrast, CO_2 contributions from river (ΔpCO_2(river)) and salt marsh (ΔpCO_2(marsh)) components were greatest closest to the coast and decreased with distance offshore. In addition, the magnitude of ΔpCO_2(marsh) was about three-fold greater than ΔpCO_2(river). Our findings also revealed that decomposition of terrestrial organic carbon was an important factor regulating the seasonal pattern of pCO_2 on the inner shelf. Despite large uncertainties, this study demonstrates the importance of terrestrial inputs, in particular those from coastal wetlands, on coastal ocean CO_2 distributions.

1 Introduction

Continental shelves play a key role in the global carbon cycle by linking terrestrial, marine and atmospheric systems (Mackenzie, 1991; Smith and Hollibaugh, 1993). Despite their relatively small size (∼ 7–8 % of the global ocean surface area), continental shelves sustain disproportionately high rates of primary production, remineralization, and organic carbon burial (Walsh, 1988; Wollast, 1993; Gattuso et al., 1998; de Hass et al., 2002). Recent studies have further shown that continental shelves are a globally important sink of atmospheric carbon dioxide (CO_2) (Borges et al., 2005; Cai et al., 2006; Chen and Borges, 2009).

The majority of continental shelves, in particular those that are both wide and aligned with a western boundary current, can be divided into two zones: the proximal (i.e., inner) shelf that is strongly impacted by land, and the distal (i.e., middle and outer) shelf that is influenced to a greater extent by open ocean waters (Rabouille et al., 2001). Relative to the distal shelf, the proximal shelf generally shows much steeper biogeochemical gradients owing to its proximity to inputs from land, including rivers, estuaries and salt marshes. Therefore, higher resolution surveys are warranted to understand the biogeochemical processes on the proximal shelf, although it has often been neglected in continental shelf CO_2 studies.

Continental shelves are strongly impacted by inputs of nutrients and organic and inorganic carbon from land (Thomas et al., 2004). As a result of nutrient inputs, proximal continental shelves typically sustain a relatively high level of biological productivity (Walsh, 1988; Wollast, 1993), which may draw down CO_2. However, this effect may be

Published by Copernicus Publications on behalf of the European Geosciences Union.

VISIT THE SCIENTIFIC PUBLICATIONS REPORT ARCHIVE

counteracted by enhanced heterotrophic activity supported by organic carbon input from land (Bauer and Bianchi, 2011; Bianchi and Bauer, 2011). In addition, direct inorganic carbon input from river waters plays an important role in enhancing pCO_2 of shelf waters (Raymond et al., 2000; Borges et al., 2006; Jiang et al., 2008b). Tidal exchange with intertidal marshes (Wang and Cai, 2004) and mangroves (Borges et al., 2003) may also raise pCO_2 in continental shelf waters. Understanding the roles of these different processes in driving carbon and CO_2 exchanges in shelf waters is critical for establishing both the relative contributions of each to coastal carbon budgets and for predicting future changes due to changes in climate, hydrology and coastal circulation.

In order to differentiate the various components contributing to shelf carbon and CO_2 sources and fluxes, we investigated the South Atlantic Bight (SAB) off the southeastern United States. The SAB is a low-latitude shallow continental shelf bordered landward by abundant salt marshes and river discharge and seaward by a major western boundary current, the Gulf Stream. This unique geographical location offers well-defined and distinct landward and seaward components. A recent study has shown that while the distal SAB shelf is an atmospheric CO_2 sink of $-1.3\,\mathrm{mol\,m^{-2}\,yr^{-1}}$, the proximal SAB shelf is a source of $1.2\,\mathrm{mol\,m^{-2}\,yr^{-1}}$ (Jiang et al., 2008a). The goal of this study is to differentiate and quantify the contributions of the annual temperature cycle, air–sea gas exchange, and inputs from rivers, salt marshes and within shelf waters to sea surface pCO_2 in this region. Evaluating the roles of these different drivers will contribute to the understanding of carbon dioxide dynamics in the coastal ocean. The present study is based on CO_2 data previously reported in Jiang et al. (2008a), and new dissolved inorganic carbon (DIC) and dissolved organic carbon (DOC) data from the same cruises.

2 Study site and methods

2.1 Site description

The SAB continental shelf has an average depth of only 30 m and is 50–75 m deep at the shelf break (Menzel, 1993). The Gulf Stream flows northward along the shelf break (Fig. 1). The shorelines of Georgia and South Carolina are characterized by extensive salt marshes ($3000\,\mathrm{km^2}$, Alexander et al., 1986). Tidal currents flood and drain intertidal salt marshes twice daily and transport materials between the marshes and the SAB (Hopkinson, 1985). Most rivers in this region are located in the central and northern part of the shelf. Discharge usually peaks in February–April, and a secondary peak may occur in fall, with a total annual discharge of about $66\,\mathrm{km^3}$ ($\sim 2.7\,\%$ of the SAB volume) (Menzel, 1993). Groundwater may also represent important additional inputs of water and other materials to the shelf waters (Moore, 2007 and references therein).

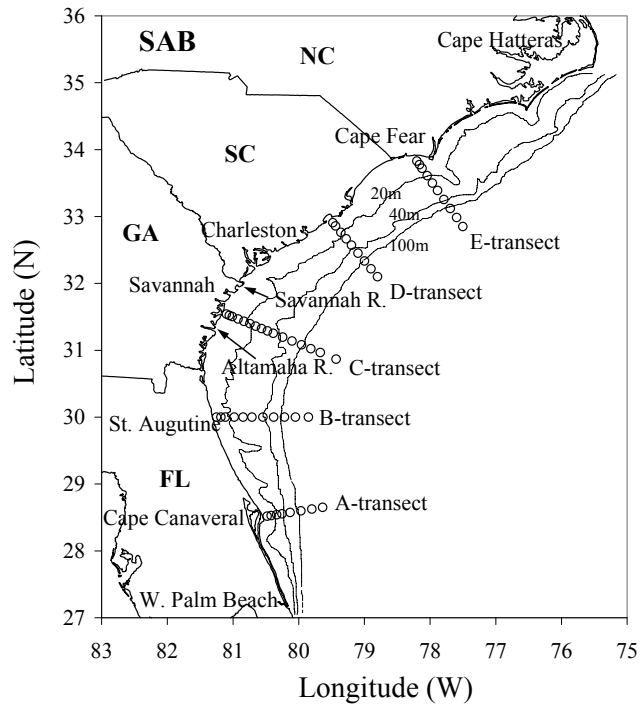

Fig. 1. Study area in the US South Atlantic Bight between Cape Lookout, North Carolina, and Cape Canaveral, Florida. Open circles indicate sampling stations, between the shoreline and extending to ~ 500 m water depth.

A coastal frontal zone (CFZ), formed by a pressure gradient induced by freshwater discharge, frequently occurs at 10–30 m isobaths, about 10–30 km offshore on the SAB shelf (Blanton, 1981). For simplicity, we refer to the shelf shoreward the CFZ as the proximal SAB (roughly equivalent to the inner shelf, as defined in Jiang et al., 2008a), and the shelf seaward the CFZ as the distal SAB (roughly equivalent to the middle and outer shelf).

The proximal SAB (inner shelf) is turbid as a result of material transport from rivers and exchange with intertidal salt marshes (Pomeroy et al., 2000). Primary production here is mainly driven by nutrients recycled in the water column (Dunstan and Atkinson, 1976; Hanson et al., 1990) and from sediments (Jahnke et al., 2005). On the distal SAB shelf (middle and outer shelf), water clarity increases dramatically, and the euphotic zone extends to the seafloor (Nelson et al., 1999). Production here is strongly influenced by intrusions induced by Gulf Stream frontal eddies (Atkinson et al., 1984).

2.2 Sampling

A whole-shelf survey consisting of five onshore–offshore transects (A-, B-, C-, D-, and E-transects from south to north, Fig. 1) was carried out in the SAB during six cruises: 5–16 January 2005, 19–30 March 2005,

VISIT THE SCIENTIFIC PUBLICATIONS REPORT ARCHIVE

27 July–5 August 2005, 7–17 October 2005, 16–21 December 2005, and 17–27 May 2006. Surface water pCO_2, temperature, salinity, and atmospheric pressure at sea level were measured while underway during all cruises (Jiang et al., 2008a). Dissolved inorganic carbon (DIC) was sampled on all five transects except for December 2005, when only E-, C-, and A-transects were covered. Dissolved organic carbon (DOC) samples were collected on D-, C-, and B-transects during January, March, and October 2005, and on all 5 transects during May 2006.

2.3 Sample analysis

DIC concentration was measured using an infrared CO_2 detector-based DIC analyzer with a precision of 0.1 % (Wang and Cai, 2004; Huang et al., 2012). DOC samples collected during the cruises of March, July, and October 2005 were measured in the Radiocarbon Laboratory of the Virginia Institute of Marine Science (VIMS) using a Shimadzu TOC-5000A high-temperature Pt-catalyzed analyzer with a mean analytical error of 1.4 $\mu mol\,L^{-1}$ (DeAlteris, 2007). DOC samples from May 2006 were analyzed in W. L. Miller's lab (University of Georgia) using a Shimadzu TOC-VCPN analyzer. Reference standards (deep Sargasso Sea seawater from D. A. Hansell's group at the University of Miami) and blanks (Milli-Q water) were analyzed every five samples to check accuracy and baseline stability and agreed within measurement error in both labs.

2.4 Calculation of temperature- and gas-exchange-corrected pCO_2

In situ pCO_2 often does not provide direct information about underlying biogeochemical processes, due to the fact that it is strongly impacted by temperature and air–sea gas exchange, as shown by Jiang et al. (2008a) in shallow coastal waters of SAB. Here we remove pCO_2 variations caused by the annual temperature cycle and air–sea gas exchange from the in situ pCO_2. The remaining pCO_2 is then assumed to be controlled primarily by biological activity and mixing. For simplicity, this temperature- and gas-exchange-corrected pCO_2 will be called TG-corrected pCO_2 hereafter, and can be calculated as

$$pCO_2(\text{TG-corrected})=pCO_2(\text{in situ})-[\Delta pCO_2(\text{temp})+\Delta pCO_2(\text{air-sea})], \quad (1)$$

where pCO_2 (TG-corrected) is the temperature- and gas-exchange-corrected sea surface pCO_2 (in µatm), pCO_2 (in situ) is the observed sea surface pCO_2, ΔpCO_2(temp) is the pCO_2 change caused by temperature deviation from the annual mean temperature, and ΔpCO_2(air-sea) is the pCO_2 change due to air–sea gas exchange (also referenced to the annual mean sea surface temperature, SST).

Water temperature changes pCO_2 both by shifting the inorganic carbon equilibrium and by altering solubility. Assuming other parameters are constant, pCO_2 in water increases with increasing water temperature. The in situ pCO_2 can be referenced to a constant temperature using the equation of Takahashi et al. (1993, 2002):

$$pCO_2(\overline{SST})=pCO_2(\text{in situ})\times\exp[0.0423\times(\overline{SST}-SST)], \quad (2)$$

where $\overline{SST}$ is the annual mean SST, and $pCO_2(\overline{SST})$ is the pCO_2 referenced to the annual mean SST. Once $pCO_2(\overline{SST})$ is calculated, the pCO_2 change due to the temperature deviation from the annual mean SST is then calculated as

$$\Delta pCO_2(\text{temp})=pCO_2(\text{in situ})-pCO_2(\overline{SST}). \quad (3)$$

It should be noted that the pCO_2 change due to temperature deviation from the annual mean SST is relative to the temperature used for the calculation.

Because aqueous CO_2 dissociates in water, the pCO_2 change due to air–sea gas exchange cannot be estimated based on linear dilution of CO_2 itself. Instead, it is calculated from changes in DIC and alkalinity (Riebesell et al., 2010). To that end, first, carbonate alkalinity (CA) is calculated from pCO_2 and DIC at in situ temperature and salinity and then is held constant during the gas exchange process. Assuming the surface mixed layer in the SAB extends to the seafloor in all sampling months (as is the case for most of the cruises except July 2005), the DIC concentration prior to air–sea gas exchange (in $mmol\,m^{-3}$) can be calculated as

$$DIC_{prior}=\frac{DIC(\text{per area})_{\text{in situ}}-\Delta DIC(\text{air-sea})}{\text{Depth}}. \quad (4)$$

Here, $DIC(\text{per area})_{\text{in situ}}$ is the integrated DIC in the water column, and ΔDIC(air-sea) is the amount of DIC gain or loss caused by air–sea gas exchange (both in $mmol\,m^{-2}$). Positive ΔDIC(air-sea) values indicate addition of CO_2 to seawater through air–sea gas exchange. As a first-order approximation, a 30-day air–sea gas exchange time was used to calculate the ΔDIC(air-sea), as mean residence time of the entire SAB is 30–90 days (Atkinson et al., 1978; Moore, 2007). Additional information about how air–sea CO_2 fluxes were calculated can be found in Jiang et al. (2008a). Once DIC_{prior} is calculated, $pCO_2(\overline{SST})_{prior}$ (pCO_2 before air–sea gas exchange at the annual mean temperature) can be calculated from DIC_{prior} and CA at the annual mean temperature and the in situ salinity. ΔpCO_2(air-sea) can then be calculated as the difference between $pCO_2(\overline{SST})$ and $pCO_2(\overline{SST})_{prior}$.

After both ΔpCO_2(temp) and ΔpCO_2(air-sea) have been estimated, TG-corrected pCO_2 can be calculated from Eq. (1). As we can see, if ΔpCO_2(temp) in Eq. (1) is substituted with the right-hand side of Eq. (3), the following is derived:

$$pCO_2(\text{TG}-\text{corrected})=pCO_2(\overline{SST})-\Delta pCO_2(\text{air-sea}). \quad (5)$$

VISIT THE SCIENTIFIC PUBLICATIONS REPORT ARCHIVE

Thus, in addition to the definition given in Eq. (1), pCO_2 (TG-corrected) may also be expressed as temperature-referenced pCO_2 corrected by the pCO_2 change due to air–sea gas exchange.

2.5 pCO_2 from river, marsh, and within-shelf sources

Contributions of pCO_2 (TG-corrected) can be divided into three components: ΔpCO_2(river), the pCO_2 change due to river inputs; ΔpCO_2(marsh), the pCO_2 change due to salt marsh inputs; and ΔpCO_2(shelf), the pCO_2 change due to biological activity and other processes on the shelf. ΔpCO_2(river), ΔpCO_2(marsh), and ΔpCO_2(shelf) can be calculated by the following equations (Fig. 2):

$$\Delta pCO_2(\text{river}) = pCO_{2_R} - pCO_{2_{base}} \quad (6)$$

$$\Delta pCO_2(\text{marsh}) = pCO_{2_{R+M}} - pCO_{2_R} \quad (7)$$

$$\Delta pCO_2(\text{shelf}) = pCO_2(\text{TG-corrected}) - pCO_{2_{R+M}}, \quad (8)$$

where pCO_2(base) is the pCO_2 if the oceanic end-member is only diluted by freshwater that contains no DIC. pCO_2(base) can be calculated from its corresponding DIC_{base} and TA_{base} that are calculated based on linear mixing of the open ocean end-members with the zero DIC and TA freshwater end-members (Fig. 2). pCO_{2_R} is the pCO_2 if the ocean end-member is only mixed with the river end-member. Similarly, pCO_{2_R} can be calculated from its corresponding DIC_R and TA_R (Fig. 2). $pCO_{2_{R+M}}$ is the pCO_2 if the ocean end-member is only mixed with the nearshore end-member, which contains inputs from both the river and marsh. Again, $pCO_{2_{R+M}}$ can be estimated from its corresponding DIC_{R+M} and TA_{R+M} using the same method (Fig. 2).

Table 1 shows the end-members used for the calculation. The river end-members were collected from Altamaha River (JayCee Landing in Jesup, Georgia, 31°67′ N, 81°85′ W). Earlier studies have shown that Altamaha River provides a good representation of the river end-members in the South Atlantic Bight (Cai and Wang, 1998; Cai et al., 2010). The nearshore and open ocean end-members were chosen as the most nearshore and offshore stations of the central transect, respectively (Table 1).

The above method has been demonstrated to work well in estuaries (Jiang et al., 2008b). However, unlike estuaries, where mixing occurs between two end-members in a restricted area, the mixing processes on the continental shelf are far more complicated (Menzel, 1993). Mixing here occurs in both cross-shelf and along-shelf directions, and is complicated by the existence of the coastal frontal zone. These complex mixing processes make it challenging to choose which specific nearshore end-members to use. As a result, the selection of nearshore end-members could cause uncertainties in the estimated ΔpCO_2(marsh) and ΔpCO_2(shelf). In addition, the nearshore end-members are not temporally stable relative to the residence time of the shelf, because primary production and respiration in the nearshore areas are highest and show the largest seasonal variation of the entire shelf (Griffith et al., 1990; Verity et al., 1993; Cai, unpublished data). This again will bring about large uncertainties (Loder and Reichard, 1981).

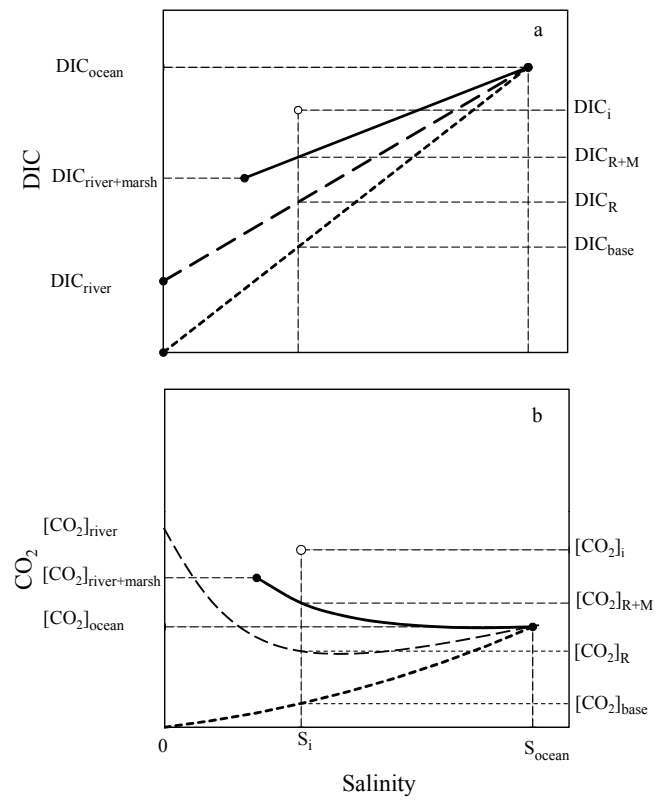

Fig. 2. Conceptual diagrams showing DIC and dissolved CO_2 concentrations during continental shelf mixing. **(a)** DIC concentration vs. salinity. On the x-axis, S_i and S_{ocean} are the salinities of station i and the ocean end-member, respectively. On the y-axis, DIC_{ocean}, $DIC_{river+marsh}$ and DIC_{river} are DIC concentrations of the oceanic end-member, nearshore end-member (containing DIC from both the river and marsh), and the river end-member, respectively. On the right side, DIC_i is the in situ DIC concentration, and DIC_{R+M}, DIC_R, and DIC_{base} are the DIC concentrations at the salinity of S_i assuming the ocean end-member is mixed only with the nearshore end-member (containing DIC from both the river and marsh), the river end-member, and zero-DIC freshwater end-member, respectively. **(b)** Dissolved CO_2 concentrations vs. salinity. The corresponding pCO_2 can be calculated according to $pCO_2 = k_H \cdot (CO_2)$, where k_H is Henry's constant.

VISIT THE SCIENTIFIC PUBLICATIONS REPORT ARCHIVE

Table 1. River, nearshore and open ocean end-members used in calculations described in Sect. 2.5. DIC and TA designate dissolved inorganic carbon and total alkalinity, respectively, with nits of μmol kg^{-1}.

Month	River end-member			Nearshore end-member			Open ocean end-member		
	Salinity	DIC	TA	Salinity	DIC	TA	Salinity	DIC	TA
Jan 2005	0.0	560.0	479.3	31.8	1943.2	2194.1	36.5	2040.0	2414.2
Mar 2005	0.0	498.0	473.1	30.7	1896.3	2104.4	36.3	2077.3	2407.5
May 2006	0.0	727.6	753.2	33.2	2019.8	2356.4	36.5	2070.3	2495.3
Jul 2005	0.0	527.2	414.3	31.2	1994.6	2235.0	35.9	2016.5	2393.8
Oct 2005	0.0	894.9	842.0	28.7	1908.9	2103.1	36.0	1985.4	2398.0

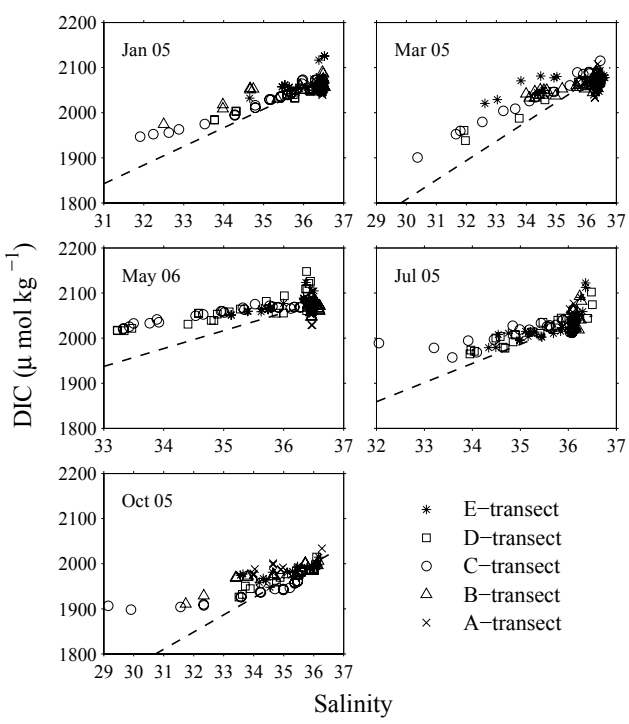

Fig. 3. Dissolved inorganic carbon (DIC) concentrations at depths shallower than 100 m vs. salinity and grouped by sampling month. The dotted lines connect the river and ocean end-members.

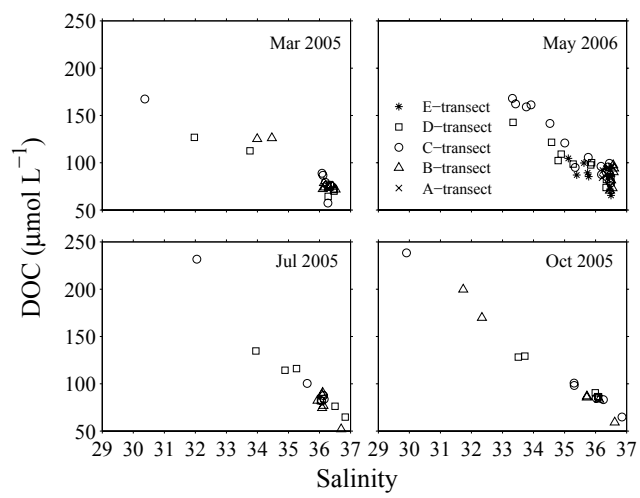

Fig. 4. Surface water dissolved organic carbon (DOC) vs. salinity in March, July, and October 2005 in the South Atlantic Bight.

3 Results

3.1 Dissolved inorganic carbon

DIC concentrations in the SAB (i.e., < 100 m water depth) ranged from 1900 to 2100 μmol kg^{-1} (Fig. 3). In all sampling months, DIC was lowest close to the coast and increased towards the shelf break. Nearshore DIC showed the largest seasonal variation, and was lowest in March and October 2005 when the shelf received the greatest amount of freshwater discharge. In comparison, DIC at the ocean end-member was relatively invariant with season. The nearshore DIC concentrations were higher than predicted from the conservative mixing line up to a salinity of 34 (Fig. 3).

3.2 Dissolved organic carbon

DOC concentrations in the SAB were negatively correlated with salinity (Fig. 4), indicating inputs of organic carbon from low salinity rivers and terrestrial sources. Spatially, the highest DOC concentrations occurred in the center (alongshore) of the inner shelf (160–170 μmol L^{-1} in March 2005 and May 2006, and 230–240 μmol L^{-1} in July and October 2005). Surface water DOC beyond the CFZ was much lower at 70–100 μmol L^{-1}. In July 2005 unusually high DOC concentrations were observed in the outer SAB (134 μmol L^{-1}) off South Carolina where low salinity waters were observed (see Fig. 3, Jiang et al., 2008a).

3.3 Impact of temperature on sea surface pCO_2

The annual temperature cycle throughout the SAB shelf resulted in lower pCO_2 in winter and spring, and higher pCO_2 in summer (Fig. 5). Area-averaged in situ pCO_2 was undersaturated across the entire shelf during winter and spring, and increased into the summer months (Fig. 5). From May to October the shelf became super-saturated, with the inner shelf showing the highest pCO_2. The magnitude of ΔpCO_2(temp)

VISIT THE SCIENTIFIC PUBLICATIONS REPORT ARCHIVE

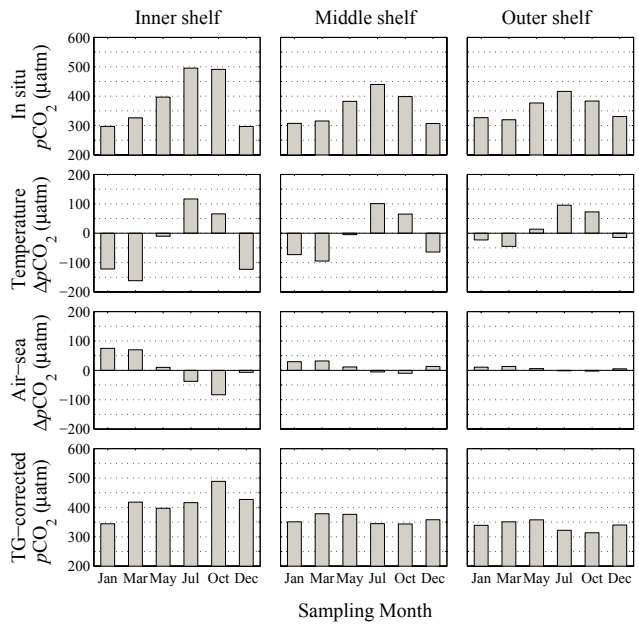

Fig. 5. Seasonal changes of area-averaged sea surface pCO_2, pCO_2 variations due to temperature deviation from the annual mean temperature (23.11 °C), pCO_2 variations due to air–sea gas exchange, and TG-corrected pCO_2 on the SAB. In situ pCO_2 is the sum of pCO_2 variations due to temperature, pCO_2 variations due to air–sea gas exchange, and TG-corrected pCO_2 (see Eq. 1 in text).

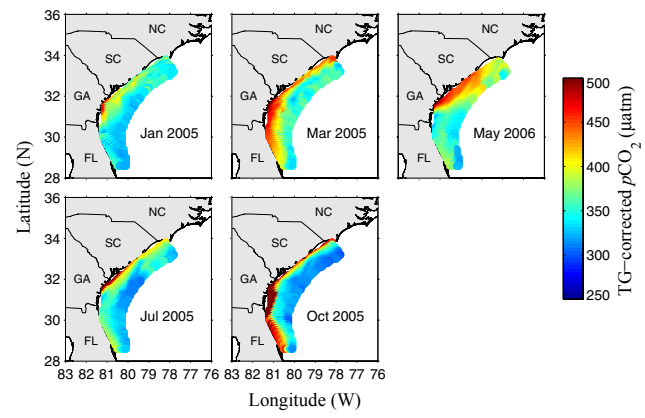

Fig. 6. Spatial distributions of surface water TG-corrected pCO_2 in the South Atlantic Bight in all sampling months except December 2005. Due to a lack of DIC data, spatial distribution of TG-corrected pCO_2 in December 2005 is not presented. The colored contours are from triangle-based liner interpolation.

on the inner shelf was larger than that on the outer shelf, partly due to the greater seasonal range of SST on the proximal SAB shelf (10–30 °C) compared with the distal SAB shelf (20–30 °C) (Jiang et al., 2008a).

3.4 Impact of air–sea gas exchange on sea surface pCO_2

Air–sea gas exchange had the net effect of modulating the seasonal changes of pCO_2 in the SAB. It increased pCO_2 in winter when sea surface pCO_2 was under-saturated and decreased it in summer when pCO_2 was supersaturated (Fig. 5). However, while air–sea gas exchange played an important role in changing pCO_2 on inner shelf, greater water depths and consequently greater integrated DIC inventory in the mixed layer on the outer shelf made air–sea gas exchange insignificant in controlling the pCO_2 there (Fig. 5).

3.5 TG-corrected pCO_2

During warm months (July and October 2005), when sea surface temperature (see Fig. 2 in Jiang et al., 2008a) was homogeneous over the entire SAB continental shelf, surface water TG-corrected pCO_2 (Fig. 6) showed similar spatial distributions as in situ pCO_2 (see Fig. 4 in Jiang et al., 2008a). Both were highest close to the coast and decreased with distance offshore. During winter (January, March, and December 2005), while TG-corrected pCO_2 was still higher close to the coast than offshore, the trend was reversed for the in situ pCO_2 (see Fig. 4 in Jiang et al., 2008a). The contrasting spatial variations in winter were due to the large onshore–offshore temperature gradients at this time of the year (SST in winter was ∼ 10–14 °C close to the coast and increased to 20–25 °C at the shelf break; Jiang et al., 2008a).

The area-averaged TG-corrected pCO_2 on the middle and outer shelf showed similar seasonal variation, i.e., increasing from January to March, leveling off in May, decreasing in July and October, and then increasing again in December (Fig. 5). On the inner shelf, the area-averaged TG-corrected pCO_2 was lowest in January, and showed the largest increase in March and October (Fig. 5) when the shelf experienced the greatest river discharges.

3.6 ΔpCO_2(river), ΔpCO_2(marsh), and ΔpCO_2(shelf)

As expected, contributions of CO_2 from rivers (ΔpCO_2(river)) were highest close to the coast and decreased with distance offshore (Fig. 7). During January and March 2005, ΔpCO_2(river) was up to 30 µatm on the inner shelf but averaged only 0–3 µatm on the outer shelf. Seasonally, ΔpCO_2(river) was highest in January, March, and October 2005 (Fig. 8). Contributions of CO_2 from salt marshes (ΔpCO_2(marsh)) showed similar spatial and seasonal distributions as ΔpCO_2(river), with the magnitude of ΔpCO_2(marsh) being about three times as high as that of ΔpCO_2(river) (Figs. 8 and 9). Contributions of CO_2 from within shelf waters (ΔpCO_2(shelf)) were highest of the three components (Figs. 8 and 10). Compared with ΔpCO_2(river) and ΔpCO_2(marsh), ΔpCO_2(shelf) showed much smaller onshore–offshore gradients in January and March 2005. Seasonally, ΔpCO_2(shelf) was highest in May 2006 and October 2005.

VISIT THE SCIENTIFIC PUBLICATIONS REPORT ARCHIVE

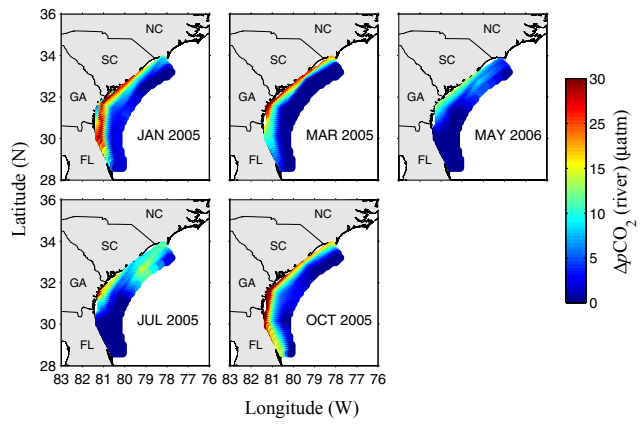

Fig. 7. Spatial distributions of ΔpCO_2(river), or the portion of sea surface pCO_2 that is due to inputs from the river (referenced to 23.11 °C). Due to a lack of DIC data, ΔpCO_2(river) in December 2005 is not presented. The colored contours are from triangle-based liner interpolation.

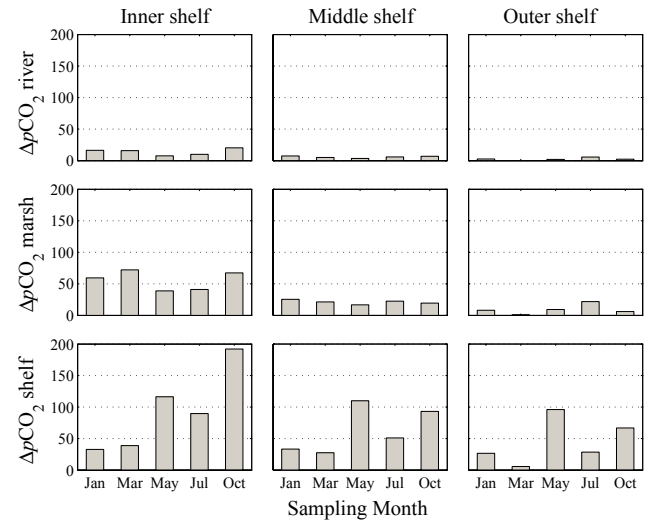

Fig. 8. Seasonal changes of area-averaged ΔpCO_2 (river), (referenced to 23.11 °C), ΔpCO_2(marsh), and ΔpCO_2(shelf).

4 Discussion

4.1 Carbon inputs from terrestrial sources

In addition to nutrients, continental shelves receive large amounts of organic and inorganic carbon from terrestrial sources. In the following discussion, "terrestrial" refers to all sources landward of the land/ocean boundary, including rivers, estuaries, salt marshes, groundwater, and other land-derived sources. Inputs of organic carbon can be readily seen from the seaward decreases of DOC concentrations (Fig. 4). In contrast to DOC, DIC transport on the shelf is less obvious. DIC on the continental shelf contains a large oceanic component that may mask the DIC signal from terrestrial sources. Therefore, seaward increases in DIC concentrations do not necessarily indicate that the shelf is transporting DIC landward (Fig. 3). To examine the DIC inputs from terrestrial sources (as well as net ecosystem metabolism, or NEM), total excess DIC ($DIC_{T\text{-excess}}$) was calculated according to Jiang et al. (2008b):

$$DIC_{T\text{-excess}} = DIC_i - \frac{S_i}{S_{ocean}} \times DIC_{ocean} \quad (9)$$

in $\mu mol\,kg^{-1}$ or $mmol\,m^{-3}$, where DIC_i and DIC_{ocean} are DIC concentrations of station i and the ocean end-member, respectively, and S_i and S_{ocean} are salinities of station i and the ocean end-member, respectively. The second term on the right-hand side of Eq. (9) ($\frac{S_i}{S_{ocean}} \times DIC_{ocean}$) represents the oceanic DIC component. Total excess DIC defined here represents all DIC sources or sinks (e.g., all terrestrial inputs as well as NEM on the shelf) except those from the open ocean.

The calculated total excess DIC was highest on the central part (alongshore) of the inner shelf (140–180 $\mu mol\,kg^{-1}$) and lowest on the outer shelf (−10 to 50 $\mu mol\,kg^{-1}$) (Fig. 11). Like DOC, the total excess DIC shows negative correlation with salinity in all sampling months, suggesting input of DIC from terrestrial sources (Fig. 11). Similarly, excess DOC was also calculated. Not surprisingly, excess DOC was also highest on the inner shelf and decreased with distance offshore (Fig. 12).

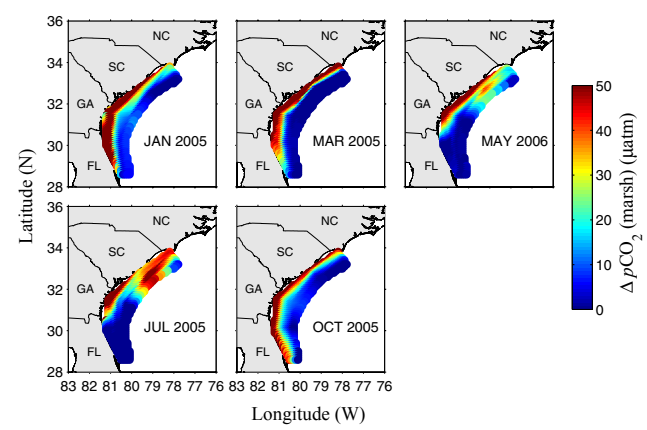

Fig. 9. Spatial distributions of ΔpCO_2(marsh) (referenced to 23.11 °C). Due to a lack of DIC data, ΔpCO_2(marsh) in December 2005 is not presented. The colored contours are from triangle-based liner interpolation.

4.2 Impact of terrestrial carbon on continental shelf CO_2

Even though the contribution of DIC from terrestrial sources is usually much smaller when compared with that from the open ocean, a larger proportion of the terrestrial DIC exists in the form of aqueous CO_2. As a result, the input of terrestrial DIC plays a critical role in elevating CO_2 concentrations in continental shelf waters. Terrestrial sources increase

VISIT THE SCIENTIFIC PUBLICATIONS REPORT ARCHIVE

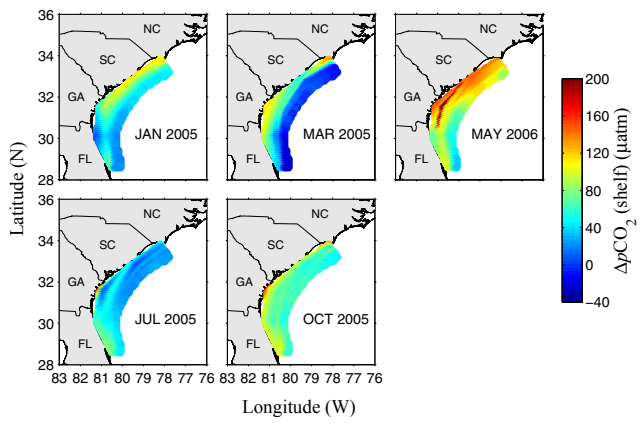

Fig. 10. Spatial distributions of ΔpCO_2(shelf) (referenced to 23.11 °C). Due to a lack of DIC data, ΔpCO_2(shelf) in December 2005 is not presented. The colored contours are from triangle-based liner interpolation.

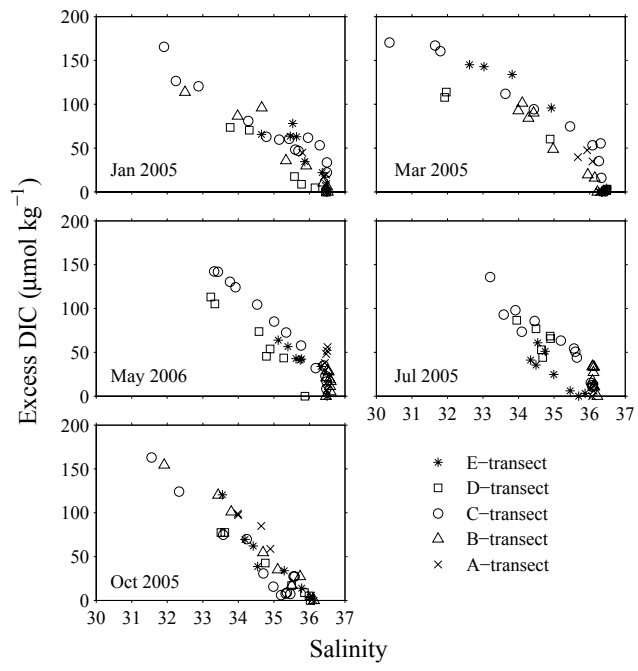

Fig. 11. Surface water total excess DIC (in excess of DIC from oceanic sources) plotted against salinity in January, March, July, October 2005 and May 2006 in the South Atlantic Bight. Due to lack of data, total excess DIC in December 2005 was not calculated.

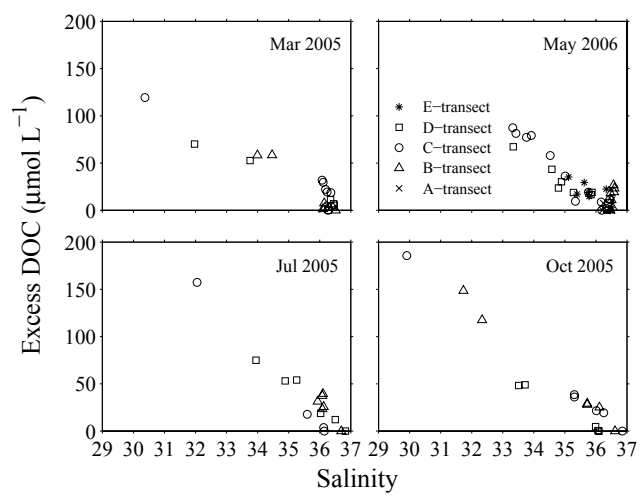

Fig. 12. Surface water excess DOC (i.e., DOC in excess of that from oceanic sources) vs. salinity in March, July, October 2005 and May 2006 in the South Atlantic Bight. Due to a lack of data, excess DOC in January and December 2005 was not calculated.

nearshore pCO_2 directly through input of inorganic carbon from rivers (Cai and Wang, 1998; Cai et al., 1999; Jiang et al., 2008b) and salt marshes (Wang and Cai, 2004), and indirectly by input of organic carbon (Moran et al., 1991; Alberts and Takács, 1999; DeAlteris, 2007) that is later remineralized to varying extents on the shelf as part of the shelf NEM.

Rivers discharging to the SAB enhance pCO_2 in shelf waters by delivering freshwater with high CO_2 concentrations that arise ultimately from microbial decomposition of organic matter in soils, river waters, and sediments (Jones and Mulholland, 1998; Neal et al., 1998; Cole and Caraco, 2001). Studies of the Altamaha and Satilla river estuaries have shown that rivers discharging to the SAB are highly supersaturated with respect to atmospheric CO_2. During summer, surface water pCO_2 in these river-dominated estuaries is as high as $\sim$4000 µatm compared with only about $\sim$400–600 µatm on the continental shelf (Cai and Wang, 1998; Jiang et al., 2008b).

Salt marshes contribute to pCO_2 in the SAB by direct release of inorganic carbon to the shelf. An important feature of this region is the extensive areas of inter-tidal salt marshes (Pomeroy and Wiegert, 1981). The dominant primary producer in these marshes is *Spartina alterniflora*, which has among the highest primary productivity of any ecosystem ($\sim$1100 to 2250 gC m^{-2} yr^{-1}; Dai and Wiegert, 1996). CO_2 that is released to intertidal marsh sediments and waters by bacterial remineralization of *Spartina*-derived organic matter can be exported to coastal waters (Cai et al., 1999; Wang and Cai, 2004; Jiang et al., 2008b) via tidal flushing (Neubauer and Anderson, 2003) and drainage of sediment interstitial waters (Jahnke et al., 2003).

Rivers and salt marshes also transport significant amounts of organic carbon to the SAB (Fig. 12), the remineralization of which by microbes (Pomeroy et al., 2000; Jahnke et al., 2005) and photochemistry (Miller and Moran, 1997) in shelf waters and sediments will further increase the nearshore pCO_2. Previous studies have shown that most nutrients entering the SAB occur in organic form that must be remineralized before they may be taken up by phytoplankton (Dunstan and Atkinson, 1976; Hanson et al., 1990; DeAlteris, 2007). The potential importance of this pathway in enhancing pCO_2

VISIT THE SCIENTIFIC PUBLICATIONS REPORT ARCHIVE

on the proximal SAB is supported by the positive correlation between TG-corrected pCO_2 and excess DOC (figure not shown).

4.3 Seasonal changes of CO_2 inputs to the proximal SAB

Seasonally, CO_2 from the SAB rivers and salt marshes is largely related to river discharge rates, and greater amounts of CO_2 will be transported to the shelf at higher discharge rates (Borges et al., 2006; Jiang et al., 2008b). This can be seen from the higher ΔpCO_2(river) and ΔpCO_2(marsh) during January and March 2005 (high flow seasons, Jiang, 2009) than in May 2006 and July 2005 (low flow seasons) (Fig. 8).

Based on the findings from the present study, CO_2 production from within shelf waters (e.g., NEM), on the other hand, is predicted to be strongly dependent on temporal changes in organic matter remineralization and shelf water residence time. Respiration rates in the inner shelf have been shown to be nearly an order of magnitude higher in summer and fall than in winter and spring (Hopkinson, 1985; Griffith et al., 1990; Jiang et al., 2010). However, the additional CO_2 released from heterotrophic processes in summer may be counterbalanced by greater CO_2 uptake due to aquatic primary production at this time of the year (Verity et al., 2002). The results of ΔpCO_2(shelf) suggest that the shelf is more likely to be heterotrophic (i.e., net release of CO_2) during summer and fall (May 2006, July and October 2005), and relatively more autotrophic (i.e., net uptake of CO_2) during winter and spring (January and March 2005) (Fig. 8). This is confirmed by the δ^{13} values of DIC in the proximal SAB, which became increasingly depleted between spring and fall (DeAlteris, 2007). The relatively lower CO_2 production during July 2005 may be further related to a Gulf Stream intrusion, which increased biological production and counterbalanced the DIC production.

5 Conclusions

Analyses of the DIC, DOC, and pCO_2 data in the SAB demonstrate how temperature, air–sea gas exchange, and terrestrial inputs control sea surface pCO_2 on the continental shelf. Terrestrial sources increase the nearshore pCO_2 by direct input of inorganic carbon from rivers and salt marshes, and indirectly by input of organic carbon that is later remineralized in the SAB (i.e., shelf NEM). This mechanism is the most likely explanation for findings of the proximal SAB (inner shelf) being a source of atmospheric CO_2 ($+1.2\,\mathrm{mol\,m^2\,yr^{-1}}$), and the distal SAB (middle and outer shelf) being a sink of $-1.3\,\mathrm{mol\,m^2\,yr^{-1}}$ (Jiang et al., 2008a). In particular, decomposition of marsh- and river-derived organic carbon is the most important factor in maintaining the high pCO_2 on the inner shelf during the fall.

Acknowledgements. This work was supported by a National Science Foundation (NSF) grant (OCE-0425153) and a National Oceanic and Atmospheric Administration (NOAA) grant (NA050AR4311161) to W.-J. Cai, and by a NSF Chemical Oceanography Program grant (OCE-0327423) and a Integrated Carbon Cycle Research Program grant (EAR-0403949) to J. Bauer. Sampling was conducted on the R/V *Cape Hatteras* and R/V *F. G. Walton Smith*. We thank Jennifer DeAlteris, Cedric Fichot, and William L. Miller for DOC analysis. We benefited from the discussion with Rik Wanninkhof, Charles S. Hopkinson, and William L. Miller. We also want to thank G. Han for laboratory support; Heike Lüger, Feizhou Chen, Justin Hartmann, Xianghui Guo, and Longjun Zhang for help with data collection during some of the cruises. Comments from C. T. Arthur Chen and an anonymous reviewer were very helpful.

Edited by: M. Dai

References

Alberts, J. J. and Takács, M.: Importance of humic substances for carbon and nitrogen transport into southeastern United States estuaries, Organic Geochem., 30, 385–395, 1999.

Alexander, C. E., Broutman, M. A., and Field, D. W.: An Inventory of Coastal Wetlands of the USA, NOAA, US Department of Commerce, Washington, DC, 1986.

Atkinson, L. P., Blanton, J. O., and Haines, E.: Shelf flushing rates based on the distribution of salinity and freshwater in the Georgia Bight, Estuar. Coast. Shelf S., 7, 465–472, 1978.

Atkinson, L. P., Yoder, J. A., and Lee, T. N.: Review of upwelling off the southeastern United States and its effect on continental-shelf nutrient concentrations and primary productivity, Rapp. P.-v. Cons. Int. Explor. Mer, 183, 70–78, 1984.

Bauer, J. E. and Bianchi, T. S.: Dissolved Organic Carbon Cycling and Transformation, in: Treatise on Estuarine and Coastal Science, edited by: Wolanski, E. and McLusky, D. S., Biogeochemistry, 5, 7–67, Waltham, Academic Press, 2011.

Bianchi, T. S. and Bauer, J. E.: Particulate Organic Carbon Cycling and Transformation, in: Treatise on Estuarine and Coastal Science, edited by: Wolanski, E. and McLusky, D. S., Biogeochemistry, 5, 69–117, Waltham, Academic Press, 2011.

Blanton, J. O.: Ocean currents along a nearshore frontal zone on the continental shelf of the southeastern United States, J. Phys. Oceanogr., 11, 1627–1637, 1981.

Borges, A. V., Djenidi, S., Lacrois, G., Théate, J.-M., Delille, B., and Frankignoulle, M.: Atmospheric CO_2 flux from mangrove surrounding waters, Geophys. Res. Lett., 30, 1558, doi:10.1029/2003GL017143, 2003.

Borges, A. V., Delille, B., and Frankignoulle, M.: Budgeting sinks and sources of CO_2 in the coastal ocean: diversity of ecosystems counts, Geophys. Res. Lett., 32, doi:10.1029/2005GL023053, 2005.

Borges, A. V., Schiettecatte, L.-S., Abril, G., Delille, B., and Gazeau, F.: Carbon dioxide in European coastal waters, Estuar. Coast. Shelf S., 70, 375–387, 2006.

Cai, W.-J. and Wang, Y.: The chemistry, fluxes, and sources of carbon dioxide in the estuarine waters of the Satilla and Altamaha Rivers, Georgia, Limnol. Oceanogr., 43, 657–668, 1998.

VISIT THE SCIENTIFIC PUBLICATIONS REPORT ARCHIVE

Cai, W.-J., Pomeroy, L. R., Moran, M. A., and Wang, Y.: Oxygen and carbon dioxide mass balance for the estuarine-intertidal marshe complex of five rivers in the southeastern U.S., Limnol. Oceanogr., 44, 639–649, 1999.

Cai, W.-J., Dai, M., and Wang, Y.: Air-sea exchange of carbon dioxide in ocean margins: A province-based synthesis, Geophys. Res. Lett., 33, L12603, doi:10.1029/2006GL026219, 2006.

Cai, W.-J., Hu, X., Huang, W.-J., Jiang, L.-Q., Wang, Y., Peng, T. H., and Zhang, X.: Alkalinity distribution in the western North Atlantic Ocean margins, J. Geophys. Res., 115, C08014, doi:10.1029/2009JC005482, 2010.

Chen, C.-T. A. and Borges, A. V.: Reconciling opposing views on carbon cycling in the coastal ocean: continental shelves as sinks and near-shore ecosystems as sources of atmospheric CO_2, Deep-Sea Res. II, 56, 578–590, 2009.

Cole, J. J. and Caraco, N. F.: Carbon in catchments: connecting terrestrial carbon losses with aquatic metabolism, Mar. Freshwater Res., 52, 101–110, 2001.

Dai, T. and Wiegert, R. G.: Estimation of the primary productivity of Spartina alterniflora using a canopy model, Ecography, 19, 410–423, 1996.

de Hass, H., van Weering, T. C. E., and de Stigter, H.: Organic carbon in shelf seas: sinks or sources, processes and products, Cont. Shelf Res., 22, 691–717, 2002.

DeAlteris, J. A.: Elemental and isotopic characterization of organic matter and carbon in the South Atlantic Bight, College of William & Mary, Williamsburg, Virginia, 196 pp., 2007.

Dunstan, W. M. and Atkinson, L. P.: Sources of new nitrogen for the South Atlantic Bight, in: Estuarine Processes I, Uses, Stresses, and Adaptation to the Estuary, edited by: Wiley, M., Academic Press, New York, 69–78, 1976.

Gattuso, J.-P., Frankignoulle, M., and Wollast, R.: Carbon and carbonate metabolism in coastal aquatic ecosystems, Annu. Rev. Ecol. Syst., 29, 405–434, 1998.

Griffith, P. C., Douglas, D. J., and Wainright, S. C.: Metabolic activity of size-fractionated microbial plankton in estuarine, nearshore, and continental shelf waters of Georgia, Mar. Ecol.-Prog. Ser., 59, 263–270, 1990.

Hanson, R. B., Robertson, C. Y., Yoder, J. A., Verity, P. G., and Bishop, S. S.: Nitrogen recycling in coastal waters of southeastern U.S. during summer 1986, J. Mar. Res., 48, 641–660, 1990.

Hopkinson, C. S.: Shallow-water benthic and pelagic metabolism: evidence of heterotrophy in the nearshore Georgia Bight, Mar. Biol., 87, 19–32, 1985.

Huang, W.-J., Wang, Y., and Cai, W.-J.: Assessment of sample storage techniques for total alkalinity and dissolved inorganic carbon in seawater, Limnol. Oceanogr.-Meth., 10, 711–717, 2012.

Jahnke, R. A., Alexander, C. R., and Kostka, J. E.: Advective pore water input of nutrients to the Satilla River Estuary, Georgia, USA, Estuar. Coast. Shelf S., 56, 641–653, 2003.

Jahnke, R., Richards, M., Nelson, J., Robertson, C., Rao, A., and Jahnke, D.: Organic matter remineralization and porewater exchange rates in permeable South Atlantic Bight continental shelf sediments, Cont. Shelf Res., 25, 1433–1452, 2005.

Jiang, L.-Q.: Biogeochemical cycling of carbon dioxide in estuaries and the continental shelf of the southeastern United States, Ph.D, Marine Science, University of Georgia, Athens, 172 pp., 2009.

Jiang, L.-Q., Cai, W.-J., Wanninkhof, R., Wang, Y., and Lüger, H.: Air-sea CO_2 fluxes on the U.S. South Atlantic Bight: spatial and seasonal variability, J. Geophys. Res., 113, C07019, doi:10.1029/2007JC004366, 2008a.

Jiang, L.-Q., Cai, W.-J., and Wang, Y.: A comparative study of carbon dioxide degassing in river- and marine-dominated estuaries, Limnol. Oceanogr., 53, 2603–2615, 2008b.

Jiang, L.-Q., Cai, W.-J., Wang, Y., Diaz, J., Yager, P., and Hu, X.: Pelagic community respiration on the continental shelf off Georgia, USA, Biogeochemistry, 98, 101–113, 2010.

Jones, J. B. and Mulholland, P. J.: Carbon dioxide variation in a hardwood forest stream: an integrative measure of whole catchment soil respiration, Ecosystems, 1, 183–196, 1998.

Loder, T. C. and Reichard, R. P.: The dynamics of conservative mixing in estuaries, Estuaries, 4, 64–69, 1981.

Mackenzie, F. T.: What is the importance of ocean margin processes in Global Change, in: Phys. Ch. Ear., edited by: Mantoura, R. F. C., Martin, J.-M., and Wollast, R., John Wiley and Sons, N.Y., 433–454, 1991.

Menzel, D. W.: Ocean Processes: U. S. Southeast Continental Shelf, U.S. Department of Energy, 112 pp., 1993.

Miller, W. L., and Moran, M. A.: Interaction of photochemical and microbial processes in the degradation of refractory dissolved organic matter from a coastal marine environment, Limnol. Oceanogr., 42, 1317–1324, 1997.

Moore, W. S.: Seasonal distribution and flux of radium isotopes on the Southeastern U.S. Continental Shelf, J. Geophys. Res., 112, C10013, doi:10.1029/2007JC004199, 2007.

Moran, M. A., Pomeroy, L. R., Sheppard, E. S., Atkinson, L. P., and Hodson, R. E.: Distribution of terrestrial derived dissolved organic matter on the southeastern U.S. continental shelf, Limnol. Oceanogr., 36, 1134–1149, 1991.

Neal, C., House, W. A., Jarvie, H. P., and Eartherall, A.: The significance of dissolved carbon dioxide in major lowland rivers entering the North Sea, Sci. Total Environ., 210–211, 187–203, 1998.

Nelson, J. R., Eckman, J. E., Robertson, C. Y., Marinelli, R. L., and Jahnke, R. A.: Benthic microalgal biomass and irradiance at the sea floor on the continental shelf of the South Atlantic Bight: spatial and temporal variability and storm effects, Cont. Shelf Res., 19, 477–505, 1999.

Neubauer, S. and Anderson, I. C.: Transport of dissolved inorganic carbon from a tidal freshwater marsh to the York River estuary, Limnol. Oceanogr., 48, 299–307, 2003.

Pomeroy, L. R. and Wiegert, R. G.: The Ecology of a Salt Marsh, Springer-Verlag, New York, 1981.

Pomeroy, L. R., Sheldon, J. E., Sheldon, W. M., Blanton, J. O., Amft, J., and Peters, F.: Seasonal changes in microbial processes in estuarine and continental shelf waters of the south-eastern U. S. A., Estuar. Coast. Shelf S., 51, 415–428, 2000.

Rabouille, C., Mackenzie, F. T., and Ver, L. M.: Influence of the human perturbation on carbon, nitrogen, and oxygen biogeochemical cycles in the global coastal ocean, Geochim. Cosmochim. Ac., 65, 3615–3641, 2001.

Raymond, P. A., Bauer, J. E., and Cole, J. J.: Atmospheric CO_2 evasion, dissolved inorganic carbon production, and net heterotrophy in the York River estuary, Limnol. Oceanogr., 45, 1707–1717, 2000.

Riebesell, U., Fabry, V. J., Hansson, L., and Gattuso, J.-P.: Guide to best practices for ocean acidification research and data reporting, 258 pp., 2010.

VISIT THE SCIENTIFIC PUBLICATIONS REPORT ARCHIVE

Smith, S. V. and Hollibaugh, J. T.: Coastal metabolism and the oceanic organic carbon balance, Rev. Geophys., 31, 75–89, 1993.

Takahashi, T., Olafsson, J., Goddard, J. G., Chipman, D. W., and Sutherland, S. C.: Seasonal variation of CO_2 and nutrients in the high-latitude surface oceans: a comparative study, Global Biogeochem. Cy., 7, 843–878, 1993.

Takahashi, T., Sutherland, S. C., Sweeney, C., Poisson, A., Metzl, N., Tilbrook, B., Bates, N., Wanninkhof, R., Feely, R. A., Sabine, C., Olafsson, J., and Nojiri, Y.: Global sea-air CO_2 flux based on climatological surface ocean pCO_2, and seasonal biological and temperature effects, Deep-Sea Res. II, 49, 1601–1622, 2002.

Thomas, H., Bozec, Y., Elkalay, K., and De Baar, H. J. W.: Enhanced open ocean storage of CO_2 from shelf sea pumping, Science, 304, 1005–1008, 2004.

Verity, P. G., Bishop, S. S., Nelson, J. R., Craven, D. B., Blanton, J. O., Robertson, C. Y., and Tronzo, C. R.: Composition, productivity, and nutrient chemistry of a coastal ocean planktonic food web, Cont. Shelf Res., 13, 741–776, 1993.

Verity, P. G., Redalje, D. G., Lohrenz, S. R., Flagg, C., and Hristov, R.: Coupling between primary production and pelagic consumption in temperate ocean margin pelagic ecosystems, Deep-Sea Res. II, 49, 4553–4569, 2002.

Walsh, J. J.: On the Nature of Continental Shelves, Academic, San Diego, 1988.

Wang, Z. and Cai, W.-J.: Carbon dioxide degassing and inorganic carbon export from a marsh dominated estuary (the Duplin River): A marsh CO_2 pump, Limnol. Oceanogr., 49, 341–352, 2004.

Wollast, R.: Interactions of carbon and nitrogen cycles in the coastal zone, in: Interactions of C, N, P and S Biogeochemical Cycles and Global Change, edited by: Wollast, R., Mackenzie, F. T., and Chou, L., Springer, Berlin, 195–210, 1993.

VISIT THE SCIENTIFIC PUBLICATIONS REPORT ARCHIVE

Environmental Science & Technology

Article

pubs.acs.org/est

Radiocesium in Pacific Bluefin Tuna *Thunnus orientalis* in 2012 Validates New Tracer Technique

Daniel J. Madigan,*[,†] Zofia Baumann,[‡] Owyn E. Snodgrass,[§] Halim A. Ergül,[∥] Heidi Dewar,[§] and Nicholas S. Fisher[‡]

[†]Hopkins Marine Station, Stanford University, 120 Ocean View Boulevard, Pacific Grove, California 93950, United States

[‡]School of Marine and Atmospheric Sciences, Stony Brook University, Stony Brook, New York 11794, United States

[§]Fisheries Research Division, Southwest Fisheries Science Center, National Marine Fisheries Service, NOAA, 8604 La Jolla Shores Drive, La Jolla, California 92037, United States

[∥]Department of Biology, Kocaeli University, 41300 Umutteppe, İzmit, Kocaeli, Turkey

Supporting Information

ABSTRACT: The detection of Fukushima-derived radionuclides in Pacific bluefin tuna (PBFT) that crossed the Pacific Ocean to the California Current Large Marine Ecosystem (CCLME) in 2011 presented the potential to use radiocesium as a tracer in highly migratory species. This tracer requires that all western Pacific Ocean emigrants acquire the ^{134}Cs signal, a radioisotope undetectable in Pacific biota prior to the Fukushima accident in 2011. We tested the efficacy of the radiocesium tracer by measuring ^{134}Cs and ^{137}Cs in PBFT (n = 50) caught in the CCLME in 2012, more than a year after the Fukushima accident. All small PBFT (n = 28; recent migrants from Japan) had ^{134}Cs (0.7 ± 0.2 Bq kg^{-1}) and elevated ^{137}Cs (2.0 ± 0.5 Bq kg^{-1}) in their white muscle tissue. Most larger, older fish (n = 22) had no ^{134}Cs and only background levels of ^{137}Cs, showing that one year in the CCLME is sufficient for ^{134}Cs and ^{137}Cs values in PBFT to reach pre-Fukushima levels. Radiocesium concentrations in 2012 PBFT were less than half those from 2011 and well below safety guidelines for public health. Detection of ^{134}Cs in all recent migrant PBFT supports the radiocesium tracer in migratory animals in 2012.

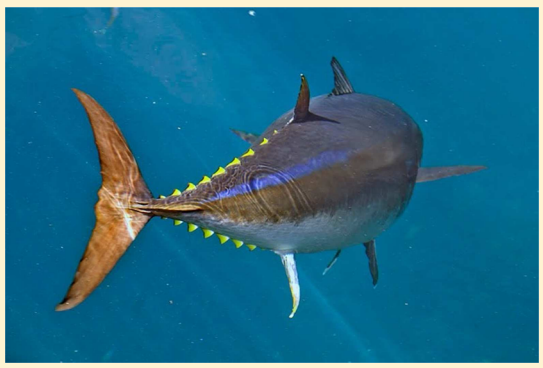

INTRODUCTION

The discharge of radionuclides into the western Pacific Ocean in 2011 from the failed Fukushima nuclear power plant has led to studies of radionuclide concentrations in seawater and marine biota, both near Japan[1−3] and in migratory marine species.[4] In 2011, radiocesium from Fukushima was detected in Pacific bluefin tuna, *Thunnus orientalis,* that had recently traversed the North Pacific Ocean, suggesting the potential for Fukushima-derived radionuclides to serve as tracers of long-distance migrations by highly migratory species in the Pacific Ocean.[4] While tools such as electronic tags have provided extensive animal movement data prospective from the date of tagging,[5] chemical tracers (such as radiocesium) can provide retrospective migration information that is often uniquely informative.[4,6−8]

Certain conditions are necessary for the reliable use of Fukushima-derived radiocesium to trace migrations. While ^{137}Cs ($t_{1/2}$ = 30.1 years) still exists throughout the Pacific in low, "background" levels as a result of nuclear weapons testing that peaked in the 1960s, the shorter lived ^{134}Cs ($t_{1/2}$ = 2.1 years) from nuclear weapons testing has long since decayed.[2] A point source of anthropogenic radionuclides such as Fukushima is therefore the only substantial source of ^{134}Cs in the Pacific Ocean, and consequently the presence of ^{134}Cs indicates recent migration from the contaminated region. For reliable application of this tracer, all animals migrating from contaminated waters must accumulate and retain measurable levels of ^{134}Cs to accurately identify their status as recent migrants from the western Pacific (to avoid interpretation of recent migrants as residents). Conversely, animals must excrete ^{134}Cs in their new environment at some determinable rate so that absence of ^{134}Cs can be interpreted as residency in the noncontaminated region for an interpretable period of time (to avoid erroneous identification of recent migrants, and to constrain the time range of a "recent" migration). Given that potential transport of Fukushima-derived radiocesium is currently being examined in a variety of migratory animals including whales, turtles, tunas, sharks, and seabirds to infer migratory patterns, it is critical to test these assumptions.

Pacific bluefin tuna (PBFT) are an ideal species for the validation and application of the radiocesium tracer. All PBFT

Received: January 16, 2013
Revised: February 5, 2013
Accepted: February 11, 2013

 © XXXX American Chemical Society

VISIT THE SCIENTIFIC PUBLICATIONS REPORT ARCHIVE

Table 1. Catch Date, Size, Estimated Age, and Radionuclide Concentrations in 50 Pacific Bluefin Tuna (PBFT) *Thunnus orientalis*, Captured in the California Current Large Marine Ecosystem in 2012[a]

PBFT no.	catch date	SL[b] (cm)	age[c] (years)	^{134}Cs (Bq kg^{-1} dry wt)	^{137}Cs (Bq kg^{-1} dry wt)	^{40}K (Bq kg^{-1} dry wt)	^{134}Cs:^{137}Cs
1	8/4/2012	63.1	1.3	0.64	1.72	385	0.37
2	8/4/2012	63.4	1.3	0.61	2.03	372	0.30
3	8/4/2012	63.5	1.3	0.33	1.61	382	0.20
4	8/4/2012	63.8	1.3	0.67	1.82	456	0.37
5	8/4/2012	64.8	1.4	0.56	2.23	275	0.25
6	8/4/2012	65.6	1.4	0.58	1.51	347	0.38
7	8/4/2012	65.8	1.4	0.61	2.03	455	0.30
8	8/4/2012	65.8	1.4	0.79	1.82	405	0.43
9	8/4/2012	65.9	1.4	0.76	2.45	500	0.31
10	8/4/2012	66.2	1.4	0.50	1.43	364	0.35
11	8/18/2012	66.6	1.4	0.59	2.71	412	0.22
12	8/4/2012	66.6	1.4	0.69	1.89	422	0.37
13	8/4/2012	66.8	1.4	1.30	2.91	446	0.45
14	8/4/2012	67.0	1.4	0.98	2.45	471	0.40
15	8/4/2012	67.1	1.4	0.60	1.93	335	0.31
16	8/4/2012	67.4	1.5	0.49	1.58	388	0.31
17	8/4/2012	67.8	1.5	0.75	1.89	487	0.39
18	8/4/2012	67.9	1.5	0.51	1.50	362	0.34
19	8/4/2012	68.5	1.5	0.54	2.23	310	0.24
20	8/18/2012	68.9	1.5	0.30	1.22	269	0.24
21	8/4/2012	68.9	1.5	0.42	1.13	269	0.37
22	8/4/2012	69.0	1.5	0.75	1.95	459	0.39
23	8/4/2012	69.1	1.5	0.68	1.66	382	0.41
24	8/18/2012	69.4	1.5	0.96	3.12	497	0.31
25	8/4/2012	69.4	1.5	0.75	2.14	324	0.35
26	8/4/2012	69.9	1.6	0.41	1.16	226	0.35
27	8/4/2012	71.8	1.6	0.54	1.88	383	0.29
28	8/22/2012	72.3	1.6	1.14	2.93	702	0.39
29	6/9/2012	73.7	1.7	nd	1.00	399	–
30	6/10/2012	76.5	1.8	0.86	2.29	439	0.38
31	6/9/2012	77.4	1.8	nd	1.33	432	–
32	6/10/2012	78.0	1.9	nd	1.98	534	–
33	8/18/2012	79.2	1.9	nd	0.98	540	–
34	8/18/2012	79.5	1.9	nd	0.94	676	–
35	8/18/2012	80.7	2.0	nd	0.96	588	–
36	8/18/2012	80.7	2.0	1.19	3.14	561	0.38
37	6/9/2012	81.0	2.0	nd	1.69	371	–
38	8/18/2012	81.0	2.0	1.26	3.81	518	0.33
39	8/4/2012	82.8	2.1	nd	0.54	438	–
40	8/18/2012	84.4	2.1	0.61	2.63	349	0.23
41	8/18/2012	87.3	2.2	1.16	4.21	564	0.28
42	6/10/2012	107.7	3.0	nd	1.43	613	–
43	6/10/2012	108.5	3.0	nd	0.86	503	–
44	6/10/2012	109.8	3.1	nd	1.71	711	–
45	6/10/2012	112.7	3.2	nd	1.37	505	–
46	6/10/2012	115.7	3.3	nd	0.36	482	–
47	5/26/2012	117.0	3.4	nd	1.28	429	–
48	6/10/2012	118.3	3.4	nd	0.53	459	–
49	6/10/2012	122.4	3.6	nd	1.08	543	–
50	5/26/2012	132.4	4.0	nd	0.97	558	–

[a]Small PBFT: nos. 1-28; larger PBFT: nos. 29-50, as defined in the text. [b]Estimated from CFL.[21] [c]Estimated from SL.[19] nd: not detected. Dash (–) indicates ^{134}Cs:^{137}Cs ratios that could not be determined due to nondetection of ^{134}Cs.

spawn in the western Pacific Ocean, and juveniles forage in the waters around Japan.[9−11] Juveniles then either remain in the western Pacific or migrate eastward to the California Current Large Marine Ecosystem (CCLME). Most PBFT are thought to migrate late in their first year or early in their second.[9] Thus, the youngest PBFT in the CCLME (approximately 1−1.5 years old) must have migrated from Japan within the preceding year. Previous studies suggest that larger, older PBFT in the CCLME are primarily residents for >1 year.[9] However, some fish migrate from Japan at older ages, and in a given year the proportion of

VISIT THE SCIENTIFIC PUBLICATIONS REPORT ARCHIVE

Japan migrants to CCLME residents is largely unknown. This information could improve fisheries modeling and management of PBFT, in which severe population declines have recently been reported.[12,13]

For radiocesium to function as a reliable tracer in PBFT, all PBFT in the CCLME below some threshold age (which must be recent migrants from Japan) must assimilate adequate concentrations of ^{134}Cs before their eastward migration and retain measurable concentrations after their trans-Pacific migration to the CCLME. Marine fish have been shown to acquire Cs from both the aqueous phase and from diet.[14] Older fish in the CCLME that are residential (>1 year in the CCLME) must lose ^{134}Cs due to excretion,[4,14,15] so that only recently migrated fish would carry measurable levels of ^{134}Cs, allowing the ^{134}Cs to distinguish recent migrants from >1 year CCLME residents.

We collected 50 samples of PBFT in 2012 and measured muscle tissue for ^{134}Cs and ^{137}Cs to determine if the acquisition of radiocesium by migrating PBFT persisted into the summer of 2012, more than a year after the Fukushima disaster. Radiocesium levels were compared to concentrations of another γ-emitting radionuclide, the naturally occurring ^{40}K, to provide context for observed radiocesium concentrations. For comparison, we also collected 5 samples of yellowfin tuna (*Thunnus albacares*) in 2012, which are known from electronic tagging studies to be residents of the CCLME and do not make migrations from the western Pacific Ocean.[5,16] We used small PBFT, known to be migrants from Japan, to test whether all migrants would demonstrate a measurable radiocesium signal from Fukushima. We examined the radiocesium levels in older fish to determine if residents and migrants could be discerned via the absence of ^{134}Cs (due to excretion during a year or more in CCLME waters) or presence of ^{134}Cs (due to recent migration from Japan). Finally, we use ratios of ^{134}Cs:^{137}Cs to estimate time of departure from Japan in recently migrated PBFT.

■ MATERIALS AND METHODS

Sampling and Radioanalysis. Tuna tissue samples were collected from PBFT and yellowfin tuna (YFT; *Thunnus albacares;* CCLME residents)[5,16] captured by recreational sport fishermen. Fish were caught within 300 km of San Diego, CA and landed in San Diego where they were filleted and frozen for human consumption. We sampled 250−500 g of white muscle tissue from the dorsal musculature behind the head. Muscle tissue was kept on dry ice (−55 °C) and shipped to Stony Brook University for radioanalysis. Muscle samples were freeze-dried and 65 ± 23 g dry wt of white muscle tissue was blended and combusted at 450 °C for 4 h. Combustion resulted in further compactness of the sample, which assured better counting efficiency during γ-radioanalysis (details below). Loss of Cs during combustion was assumed to be negligible, as shown previously.[17] Ash was further ground with a mortar and pestle to achieve a uniform matrix, placed inside plastic jars, and stored at 60 °C prior to radioanalysis.

For γ-radioanalysis of ^{134}Cs, ^{137}Cs, and ^{40}K we used high purity germanium detectors (HPGe; Canberra Industries). Sample counting times were adjusted to allow propagated counting errors of <10% for ^{137}Cs (662 keV), <15% for ^{134}Cs (605 keV) and <3% for ^{40}K (1461 keV). Most samples were counted for up to 3 days. Genie 2000 software (Canberra) was used to analyze the peaks in the energy spectrum. The lowest detection limits were 0.1 Bq kg^{-1} for both ^{134}Cs and ^{137}Cs and 0.9 Bq kg^{-1} for ^{40}K. These detection limits were calculated for each individual fish muscle sample using the "well-known blank" method.[18] Counting geometry was taken into consideration by varying the fullness of the jar when testing standards made of known quantities of ^{75}Se, ^{134}Cs, ^{137}Cs, and ^{40}K emitting over a broad energy spectrum (265, 605, 662, and 1461 keV, respectively). ^{134}Cs and ^{137}Cs concentrations in tuna muscle samples were decay-corrected to catch dates in the CCLME (Table 1). No decay correction was required for ^{40}K due to its long half-life ($t_{1/2}$ = 1.2 × 10^9 years).

Age Estimation. Age (age$_{est}$) was estimated from standard length (SL; cm) for PBFT and YFT according to Bayliff et al.[19] and Wild.[20] SL was calculated from curved fork length (CFL; cm) for PBFT according to Farwell.[21] and for YFT according to Scida et al.[22] When possible we measured the length from rostrum to operculum (operculum length, or OL, cm) and curved fork length (CFL, cm) of whole fish and calculated a regression for PBFT:

$$\mathrm{CFL} = 2.8373\mathrm{OL} + 12.307 \quad (1)$$

to estimate CFL from OL (Supporting Information (SI) Figure S1). The linear equation had an r^2 value of 0.98 (SI Figure S1).

Back-Calculated Departure Date. The ratio of radioactive Cs isotopes (^{134}Cs:^{137}Cs = R) was used to back-calculate the time at which individual PBFT left the Fukushima-contaminated waters around Japan. This ratio would decrease in PBFT after their departure due to continued exposure to ^{137}Cs at background levels (1 mBq L^{-1}) but no ^{134}Cs in central and eastern Pacific waters, and the faster decay rate of ^{134}Cs. A model based on that from Madigan et al.[4] was used to estimate how ^{134}Cs:^{137}Cs ratios in PBFT would change over time after leaving waters around Japan. Briefly, eq 2 describes the processes that impact the change of ^{134}Cs:^{137}Cs ratio over time t. These processes are: radioactive decay (λ_1 and λ_2 for ^{137}Cs and ^{134}Cs; $t_{1/2}$ = 30.2 and 2.1 years, respectively) and efflux (k_e: 0.02 d^{-1})[15] of previously accumulated Cs.[14] Background ^{137}Cs in PBFT muscle (measured in pre-Fukushima PBFT) is represented by A (here, A = 1 Bq kg^{-1} dry wt), which is the same for YFT never exposed to Fukushima radionuclides, PBFT residents of the CCLME >1 year, and PBFT before Fukushima (2008).[4] Background ^{137}Cs (from nuclear weapons testing fallout) in PBFT is a result of uptake of ^{137}Cs from seawater and food (collectively, k_a) and loss of previously accumulated ^{137}Cs (k_e).[4] Since PBFT concentrations of ^{134}Cs and ^{137}Cs change differently over time due to different decay rates and acquisition of weapons fallout ^{137}Cs but not ^{134}Cs after leaving contaminated waters, estimated time since departure (t) will depend not only on the initial R calculation (R_0) but also on absolute concentrations of ^{134}Cs and ^{137}Cs in PBFT. The contribution of ^{137}Cs from weapons fallout (1.0 Bq kg^{-1} dry wt) will contribute relatively more ^{137}Cs to the total pool of ^{137}Cs in PBFT muscle in PBFT that acquire low amounts of Cs in contaminated waters. Consequently, fish that acquire relatively low amounts of ^{134}Cs and ^{137}Cs in contaminated waters will have R values that decrease more rapidly, with ^{134}Cs decreasing more rapidly than ^{137}Cs. In contrast, PBFT that acquire more ^{134}Cs and ^{137}Cs in contaminated waters will have slower rates of decrease of R, as both ^{134}Cs and ^{137}Cs concentrations will decrease at fairly similar rates until the ^{137}Cs concentration decreases to levels where background ^{137}Cs (A) contributes an appreciable proportion of ^{137}Cs to the total pool of ^{137}Cs in PBFT muscle:

VISIT THE SCIENTIFIC PUBLICATIONS REPORT ARCHIVE

$$R_t = \frac{[^{134}\mathrm{Cs}]_t e^{-t(\lambda_2+k_e)}}{([^{137}\mathrm{Cs}]_t - A)e^{-t(\lambda_1+k_e+k_a)} + A} \quad (2)$$

Background ^{137}Cs concentration in PBFT (A) is a product of ^{137}Cs concentration in seawater (1 mBq L^{-1}) and the Cs uptake rate constant (k_a) divided by the sum of efflux (k_e), radioactive decay (λ_1) and accumulation (k_a) rate constants:

$$A = \frac{(^{137}\mathrm{Cs}_w)k_a}{\lambda_1 + k_e + k_a} \quad (3)$$

It is assumed that ^{134}Cs and ^{137}Cs have identical rate constants of uptake and loss in fish. In 2012, accumulation rate constants (k_a) and efflux rate constants (k_e) yield A values = 1 Bq kg^{-1} of ^{137}Cs. PBFT that migrate away from Fukushima-contaminated waters will lose previously accumulated Cs from muscle tissue, and the concentration of ^{137}Cs and ^{134}Cs in PBFT muscle will asymptotically approach A (1 Bq kg^{-1} dry wt) and 0, respectively. Dividing A by the concentration of ^{137}Cs in surface seawater in the Pacific yields a dry wt concentration factor in PBFT muscle of 1000, and a wet wt concentration factor of 244, somewhat higher than the value of 100 calculated for generic marine fish.[23]

Back-calculations of departure date from Japan require an assumed initial value for ^{134}Cs:^{137}Cs ratio (R) to solve for time t. R at the date of maximum discharge was approximately 1.[2] For PBFT in 2012, we calculated an assumed value of R for April 6, 2012, one year after peak discharge of radionuclides[2] that would result from the different decay rates of ^{134}Cs and ^{137}Cs. This value (0.73) was used in estimates of departure date from Japan for individual PBFT (SI Table S2).

Statistical Analysis. Mann−Whitney U-tests were used to compare the ^{134}Cs and ^{137}Cs concentrations of small (63.4−72.3 cm SL) PBFT, larger PBFT migrants (^{134}Cs present), larger PBFT residents (^{134}Cs absent), PBFT migrants from 2011,[4] and YFT residents in the CCLME. Mann−Whitney U-test p-values were considered significant at $p = 0.05$. Pearson's linear correlation was used to assess the potential linear correlation between PBFT age and estimated time since migration from waters around Japan (calculated from ^{134}Cs:^{137}Cs ratios, eq 2), with p-values significant at $p = 0.05$ and H_0 = no correlation between variables.

RESULTS

We collected 50 Pacific bluefin tuna in 2012 in May, June, and August (Table 1). PBFT ranged from 63.1 to 132.4 cm SL (79.4 ± 18.6 cm), corresponding to estimated ages of 1.3−4.0 years (1.9 ± 0.7 years) (Table 1). ^{134}Cs was detected in 33 fish and concentrations of ^{137}Cs and ^{40}K are reported for all PBFT. All of the small PBFT (63.1−72.3 cm SL; age$_{est}$ = 1.3−1.6 years; n = 28; hereafter "small PBFT") had measurable concentrations of ^{134}Cs (0.7 ± 0.2 Bq kg^{-1}), whereas only 5 of the 22 larger PBFT (73.7−132.4 cm SL; age$_{est}$ = 1.7−4.0 years) had detectable concentrations of ^{134}Cs (1.02 ± 0.27 Bq kg^{-1}) (Table 1 and S1). When detected, ^{134}Cs concentrations ranged from 0.3−1.3 Bq kg^{-1} dry wt (0.7 ± 0.3 Bq kg^{-1}), approximately 18% of the mean concentration reported in 2011 PBFT (4.0 ± 1.4 Bq kg^{-1}).[4] For PBFT containing ^{134}Cs above the detection limit, the mean ^{134}Cs:^{137}Cs ratio was 0.33 ± 0.06 (Table 1). YFT had no ^{134}Cs and only background levels (0.84 ± 0.12) of ^{137}Cs (Table 2). Concentrations of naturally occurring ^{40}K ranged from 226 to 711 Bq kg^{-1}, and ratios of radioactivity from ^{40}K to $^{134+137}$Cs in PBFT ranged from 99 (PBFT no. 5) to 719 (PBFT no. 34) (Tables 1 and S1).

PBFT sampled in the CCLME are either recent Japan migrants or CCLME residents (Figure 1A), and radiocesium concentrations enabled us to classify PBFT as migrants or residents (Table 1, Figure 1B). All fish ≤ 1.6 years old were migrants, while only 5 of 22 PBFT age 1.7−4 years were

Table 2. Catch Date, Size, and Radionuclide Concentrations in Five Yellowfin Tuna (YFT) *Thunnus albacares*, Captured in the California Current Large Marine Ecosystem in 2012. ^{134}Cs Was Undetectable in All YFT

YFT no.	catch date	SL[a] cm	age[b] years	^{137}Cs Bq kg^{-1} dry wt	^{40}K Bq kg^{-1} dry wt
1	9/22/2012	64.6	1.2	0.90	630
2	9/22/2012	62.7	1.2	0.85	575
3	9/22/2012	66.1	1.2	0.92	636
4	9/22/2012	61.3	1.2	0.90	650
5	9/22/2012	67.0	1.2	0.62	404
average		64.4	1.2	0.84	579
SD		2.4	0	0.12	102

[a]Estimated from CFL.[22] [b]Estimated from SL.[20]

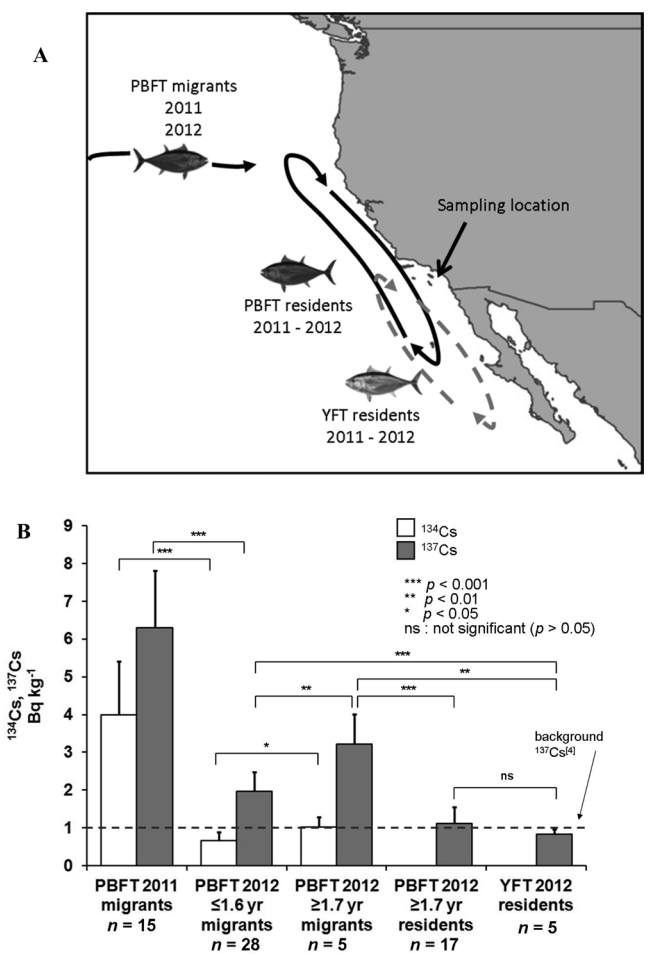

Figure 1. Map of simplified movement patterns (A) and concentrations of ^{134}Cs and ^{137}Cs (B) in Pacific bluefin tuna (migrants and residents) and yellowfin tuna (residents) in the CCLME. Radiocesium concentrations in (B) are mean values (Bq kg^{-1} dry wt) + SD P-values shown are for Mann−Whitney U-tests.

VISIT THE SCIENTIFIC PUBLICATIONS REPORT ARCHIVE

migrants. Small migrant 2012 PBFT had lower concentrations than larger migrant PBFT of both ^{134}Cs ($p < 0.05$) and of ^{137}Cs ($p < 0.01$) (Figure 1B). Both 2012 migrant groups had lower concentrations than recent migrants sampled in 2011. Larger resident PBFT and YFT had no detectable ^{134}Cs and only background levels of ^{137}Cs (Tables 1 and 2, Figure 1B), and radiocesium levels between these groups was not significantly different (Figure 1B). The smallest fish categorized as a CCLME resident of >1 year was 73.7 cm SL (age_{est} = 1.7 years) (Table 1), establishing this size and age as the threshold in this study between the 100% migrant group (small PBFT) and the mixed group of residents and migrants (larger PBFT) (Figure 2).

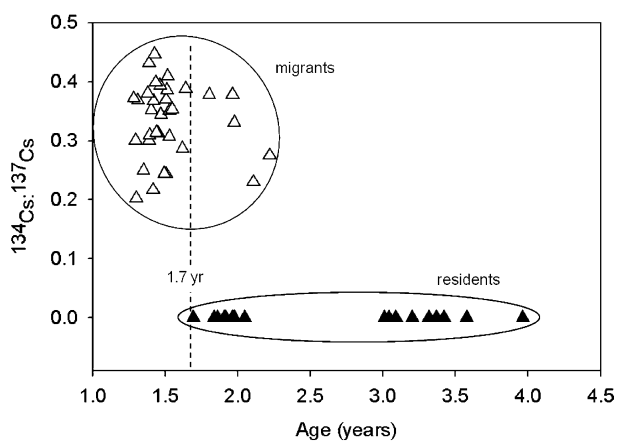

Figure 2. Ratios of ^{134}Cs:^{137}Cs in Pacific bluefin tuna caught in the CCLME from June through August 2012. Open triangles indicate recent Japan migrants, and filled triangles indicate fish that are resident (>1 year) to CCLME. Cs ratios equal to 0 are due to absence of ^{134}Cs in these fish and are only observed in older fish (*x*-axis: ≥1.7 years old). ^{134}Cs:^{137}Cs ratios greater than zero in PBFT >1.7 years represent PBFT that migrated from Japan at older ages.

There was a positive correlation between fish age and time since departure from Japan (estimated from ^{134}Cs:^{137}Cs ratios) ($p < 0.01$, $r^2 = 0.36$; Figure 3A) indicating that larger PBFT left Japan earlier. Estimated departure times from Japan suggest that most migrants left Japan in early mid June, with a few departing in April and July (Figure 3B).

DISCUSSION

Our results demonstrate that PBFT continue to transport Fukushima-derived radiocesium across the Pacific Ocean to the CCLME. These findings support the use of Fukushima-derived radiocesium in Pacific bluefin tuna to determine whether PBFT in the eastern Pacific Ocean have recently migrated from Japan or have been residential in the CCLME for at least one annual cycle, at which point ^{134}Cs is undetectable and ^{137}Cs decreases to background levels.

Prior to this study it was unknown whether concentrations of radiocesium in PBFT in 2012 would be higher or lower than those measured in 2011. Concentrations of Cs in PBFT could decrease over time due to dilution of radiocesium in waters around Japan, the decay of ^{134}Cs, and the potential for decreasing radiocesium concentrations in PBFT prey due to Cs dilution in seawater. However, PBFT captured in the CCLME in 2012 spent more time in contaminated waters than those sampled in 2011. PBFT in 2011 likely spent only 1−3 months in contaminated waters prior to eastward migration, and

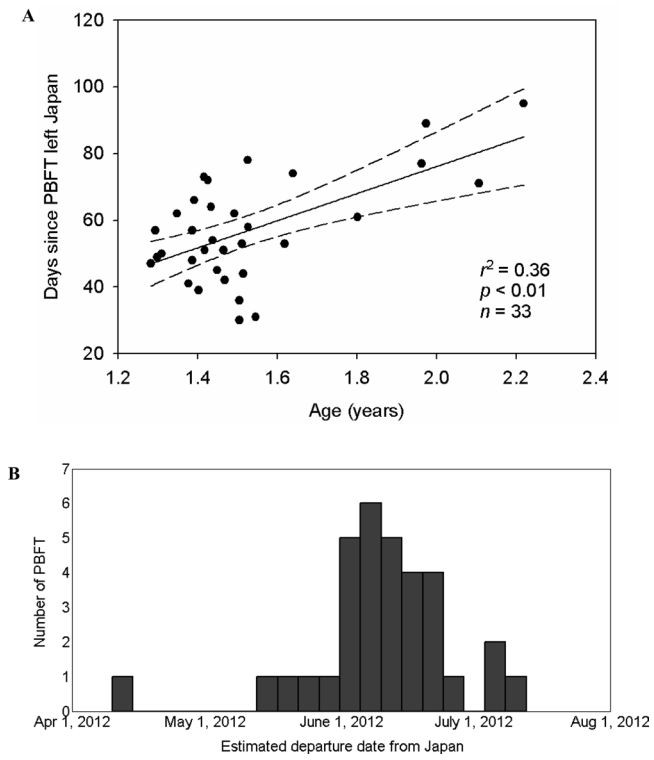

Figure 3. Relationship between PBFT age and estimated time since departure (days) from Japan for the 33 PBFT that contained ^{134}Cs (A) and histogram of estimated departure dates from Japan (B) for recent migrant PBFT. *P*-value and r^2 reported in (A) are for Pearson's linear correlation test. Solid line represents linear fit to data, dashed lines show 95% CI. Departure dates in (B), estimated from ^{134}Cs:^{137}Cs ratios, were centered on early June.

estimations of departure dates suggest that some may have spent less than one month in contaminated waters before their trans-Pacific migration.[4] Small PBFT in 2012 potentially spent their entire first year in coastal waters around Japan before migrating eastward. There is also the potential for trophic biomagnification of Cs in juvenile PBFT,[14,24] which are mid- to high-trophic level predators that feed on crustaceans, forage fish, and squid.[11] The potential biomagnification of Cs in PBFT presents the possibility of a time lag between maximum radiocesium concentrations in seawater and maximum concentrations in tuna (and other high trophic level predator) muscle tissue. Longer exposure times and potential trophic biomagnification presented the potential for higher concentrations of Cs in 2012 PBFT. Our results show that migrant PBFT concentrations of ^{134}Cs in 2012 dropped to approximately 18% of those in 2011. Total radiocesium ($^{134+137}$Cs) also dropped, from 10.3 ± 2.9 in 2011[4] to 2.9 ± 1.0 Bq kg^{-1} in 2012 (Table 1), suggesting that radiocesium levels declined significantly in PBFT from 2011 to 2012 in the CCLME. This suggests that any enhanced bioaccumulation of $^{134+137}$Cs in PBFT over the longer exposure period was outweighed by the year-long dilution of radiocesium in contaminated waters in 2012. This is in contrast to the report that $^{134+137}$Cs concentrations remained steady (though highly variable) in demersal, coastal fish off Fukushima in 2012.[3] It is likely that differences in radiocesium concentrations in both seawater and prey lead to differences in Cs concentrations between demersal coastal fish and pelagic fish such as PBFT.

VISIT THE SCIENTIFIC PUBLICATIONS REPORT ARCHIVE

The radionuclides in PBFT from the Fukushima nuclear power plant accounted for an even smaller fraction of the total radioactivity in 2012 PBFT than in 2011 PBFT[4] and remained well below safety limits set by the most stringent government regulations (100 Bq kg^{-1} wet wt, or about 400 Bq kg^{-1} dry wt). The radioactivity from the naturally occurring ^{40}K exceeded that of radiocesium by 2−3 orders of magnitude. Another naturally occurring radionuclide, ^{210}Po, is present in tuna muscle provides a radioactive dose to seafood consumers that is orders of magnitude above the dose resulting from the Fukushima radionuclides.[25,26]

The differences between migrant and resident PBFT (Figure 1B) demonstrate that recent migrants to the CCLME can easily be discerned from CCLME residents of at least one year using radiocesium concentrations; this is particularly apparent in concentrations of ^{134}Cs. ^{134}Cs was detected in only 23% (5 of 22 individuals) of older PBFT (Table 1, Figures 1 and 2). This is an expected result, as many older PBFT in the CCLME are assumed to have migrated during their first year, although some variable proportion migrates in subsequent years.[19] The 5 older fish with detectable ^{134}Cs demonstrate the utility of the radiocesium tracer to discern recent migrants from residents in older fish, for which migration status is unknown.[9,19] The higher concentrations of ^{134}Cs and ^{137}Cs in larger vs smaller migrants may be the result of trophic biomagnification, as young PBFT off Japan show a diet shift to higher trophic level prey during their first year, and larger fish would thus be feeding on higher trophic levels in waters around Japan for a longer time period.[11] Efflux rate constants for Cs may also be greater in smaller versus larger fish, though this has not been measured.

Radiocesium levels in older resident PBFT were not significantly different from those in YFT, which do not migrate from the western Pacific and are residential to the CCLME[5,16] and show no detectable ^{134}Cs and only background levels of ^{137}Cs (Table 2) over two years of data analysis.[4] This suggests that older PBFT which carried radiocesium in 2011 eliminated ^{134}Cs to nondetectable and ^{137}Cs to background (∼1 Bq kg^{-1}) levels within one year of residency in the CCLME. Therefore, all PBFT in the CCLME for one year or more can be expected to carry radiocesium levels comparable to pre-Fukushima conditions. This makes identification of CCLME residents particularly straightforward, as presence or absence of ^{134}Cs discerns migrants from residents. All PBFT that are 3−4 years old carried no ^{134}Cs, distinguishing all of these PBFT ($n = 9$) as >1 year CCLME residents (Figure 2).

The significant linear relationship between PBFT age and time since departure from Japan (Figure 3A) suggests that older fish may have migrated from the western Pacific Ocean before younger fish. Older fish had similar ^{134}Cs:^{137}Cs ratios to smaller fish, and greater estimated time since departure in older fish is a consequence of the greater concentrations (Figure 1B) of ^{134}Cs and ^{137}Cs in older fish than those in younger fish (see description of eq 2 in Materials and Methods). Estimated time since Japan departure, based on ^{134}Cs:^{137}Cs ratios, ranged from 30 to 95 days (SI Table S2) with an average time since departure of approximately two months (57 ± 16 days). This average matches the crossing time (65 days) of an electronically tagged juvenile PBFT making its first trans-Pacific migration, and the shortest time since departure in our study (30 days) is possible given the daily swimming speed (172.3 ± 41.7 km d^{-1}) in that study.[27] If our lowest estimate of 30 d is accurate, it is the fastest reported trans-Pacific migration by a PBFT.

Time since departure for larger PBFT (>1.7 years) was nearly a month longer (79 ± 14 day) (SI Table S2). Variability in the timing of offshore migration has been demonstrated in conventional tagging studies,[19] and it is possible that older, larger fish follow different cues for the initiation of offshore migration. Larger fish would have a higher tolerance for colder waters and would potentially be less affected by oceanographic conditions that may limit migration ability during periods of cooler water before spring and early summer.

Departure from Japan began in late spring, centered on early June (Figure 3B), corresponding with conventional tagging studies that show many PBFT initiate their eastward migration during spring-summer.[19] This early summer departure from Japan may explain why most recent Japan migrants to the CCLME were captured in August and not in earlier summer months in the CCLME (Table 1). Departure-date estimates rely on a predictable and consistent ^{134}Cs:^{137}Cs ratio in PBFT muscle before leaving Japan. Our estimate of an initial ^{134}Cs:^{137}Cs ratio in tuna muscle of 0.73 (SI Table S2) was based on the initial release ratio of 1[2] and the different decay rates of ^{134}Cs and ^{137}Cs; more consistent and publicly accessible measurements of PBFT off Japan would provide the actual data to validate or modify this estimate. However, the average ^{134}Cs:^{137}Cs ratio for coastal and pelagic predatory fish species caught on April ninth 2012, approximately one year after maximum discharge of radiocesium, was approximately equal (0.74 ± 0.18, $n = 10$ fish species; for more information see SI).[28] These data support our use of this initial ^{134}Cs:^{137}Cs ratio value (0.73) in PBFT off Japan.

The approach used here, especially applied to large data sets or used to interpret data from other chemical tracers, can improve our understanding of movement patterns of PBFT in the North Pacific Ocean. Understanding the relative proportions of migrants to CCLME residents in relation to oceanographic (e.g., ENSO events) or biological (e.g., sardine or anchovy abundance) conditions can help identify the drivers of the eastward migration of PBFT from Japan to the CCLME. Such studies could be applied to fisheries models which can benefit from migratory information.[12]

One source of error in this study is the use of length as a proxy for age, as there is significant variability in this relationship.[19] Aging using otoliths is a more precise (albeit time-intensive) method,[29] although otoliths were not available for every individual sampled for white muscle tissue. Data for fisheries models in particular may require aging using otoliths. It is also possible that time of departure from Japan is more representative of the time of departure from a broader area now contaminated by Fukushima radiocesium due to dispersal. It has recently been shown that Fukushima-derived radioactive Cs is dispersing further away from the Japanese shoreline and could be reaching waters as far as ∼170°E in 2012.[30]

The applicability of our results and approach to other Pacific species that migrate from Japan to distant ecoregions is important. Albacore tuna *Thunnus alalunga*,[31] blue sharks *Prionace glauca*,[32] Pacific loggerhead sea turtles *Caretta caretta*,[33] sooty shearwaters *Puffinus griseus*,[34] salmon sharks *Lamna ditropis*,[35] common minke whales *Balaenoptera acutorostrata*,[36] and other highly migratory species are all known to forage in the Kuroshio Current off eastern Japan and subsequently migrate to regions such as the Okhotsk Sea, the Aleutian Islands, the CCLME, and regions of the South Pacific Ocean. Detection of ^{134}Cs and elevated ^{137}Cs in 100% of small, recently migrated PBFT in 2012 suggests that other species that

VISIT THE SCIENTIFIC PUBLICATIONS REPORT ARCHIVE

forage near Japan have a high probability of acquiring ^{134}Cs and ^{137}Cs, and the model in eq 2 could be applied to radiocesium data in other migratory species. However, the movement patterns and feeding habits of each study species while near Japan should be taken into account when utilizing this tracer, as PBFT are known to feed specifically in waters near Japan during their juvenile stage, making use of the Kuroshio Current before migrating eastward.[10,11,27] Complementary data (e.g., known life history patterns, electronic tagging, or other chemical tracers) may help interpret radiocesium tracer data in other highly migratory taxa.

Previous studies that measured radionuclides from the Bikini atoll weapons tests in the 1940s−1960s attempted to infer migration patterns of pelagic animals, including yellowfin tuna *T. albacares*[6] and albacore tuna *Thunnus alalunga*.[37−39] However, nuclear detonations led to extensive, widespread fallout from the atmosphere,[40] and results of those pioneering studies could only provide general, highly inferential results. In contrast, the Fukushima plant failure represents a more discrete point source of radionuclides. This unique attribute of Fukushima together with the unique migratory biology of PBFT (i.e., that all small PBFT in the CCLME must be migrants from Japan) provides an unprecedented opportunity to test and apply concentrations of anthropogenic radionuclides to trace animal movement.

Despite the assumptions and gaps in knowledge that result from the Fukushima accident and observations of radioisotopes in marine biota, these radiocesium data present a clear and coherent picture of PBFT migrations that can be interpreted unequivocally. The data shown here are the strongest results possible for the evaluation of radiocesium as a tracer in PBFT and validate its use for the study of large-scale Pacific migrations, as was suggested in 2011.[4] We expect this new tool to produce novel data on the recent migration patterns of keystone pelagic predators, which have been historically difficult to obtain.

■ ASSOCIATED CONTENT

Supporting Information

A description of the fish species (sampled near Japan) used to estimate initial ^{134}Cs:^{137}Cs ratios in fish off Japan around April 6th, 2012 and mean ^{134}Cs:^{137}Cs values of these fish, Table S1 showing error values for ^{134}Cs, ^{137}Cs, and ^{40}K measurements and calculated ^{134}Cs:^{137}Cs ratios, Table S2 with estimated time since departure for individual PBFT, and Figure S1 showing relationship between operculum length (OL) and curved fork length (CFL) used to estimate CFL from OL in PBFT. This material is available free of charge via the Internet at http://pubs.acs.org.

■ AUTHOR INFORMATION

Corresponding Author

*Phone: (831) 655-6240; fax: (831) 375-0793; e-mail: dmadigan@stanford.edu.

Notes

The authors declare no competing financial interest.

■ ACKNOWLEDGMENTS

We thank Cheng-Shiuan Lee and Shelagh Zegers for laboratory assistance, Masatoshi Sugeno for Japanese translation of articles, and Shin-ichi Ito and Motoyoshi Ikeda for assistance with interpretation of Japanese PBFT data. This research was supported by grants from the Gordon and Betty Moore Foundation and NOAA.

■ REFERENCES

(1) Buesseler, K. O.; Jayne, S. R.; Fisher, N. S.; Rypina, I. I.; Baumann, H.; Baumann, Z.; Breier, C. F.; Douglass, E. M.; George, J.; Macdonald, A. M.; Miyamoto, H.; Nishikawa, J.; Pike, S. M.; Yoshida, S. Fukushima-derived radionuclides in the ocean and biota off Japan. *Proc. Natl. Acad. Sci. U.S.A.* **2012**, *109* (16), 5984−5988.

(2) Buesseler, K. O.; Aoyama, M.; Fukasawa, M. Impacts of the Fukushima nuclear power plants on marine radioactivity. *Environ. Sci. Technol.* **2011**, *45* (23), 9931−9935.

(3) Buesseler, K. O. Fishing for answers off Fukushima. *Science* **2012**, *338* (6106), 480−482.

(4) Madigan, D. J.; Baumann, Z.; Fisher, N. S. Pacific bluefin tuna transport Fukushima-derived radionuclides from Japan to California. *Proc. Natl. Acad. Sci. U.S.A.* **2012**, *109* (24), 9483−9486.

(5) Block, B. A.; Jonsen, I. D.; Jorgensen, S. J.; Winship, A. J.; Shaffer, S. A.; Bograd, S. J.; Hazen, E. L.; Foley, D. G.; Breed, G. A.; Harrison, A. L.; Ganong, J. E.; Swithenbank, A.; Castleton, M.; Dewar, H.; Mate, B. R.; Shillinger, G. L.; Schaefer, K. M.; Benson, S. R.; Weise, M. J.; Henry, R. W.; Costa, D. P. Tracking apex marine predator movements in a dynamic ocean. *Nature* **2011**, *475*, 86−90.

(6) Suzuki, Z.; Tomlinson, P. K.; Honma, M. Population structure of Pacific yellowfin tuna. *Inter-Am. Trop. Tuna Comm., Bull.* **1978**, *17*, 277−358.

(7) Rooker, J. R.; Secor, D. H.; Metrio, G. D.; Schloesser, R.; Block, B. A.; Neilson, J. D. Natal homing and connectivity in Atlantic bluefin tuna populations. *Science* **2008**, *322* (5902), 742−744.

(8) Ramos, R.; González-Solís, J. Trace me if you can: The use of intrinsic biogeochemical markers in marine top predators. *Front. Ecol. Environ.* **2012**, *10* (5), 258−266.

(9) Bayliff, W. H. A review of the biology and fisheries for northern bluefin tuna, *Thunnus thynnus*, in the Pacific Ocean. *FAO Fish. Tech. Pap.* **1994**, *336*, 244−295.

(10) Inagake, D.; Yamada, H.; Segawa, K.; Okazaki, M.; Nitta, A.; Itoh, T. Migration of young bluefin tuna, *Thunnus orientalis* Temminck et Schlegel, through archival tagging experiments and its relation with oceanographic conditions in the Western North Pacific. *Bull. Natl. Res. Inst. Far Seas Fish.* **2001**, *38*, 53−81.

(11) Shimose, T.; Watanabe, H.; Tanabe, T.; Kubodera, T. Ontogenetic diet shift of age-0 year Pacific bluefin tuna *Thunnus orientalis*. *J. Fish Biol.* **2012**, DOI: 10.1111/j.1095-8649.2012.03483.x.

(12) Whitlock, R. E.; McAllister, M. K.; Block, B. A. Estimating fishing and natural mortality rates for Pacific bluefin tuna (*Thunnus orientalis*) using electronic tagging data. *Fish. Res.* **2012**, *119−120*, 115−127.

(13) Pacific Bluefin Stock Assessment; International Scientific Committee for Tuna and Tuna-like Species in the North Pacific Ocean, 2012. http://isc.ac.affrc.go.jp/pdf/Stock_assessment/Final_Assessment_Summary_PBF.pdf.

(14) Mathews, T.; Fisher, N. S. Dominance of dietary intake of metals in marine elasmobranch and teleost fish. *Sci. Total Environ.* **2009**, *407* (18), 5156−5161.

(15) Mathews, T.; Fisher, N. S.; Jeffree, R. A.; Teyssie, J. L. Assimilation and retention of metals in teleost and elasmobranch fishes following dietary exposure. *Mar. Ecol.: Prog. Ser.* **2008**, *360* (1), 1−12.

(16) Schaefer, K.; Fuller, D.; Block, B. Movements, behavior, and habitat utilization of yellowfin tuna (*Thunnus albacares*) in the northeastern Pacific Ocean, ascertained through archival tag data. *Mar. Biol.* **2007**, *152* (3), 503−525.

(17) Buesseler, K. O.; Casso, S. A.; Hartman, M. C.; Livingston, H. D. Determination of fission-products and actinides in the Black Sea following the Cherynobyl accident. *J. Radioanal. Nucl. Chem.* **1990**, *138* (1), 33−47.

(18) Currie, L. A. Limits for qualitative detection and quantitative determination. Application to radiochemistry. *Anal. Chem.* **1968**, *40* (3), 586−593.

VISIT THE SCIENTIFIC PUBLICATIONS REPORT ARCHIVE

(19) Bayliff, W. H.; Ishizuka, Y.; Deriso, R. Growth, movement, and attrition of northern bluefin tuna, *Thunnus thynnus*, in the Pacific Ocean, as determined by tagging. *Inter-Am. Trop. Tuna Comm., Bull.* **1991**, *20*, 3−94.

(20) Wild, A. A review of the biology and fisheries for yellowfin tuna, *Thunnus albacares*, in the Eastern Pacific Ocean. *FAO Fish. Tech. Pap.* **1994**, *336*, 52−107.

(21) Farwell, C. J. Based on a regression by C. Farwell. *Tuna Research and Conservation Center* **2000**, 1.

(22) Scida, P.; Rainosek, A.; Lowery, T. Length conversions for yellowfin tuna (*Thunnus albacares*) caught in the western North Atlantic Ocean. *Collect. Vol. Sci. Pap. ICCAT* **2001**, *52* (2), 528−532.

(23) IAEA. *Sediment Distribution Coefficients and Concentration Factors for Biota in the Marine Environment*. International Atomic Energy Agency: Vienna, Austria, 2004.

(24) Wang, W.-X.; Ke, C.; Yu, K. N.; Lam, P. K. S. Modeling radiocesium bioaccumulation in a marine food chain. *Mar. Ecol.: Prog. Ser.* **2000**, *208*, 41−50.

(25) Yamamoto, M.; Abe, T.; Kuwabara, J.; Komura, K.; Ueno, K.; Takizawa, Y. Polonium-210 and lead-210 in marine organisms: Intake levels for Japanese. *J. Radioanal. Nucl. Chem.* **1994**, *178* (1), 81−90.

(26) Fisher, N. S., Beaugelin-Seiller, K., Hinton, T. G., Baumann, Z., Madigan, D. J., &Garnier-LaPlace, J. An evaluation of radiation doses and associated risk from the Fukushima nuclear accident to marine biota and human consumers of seafood. *Proc. Natl. Acad. Sci. U.S.A.*, submitted.

(27) Kitagawa, T.; Kimura, S.; Nakata, H.; Yamada, H.; Nitta, A.; Sasai, Y.; Sasaki, H. Immature Pacific bluefin tuna, *Thunnus orientalis*, utilizes cold waters in the Subarctic Frontal Zone for trans-Pacific migration. *Environ. Biol. Fish.* **2009**, *84* (2), 193−196.

(28) *Results of the Inspection on Radioactivity Materials in Fisheries Products*; Japanese Ministry of Agriculture, Forestry, and Fisheries: Tokyo, 2011; http://www.jfa.maff.go.jp/e/inspection/index.html.

(29) Shimose, T.; Tanabe, T.; Chen, K.-S.; Hsu, C.-C. Age determination and growth of Pacific bluefin tuna, *Thunnus orientalis*, off Japan and Taiwan. *Fish. Res.* **2009**, *100* (2), 134−139.

(30) Nakano, M.; Povinec, P. P. Long-term simulations of the 137Cs dispersion from the Fukushima accident in the world ocean. *J. Environ. Radioact.* **2012**, *111*, 109−115.

(31) Childers, J.; Snyder, S.; Kohin, S. Migration and behavior of juvenile North Pacific albacore (*Thunnus alalunga*). *Fish. Oceanogr.* **2011**, *20* (3), 157−173.

(32) Nakano, H. Age reproduction and migration of blue shark in the North Pacific Ocean. *Bull. Natl. Res. Inst. Far Seas Fish.* **1994**, *31*, 141−256.

(33) Peckham, S. H.; Diaz, D. M.; Walli, A.; Ruiz, G.; Crowder, L. B.; Nichols, W. J. Small-scale fisheries bycatch jeopardizes endangered Pacific loggerhead turtles. *PLoS ONE* **2007**, *2* (10), e1041.

(34) Shaffer, S. A.; Tremblay, Y.; Weimerskirch, H.; Scott, D.; Thompson, D. R.; Sagar, P. M.; Moller, H.; Taylor, G. A.; Foley, D. G.; Block, B. A.; Costa, D. P. Migratory shearwaters integrate oceanic resources across the Pacific Ocean in an endless summer. *Proc. Natl. Acad. Sci. U.S.A.* **2006**, *103* (34), 12799−12802.

(35) Nagasawa, K. Predation by salmon sharks (*Lamna ditropis*) on Pacific salmon (*Oncorhynchus* spp.) in the North Pacific Ocean. *North Pac. Anadr. Fish Comm. Bull.* **1998**, *1*, 419−433.

(36) *Report of the Sub-Committee on Minke Whales*; International Whaling Commission: Cambridge, 1983; http://www.iwcoffice.org/annual-reports.

(37) Hodge, V. F.; Folsom, T. R.; Young, D. R. Retention of fall-out constituents in upper layers of the Pacific Ocean as estimated from studies of a tuna population. In *IAEA Symposium on the Interaction of Radioactive Contaminants with the Constituents of the Marine Environment*, Seattle, Washington, 1972.

(38) Young, D. R.; Folsom, T. R.; Hodge, V. F. ^{137}Cs and ^{40}K in the flesh of Pacific albacore, 1964−1974. *Health Phys.* **1975**, *29* (5), 689−694.

(39) Suda, A. Hoshano maguro (Tunas contaminated by radioactivity) (in Japanese). *Suisan Kenkyusha Kyogikai, Suisan Kagaku* **1956**, *6* (1), 16−22.

(40) Volchok, H. L., Bowen, V. T., Folsom, T. R., Broecker, W. S., Schuert, E. A., &Bien, G. S. Oceanic distributions of radionuclides from nuclear explosions. In *Radioactivity in the Marine Environment*; National Academy of Sciences: Washington, DC, 1971; pp 42−89.

VISIT THE SCIENTIFIC PUBLICATIONS REPORT ARCHIVE

Probability of taking a western North Pacific gray whale during the proposed Makah hunt

Jeffery E. Moore and David W. Weller

U.S. Department of Commerce
National Oceanic and Atmospheric Administration
National Marine Fisheries Service

NOAA Technical Memorandum NMFS-SWFSC-506
January 2013

VISIT THE SCIENTIFIC PUBLICATIONS REPORT ARCHIVE

Probability of taking a western North Pacific gray whale during the proposed Makah hunt

Jeffery E. Moore and David W. Weller

Protected Resources Division
Southwest Fisheries Science Center
National Marine Fisheries Service
National Oceanic and Atmospheric Administration
8901 La Jolla Shores Drive
La Jolla, CA 92037-1022 USA

U.S. Department of Commerce
Gary Locke, Secretary

National Oceanic and Atmospheric Administration
Jane Lubchenco, Ph.D., Administrator

National Marine Fisheries Service
Eric C. Schwaab, Assistant Administrator for Fisheries

VISIT THE SCIENTIFIC PUBLICATIONS REPORT ARCHIVE

ABOUT THIS DOCUMENT

The mission of the National Oceanic and Atmospheric Administration (NOAA) is to understand and predict changes in the Earth's environment and to conserve and manage coastal and oceanic marine resources and habitats to help meet our Nation's economic, social, and environmental needs. As a branch of NOAA, the National Marine Fisheries Service (NMFS) conducts or sponsors research and monitoring programs to improve the scientific basis for conservation and management decisions. NMFS strives to make information about the purpose, methods, and results of its scientific studies widely available. NMFS Southwest Fisheries Science Center uses the **NOAA Technical Memorandum NMFS** series to achieve timely dissemination of scientific and technical information that is of high quality but inappropriate for publication in the formal peer-reviewed literature. The contents are of broad scope, including technical workshop proceedings, large data compilations, status reports and reviews, lengthy scientific or statistical monographs, and more. NOAA Technical Memoranda published by the Southwest Fisheries Science Center although informal, are subjected to extensive review and editing and reflect sound professional work. Accordingly, they may be referenced in the formal scientific and technical literature.

A **NOAA Technical Memorandum NMFS** issued by the Southwest Fisheries Science Center may be cited in following manner:

Moore, J.E. and Weller, D.W. 2013. Probability of taking a western North Pacific gray whale during the proposed Makah hunt. U.S. Dep. Commer., NOAA Tech. Memo. NMFS-SWFSC-506, 13 p.

A copy of this report may be obtained from:
Protected Resources Division
Southwest Fisheries Science Center
National Marine Fisheries Service
National Oceanic and Atmospheric Administration
8901 La Jolla Shores Drive
La Jolla, CA 92037-1022 USA

ACKNOWLEDGEMENTS

We are grateful to the Alaska Fisheries Science Center, Cascadia Research Collective, International Whaling Commission, National Marine Mammal Laboratory, NOAA Northwest Regional Office, Southwest Fisheries Science Center for their contributions and support of this work. We thank Jeff Laake for providing data and significant insight and advice on how to approach the analysis. We also extend our appreciation to John Brandon, Bob Brownell, John Calambokidis, Greg Donovan, Aimee Lang, Andre Punt and Jon Scordino for their input.

VISIT THE SCIENTIFIC PUBLICATIONS REPORT ARCHIVE

EXECUTIVE SUMMARY

Recent observations of gray whales (*Eschrichtius robustus*) identified in the western North Pacific (WNP) migrating to areas off the coast of North America (Alaska to Mexico) raise concern about the possibility of the small western population being subjected to the gray whale hunt proposed by the Makah Indian Tribe in northern Washington, USA. To address this concern, we estimated the probability of striking (i.e. killing or seriously injuring) a WNP whale during the Makah hunt using six models from 4 model sets that varied based on the assumptions and types of data used for estimation. Model set 1 used WNP and ENP abundance estimates. Model set 2 used these abundance estimates, as well as sightings data from the proposed hunt area. Model sets 3 and 4 used only the sightings data. Within model sets 1 and 2, two models (A and B) differed based upon whether migrating ENP and WNP whales were assumed to be equally available to the hunt per capita (A) or whether this assumption is relaxed (B). We consider Model 2B the most plausible of all models because model set 2 makes use of all available information and 2B contains fewer assumptions than 2A. Based on model 2B, the probability of striking ≥1 WNP whale in a single season ranges from 0.007 to 0.036, depending on if the median or upper 95th percentile estimate is used and on which maximum is used for the total number of whales struck. The probability of striking ≥1 WNP whale out of 5 seasons ranges from 0.036 to 0.170 across the same scenarios. The expected number to be struck in a single year ranges from 0.01 to 0.04 and from 0.04 to 0.19 across 5 years. For context, these strike estimates were compared to different possible values of Potential Biological Removal (PBR). We also summarized analogous estimates for the number of WNP whales that would be "taken" non-lethally, in terms of the number of attempted but unsuccessful strikes as well as the number of animals approached and pursued during the hunt.

VISIT THE SCIENTIFIC PUBLICATIONS REPORT ARCHIVE

INTRODUCTION

Gray whales (*Eschrichtius robustus*) are recognized as comprising two populations in the North Pacific Ocean. Significant mitochondrial and nuclear genetic differences have been found between whales in the western North Pacific (WNP) and those in the eastern North Pacific (ENP) (Lang *et al*., 2011). The ENP population ranges from wintering areas in Baja California, Mexico, to feeding areas in the Bering, Beaufort, and Chukchi Seas (Fig. 1). An exception to this generality is the relatively small number (100s) of whales that summer and feed along the Pacific coast between Kodiak Island, Alaska, and northern California (Calambokidis *et al*. 2012). These whales are collectively called the Pacific Coast Feeding Group (PCFG). U.S. domestic policy defines the PCFG as gray whales observed between 1 June and 30 November from Northern California through Northern British Columbia. The International Whaling Commission (IWC) has refined this definition to be: PCFG whales are those observed between 1 June and 30 November from 41°N to 52°N in two or more years (IWC, 2012). The WNP population feeds in the Okhotsk Sea off Sakhalin Island, Russia (Weller *et al*., 1999; Weller *et al*. 2012), and in nearshore waters of the southwestern Bering Sea off the southeastern Kamchatka Peninsula (Tyurneva *et al*., 2010).

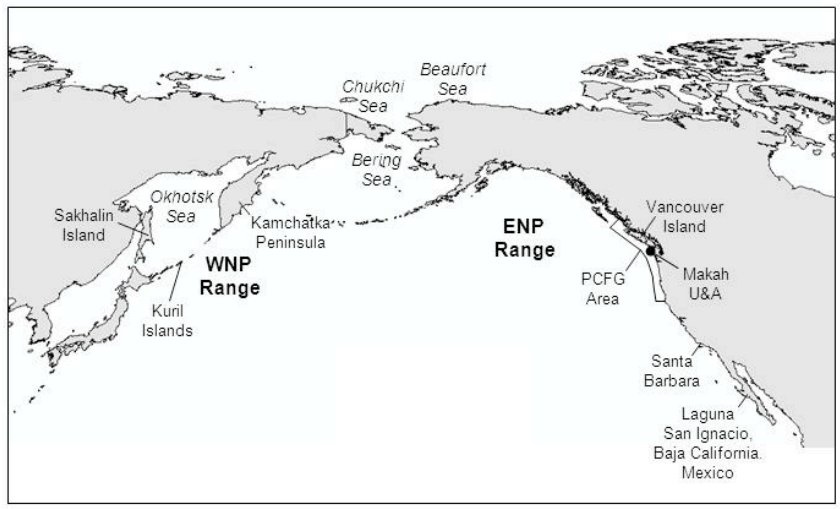

Figure 1. Areas in the western and eastern North Pacific mentioned in the report.

The historical distribution of gray whales in the Okhotsk Sea greatly exceeded what is found today (Reeves *et al*., 2008). Whales associated with the Sakhalin feeding area can be absent for all or part of a given feeding season (Bradford *et al*., 2008), indicating they use other areas during the summer and fall feeding period. Some of the whales identified feeding in the coastal waters off Sakhalin, including reproductive females and calves, have also been documented off the southern and eastern coast of Kamchatka (Tyurneva *et al*., 2010). Whales observed off Sakhalin have also been sighted off the northern Kuril Islands in the eastern Okhotsk Sea and Bering Island in the western Bering Sea (Weller *et al*., 2003).

Recently, mixing of whales identified in the WNP and ENP has been observed (Weller *et al*., 2012). Lang (2010) reported that two adult individuals from the WNP, sampled off Sakhalin in 1998 and 2004, matched the microsatellite genotypes, mtDNA haplotypes, and sexes (one male,

VISIT THE SCIENTIFIC PUBLICATIONS REPORT ARCHIVE

one female) of two whales sampled off Santa Barbara, California in March 1995. Mate and colleagues (Mate *et al*., 2011) satellite-tracked three whales from the WNP to the ENP (Mate *et al*., 2011; IWC, 2012). Finally, photographic matches between the WNP and ENP, including resightings between Sakhalin and Vancouver Island and Laguna San Ignacio, have further confirmed use of areas in the ENP by whales identified in the WNP (Weller *et al*., 2012, Urbán *et al*., 2012). Despite this level of mixing, significant mtDNA and nuclear genetic differences between whales in the WNP and ENP have been found (Lang *et al*., 2011).

Observations of gray whales identified in the WNP migrating to areas off the coast of North America (Alaska to Mexico) raise concern about placing the WNP population at potential risk of being harmed or killed incidental to the ENP gray whale hunt proposed by the Makah Indian Tribe off northern Washington, USA (IWC, 2012). Given the ongoing concern about conservation of the WNP population, in 2011 the Scientific Committee of the International Whaling Commission (IWC) emphasized the need to estimate the probability of a western gray whale being killed during aboriginal gray whale hunts (IWC, 2012). Additionally, NOAA is required to prepare an Environmental Impact Statement (EIS) pertaining to the Makah's request for a waiver under the U.S. Marine Mammal Protection Act (MMPA) in order to hunt gray whales (NOAA, 2008). The EIS will include an estimate of the likelihood of Makah hunters approaching, pursuing, and attempting to strike a WNP whale in addition to the likelihood of actual strikes (assumed to result in death or serious injury).

The objective of this analysis was therefore to estimate the probability that one or more whales identified in the WNP might be lethally or non-lethally "taken[1]" during the hunt proposed by the Makah Indian Tribe. This report updates the analysis of mortality risk provided by Moore and Weller (2012), by incorporating feedback from the IWC Scientific Committee on that report and by including an analysis of the likelihood of non-lethal as well as lethal take.

METHODS

The probability of striking or taking a WNP whale during the proposed Makah hunt was estimated using four different sets of models (6 models total). Models were based on the following information: (1) the most recent estimates of WNP and ENP population abundance; (2) sightings data from spring 1999-2010 off the coast of northern Washington (NWA) in the Makah Usual and Accustomed (MUA) fishing grounds, where the proposed hunt would take place; and (3) minimum estimates of the proportion of the WNP population that migrate to ENP areas along the North American coast.

Data

Abundance estimates

The most recent WNP abundance estimate (for 2012) is 155, with 95% CI = 142 – 165 (IUCN, 2012). The most recent ENP estimate (for 2007) is 19,126, with CV = 0.071 (Laake *et al*., 2009). In the models, these estimates were expressed as log-normally distributed random variables with parameters $\mu_{WNP} = 5.043$, $\sigma_{WNP} = 0.0387$, and $\mu_{ENP} = 9.856$, $\sigma_{ENP} = 0.0709$.

[1] Under the U.S. Marine Mammal Protection Act, "take" is defined as "harass, hunt, capture, kill or collect, or attempt to harass, hunt, capture, kill or collect."

VISIT THE SCIENTIFIC PUBLICATIONS REPORT ARCHIVE

Sightings in the Makah Usual and Accustomed (MUA) Fishing Grounds
During spring surveys (1 March to 31 May) in 1999-2009, there were 118 "whale-days" in the MUA off the NWA coast (Calambokidis *et al*., 2012), where all sightings of an individual on a particular day collectively count as 1 "whale-day" (e.g., multiple sightings of the same individual on the same day count as just 1 whale-day, but the same individual seen the next day would count as a second whale-day). There were 9 gray whale sightings in March. All other sightings were in April or May. None of the 118 whale-days observed included WNP whales[2]; 35 (29.7%) were considered "Pacific Coast Feeding Group" (PCFG) whales; and the rest (83, or 70.3%) were assumed to be migrating ENP whales. The photo-identification catalog for whales identified in the WNP off Sakhalin Island is characterized by extremely high (> 95%) resighting rates since 2002 (Burdin *et al*., 2012). Therefore, we assumed in this analysis that the absence of WNP sightings is not likely due to false negative identification (although it is possible that WNP whales were missed during days when MUA surveys were or were not conducted).

Proportion of WNP whales migrating with ENP whales
The proportion of the WNP population that migrates along the North American coast is unknown but based on recent photo-identification, telemetry, and genetic matches of WNP whales to ENP areas, we estimate the value to be at least 0.15, based on there being 23 known matches out of an estimated population size of 155 (Mate *et al*., 2011; IWC, 2012; Urbán *et al*., 2012; Weller *et al*. 2012).

Models
Model set 1
Model set 1 makes use of the ENP and WNP abundance estimates but ignores information obtained from sightings in the MUA off the NWA coast. The potential justification for ignoring the sightings data is that these may not be representative of the whale compositions that would be encountered by hunters, perhaps because of a timing mismatch (if hunt does not occur in April/May) or if whales approached by field researchers in motorized boats behave fundamentally differently than those approached by hunters in non-motorized boats.

Model 1A - All whales migrating through the MUA area -- WNP and ENP -- are assumed to be equally available to the hunt, so that the probability of taking a WNP whale is:

$$P_{WNP} = mN_{WNP}/N_{ENP}$$
$$m \sim \text{uniform}(0.15, 1)$$
$$N_{WNP} \sim \text{log-normal}\ (\mu_{WNP}, \sigma_{WNP})$$
$$N_{ENP} \sim \text{log-normal}\ (\mu_{ENP}, \sigma_{ENP}),$$

where m is the proportion of WNP whales that migrate with ENP whales along the North American coast and abundance parameters are as above (see Data section). The lower limit for m, 0.15, is based on genetic and photo-identification matching data (see Data section). The upper limit of 1 for m is precautionary, as the true value is unknown but could be high. We used Monte Carlo simulation based on drawing 100,000 random samples from the above distributions to estimate the distribution for P_{WNP}.

Model 1B – Rather than assuming P_{WNP} to be directly proportional to the ratio of abundances (N_{WNP}/N_{ENP}), we express our uncertainty in P_{WNP} as a uniform distribution with the upper limit

[2] Although not in the MUA, Weller *et al*. 2012 report observing three WNP whales on 2 May 2004 and three more on 25 April 2008 near Barkley Sound off the west coast of southern Vancouver Island, British Columbia, Canada.

VISIT THE SCIENTIFIC PUBLICATIONS REPORT ARCHIVE

for P_{WNP} based on the maximum (99th percentile) estimate for the number of WNP whales available to the hunt divided by a minimum (1st percentile) estimate for the ENP population, i.e.,

$$P_{WNP} \sim \text{uniform}(0, P_{max})$$
$$P_{max} = m \cdot N_{99,WNP}/N_{01,ENP}.$$

The interpretation of this model is that, within some plausible upper bound (defined as P_{max}), we have no information about the per capita probability of taking a WNP whale, given unknown differences in migration patterns between WNP and ENP animals. Just as for Model 1A, we use a Monte Carlo approach (100,000 samples) to estimate a distribution for P_{WNP}. For each sample, P_{WNP} is drawn from the uniform distribution specified by P_{max}. P_{max} varies with each sample based on the draw for m, while the ratio $N_{99,WNP}/N_{01,ENP}$ is fixed. Analysis for Model set 1 was conducted in R.

Model set 2

Model sets 2, 3, and 4 differ from Model set 1 in that they use the information from the sightings data in the MUA. In these models, it is assumed that the sightings data from the MUA are representative of the composition of whales (three groups: ENP, WNP, PCFG) that would be available to the hunt. In other words, whales that are most likely to be photographed (i.e., approachable in a small boat) are also the most likely to be approached by hunters.

Model set 2 makes use of the MUA sightings data, as well as WNP and ENP abundance estimates. WNP whales are assumed to be moving with the ENP migrants, so that the marginal probability of a WNP whale being taken is the probability of being a migrant, P_{mig} (i.e., probability of not being a whale from the PCFG), multiplied by the conditional probability of being a WNP whale given that it is a migrant ($P_{WNP|mig}$), i.e., $P_{WNP} = P_{mig}P_{WNP|mig}$. P_{mig} is estimated using Bayesian MCMC methods assuming that $n_{mig} \sim$ Binomial (N, P_{mig}), where n_{mig} is the number of non-PCFG migrants (83) out of N (118) sightings in the MUA sightings data set. Models 2A and 2B differ in how the conditional probability $P_{WNP|mig}$ is estimated.

<u>Model 2A</u> - The distribution for $P_{WNP|mig}$ is given by the estimator for P_{WNP} in Model 1A. Thus, it is assumed the per capita probabilities of an ENP or WNP whale being taken are the same.

<u>Model 2B</u> - The distribution for $P_{WNP|mig}$ is given by the estimator for P_{WNP} in 1B. Thus, this model asserts that we have no information (apart from specifying a reasonable upper bound) about the per capita likelihood of a WNP whale being killed relative to that of an ENP whale.

Model 3

This uses the MUA sightings data but does not make use of information about WNP population size or the proportion of WNP whales that migrate with ENP whales. Thus, P_{WNP} estimates are solely based on the proportion of animals in the MUA sightings data set that are from the WNP. The posterior distribution for P_{WNP} is estimated using MCMC methods assuming that $n_{WNP} \sim$ Binomial (N, P_{WNP}), where $n_{WNP} = 0$, and N = 118. The justification for this model (i.e., for ignoring information about WNP abundance) would be that the relative per capita probability of taking WNP vs. ENP animals is totally unknown apart from the information contained in the sightings data set. For example, WNP whales could be much more (or less) available to the hunt than ENP whales due to differences in migration timing or behavior, such that our knowledge about the WNP population being very small is irrelevant to the estimates.

VISIT THE SCIENTIFIC PUBLICATIONS REPORT ARCHIVE

Model 4
Model 4 is a variant of Model 3, explained below.

Bayesian estimation
Analyses for Models 2, 3, and 4 were conducted in WinBUGS. Posterior distributions for parameters were summarized from two MCMC chains, each 50,000 samples in length (100,000 samples total) following a burn-in of 20,000 samples. These simple models converged quickly and clearly (chains well mixed) in all cases (Fig. 2). A uniform [0, 1] prior was used for P_{mig} in model set 2 and for P_{WNP} in model 3 and 4; these are the only parameters for which the prior is updated by data (the MUA sightings data) to obtain a new posterior. The posterior distributions for $P_{WNP|mig}$ in Models 2A and 2B were not informed by the sightings data and thus are essentially determined by informative priors given by the above estimators for these parameters.

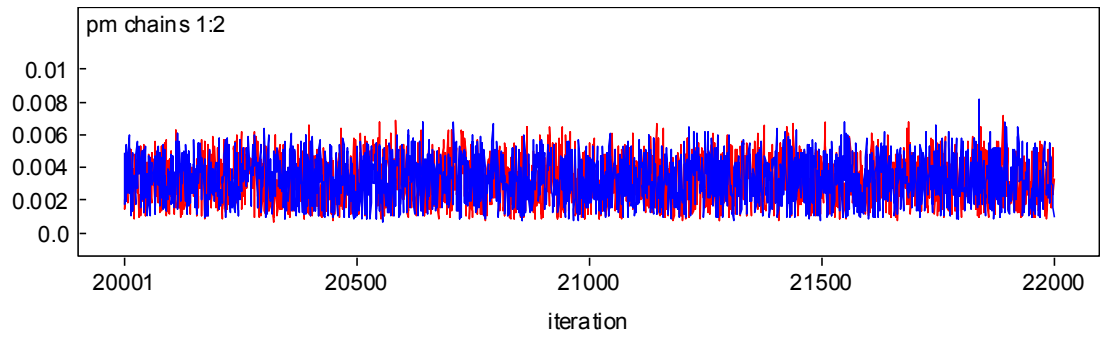

Figure. 2. Example from Model 2A of two MCMC chains (red and blue) mixing for the parameter P_{WNP}.

Estimated parameters
Based on estimates of P_{WNP} for each model, we calculated the probability of striking at least one WNP whale (i.e., P(x>0)) out of X total strikes (strikes are treated as lethal takes), the probability of non-lethally taking at least one WNP whale out of Y strike attempts (P(y>0)), or the probability of non-lethally taking at least one WNP whale out of Z approaches (P(z>0)). We also estimated the expected number of WNP takes out of X, Y or Z total takes. These are calculated as follows:

$$P(x > 0) = 1 - (1 - P_{WNP})^X$$
$$P(y > 0) = 1 - (1 - P_{WNP})^Y$$
$$P(z > 0) = 1 - (1 - P_{WNP})^Z$$
$$E(x) = P_{WNP}X$$
$$E(y) = P_{WNP}Y$$
$$E(z) = P_{WNP}Z$$

For model sets 1, 2, and 3, let X = X* = 5, 7, 20, and 35 gray whale strikes. These were based on the description of the Makah Tribe's proposed gray whale hunt (IWC, 2012 Annex D), which states the following: 5 is the maximum allowable number of landed whales per year; 7 is the maximum number of struck whales allowed per year; 20 is the maximum number allowed to be landed over a 5-year period; and 35 is the maximum number that could be struck over a 5-year period.

VISIT THE SCIENTIFIC PUBLICATIONS REPORT ARCHIVE

For model sets 1, 2, and 4, let X = X** = 3 or 4 strikes in one year and 15 or 20 strikes in 5 years of *non-PCFG whales*. The justification for considering this scenario is that, given other management measures within the Makah plan – most importantly the provision to cease the annual hunt if a certain number of PCFG whales are struck – it may be unlikely that the maximum strike limits in the proposal will be achieved. Implementation trials conducted by the Aboriginal Whaling Management Procedure (AWMP) subgroup of the IWC scientific committee suggest that, when management measures are considered, the expected number of strikes per year *to non-PCFG whales* would typically be between 3 and 4 (J. Scordino, pers. comm.).

For Model set 1, estimates for when X = X** are calculated the same as for when X = X*. For Model set 2, since it is given that X** are for *non-PCFG* whales (i.e., migrant whales), then it follows that $P_{mig} = 1$, so the model 2 estimators for P_{WNP} reduce from $P_{mig}P_{WNP|mig}$ to just $P_{WNP|mig}$, which are the same estimators as for Model set 1. When X = X**, we use Model 4 as a variant of Model 3 (which is for X = X*). In Model 3, $n_{WNP} \sim$ Binomial (N_{tot}, P_{WNP}), where $n_{WNP} = 0$, and $N_{tot} = 118$ total whale-day sightings, 35 of which were PCFG whales and 83 of which were migrating ENP whales. In Model 4, $n_{WNP} \sim$ Binomial (N_{mig}, $P_{WNP|mig}$), where $N_{mig} = 83$ whale-day sightings of non-PCFG migrant whales (i.e., we are only evaluating conditional probability of being a WNP whale given being migrant whale.

Values of Y for each model were calculated as 4X, and values for Z were calculated as 20X. In other words, for every struck whale, there are an estimated 4 strike attempts and 20 whales approached in attempt to strike. These numbers are based on the Makah tribe's experience in the 1999 and 2000 hunts, for which they stated that for every struck whale, there would be approximately 4 attempted strikes and 10 individuals pursued, which are assumed to affect 20 whales, given an average pod size of two whales (NOAA, 2008).

Comparison to Potential Biological Removal (PBR)

To contextualize the Table 1 estimates of lethal takes, we provide 5-year estimates of PBR[3]) for comparison. PBR is conventionally calculated as $0.5R_{max}N_{min}F_R$, where R_{max} is the maximum productivity rate estimate for the population (we used 0.062 based on the 2012 Draft Stock Assessment Report; NMFS, 2012), N_{min} is the 20th percentile abundance estimate (we used 150 based on WNP abundance parameters), and F_R is a recovery factor. We provide PBR estimates for $F_R = 0.1$, 0.5, and 1.0. $F_R = 0.1$ is typically used for stocks of endangered species, noting that the WNP gray whale stock is listed as Endangered under the U.S. Endangered Species Act and Critically Endangered on the IUCN Red List. $F_R = 0.5$ is a recommended default for most stocks (NMFS 2005), whereas $F_R = 1.0$ may be appropriate for stocks with known and favorable population status. The PBR estimate is also supposed to take into the account (be discounted by) the proportion of the stock using US waters and the proportion of time it is there (NMFS, 2005). The proportion of the WNP migrating in the ENP range is unknown but characterized in our models by a uniform (0.15, 1) distribution. The proportion of time spent in US waters is difficult to estimate for migratory animals but is probably on the order of 3 months or 0.25 years. Thus, for each value of F_R, we calculated a distribution for the 5-year PBR estimate, by multiplying the standard equation by 0.25 and by a uniform (0.15, 1) distribution.

[3] Under the U.S. Marine Mammal Protection Act, PBR level is defined as "the maximum number of animals, not including natural mortalities, that may be removed from a marine mammal stock while allowing that stock to reach or maintain its optimum sustainable population."

VISIT THE SCIENTIFIC PUBLICATIONS REPORT ARCHIVE

a b

RESULTS

Take estimates

Estimated parameters from all model sets are in Tables 1 – 3. Table 1 presents estimates for the probability of striking a WNP whale during a single strike event (P_{WNP}), and of striking at least one WNP whale (P(x>0)) and the expected number of WNP whales (E(x)) that would be struck given X = X* (number of gray whales struck) or X** (number of *non-PCFG* whales struck). Table 2 presents the analogous estimates for the number of attempted strikes (Y = Y* or Y**), and Table 3 presents the analogous estimates for the number of whales approached (Z = Z* or Z**). We present median estimates and, for precautionary purposes, 95th percentile estimates from the Monte Carlo or Bayesian posterior distributions.

For X = X*, Y = Y*, and Z = Z* (i.e., out of the total number of events affecting gray whales, irrespective of the putative stock affected), parameter estimates were higher for Model set 1 than Model set 2. Within these models sets, median parameter estimates were higher for version A than B, although upper (95th percentile) estimates were similar. Estimates for Model 3 were higher than for the other models, particularly when looking at upper bound (95th percentile) estimates, because of the highly skewed and unconstrained posterior for P_{WNP} (Fig. 3).

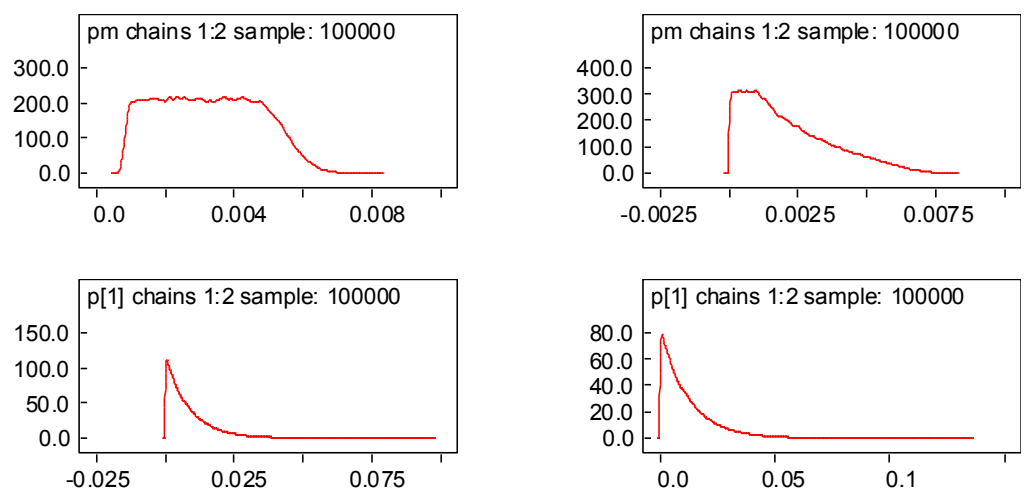

Figure 3. Comparison of Bayesian posterior distributions for P_{WNP} for Models 2A (a), 2B (b), 3 (c), and 4 (d).

For X = X**, Y = Y**, Z = Z** (i.e., out of the total number of events affecting *non-PCFG* whales), model set 1 and model set 2 results are the same (because the estimators are the same), but median estimates were higher for version A than B in these model sets (although 95th percentile estimates were similar). Estimates for Model 4 were higher than for the other models.

In Tables 1 – 3, we highlight (bold) estimates from Model 2B because Model set 2 makes the greatest use of available information (i.e., uses all datasets), and model 2B is based on fewer assumptions than 2A, and thus we favor Model 2B estimates as the most plausible (see Discussion). Estimates from this model for the proposed 5-year hunt period are as follows. The median (and 95th percentile) probability of striking a WNP whale within the 5-year permit period

VISIT THE SCIENTIFIC PUBLICATIONS REPORT ARCHIVE

ranged from 0.036 (0.107) to 0.058 (0.170) as X increased from 15 *non-PCFG* whales to 35 whales of any putative stock, and the expected number of whales that would be struck ranged from 0.04 (0.11) to 0.06 (0.19). The probability of an attempted strike on a WNP whale ranged from 0.136 (0.365) to 0.212 (0.524), and the expected number of attempts on WNP whales ranged from 0.15 (0.45) to 0.24 (0.74). Finally, the probability that a WNP whale would be pursued or approached by a hunter ranged from 0.519 (0.897) to 0.697 (0.976), and the expected number of WNP whales that would be approached ranged from 0.73 (2.26) to 1.19 (3.70).

In summary, we estimate based on Model 2B a fairly high probability that at least one WNP would be taken in the broadest sense of being pursued or approached by Makah hunters (i.e., P(z>0) = 0.52 – 0.98, depending on Z and whether the median or upper estimate is used). The probability of an attempted strike on least one WNP whale in 5 years was relatively moderate (i.e., P(y>0) = 0.14 – 0.52). The probability of actually striking at least one WNP whale during the 5-year period was relatively low but non-trivial (i.e., P(z>0) = 0.04 – 0.17).

Table 1. Summary statistics for six models from four model sets. P_{WNP} is probability of taking (striking) a WNP whale during a given take event. $P(x>0)_X$ are probabilities of striking at least 1 WNP whale out of X events. $E(x)_X$ is the expected number of struck WNP whales out of X total events. X=X** indicates that events are known to affect *non-PCFG* whales (otherwise X = X*, the number of events to gray whales in general). Cell entries are median and upper (95th percentile) probabilities.

	Model 1A	Model 1B	Model 2A	**Model 2B**	Model 3	Model 4
P_{WNP}	0.005 (0.008)	0.002 (0.008)	for X = X* 0.003 (0.006) for X = X** 0.005 (0.007)	**for X = X*** **0.002 (0.005)** **for X = X**** **0.002 (0.008)**	0.006 (0.025)	0.008 (0.035)
1 year						
$P(x>0)_{3**}$	0.014 (0.024)	0.007 (0.023)	0.014 (0.023)	**0.007 (0.022)**	NA	0.024 (0.102)
$P(x>0)_{4**}$	0.018 (0.031)	0.010 (0.030)	0.018 (0.031)	**0.010 (0.030)**	NA	0.033 (0.134)
$P(x>0)_5$	0.023 (0.039)	0.012 (0.037)	0.016 (0.028)	**0.008 (0.026)**	0.029 (0.119)	NA
$P(x>0)_7$	0.032 (0.054)	0.017 (0.052)	0.022 (0.039)	**0.012 (0.036)**	0.040 (0.162)	NA
$E(x)_{3**}$	0.01 (0.02)	0.01 (0.02)	0.01 (0.02)	**0.01 (0.02)**	NA	0.03 (0.11)
$E(x)_{4**}$	0.02 (0.03)	0.01 (0.03)	0.02 (0.03)	**0.01 (0.03)**	NA	0.03 (0.14)
$E(x)_5$	0.02 (0.04)	0.01 (0.04)	0.02 (0.03)	**0.01 (0.03)**	0.03 (0.13)	NA
$E(x)_7$	0.03 (0.06)	0.02 (0.05)	0.02 (0.04)	**0.01 (0.04)**	0.04 (0.18)	NA
5 year						
$P(x>0)_{15**}$	0.067 (0.113)	0.036 (0.108)	0.067 (0.112)	**0.036 (0.107)**	NA	0.117 (0.416)
$P(x>0)_{20**}$	0.089 (0.147)	0.048 (0.141)	0.089 (0.146)	**0.048 (0.141)**	NA	0.152 (0.512)
$P(x>0)_{20}$	0.089 (0.147)	0.048 (0.141)	0.063 (0.106)	**0.034 (0.101)**	0.110 (0.397)	NA
$P(x>0)_{35}$	0.151 (0.244)	0.082 (0.233)	0.107 (0.178)	**0.058 (0.170)**	0.185 (0.587)	NA
$E(x)_{15**}$	0.07 (0.12)	0.04 (0.11)	0.07 (0.12)	**0.04 (0.11)**	NA	0.12 (0.53)
$E(x)_{20**}$	0.09 (0.16)	0.05 (0.15)	0.09 (0.16)	**0.05 (0.15)**	NA	0.17 (0.70)
$E(x)_{20}$	0.09 (0.16)	0.05 (0.15)	0.06 (0.11)	**0.03 (0.11)**	0.12 (0.50)	NA
$E(x)_{35}$	0.16 (0.28)	0.09 (0.26)	0.11 (0.20)	**0.06 (0.19)**	0.20 (0.87)	NA

VISIT THE SCIENTIFIC PUBLICATIONS REPORT ARCHIVE

Table 2. Summary statistics for six models from four model sets. P_{WNP} is probability of taking (attempted strike) a WNP whale during a given take event. $P(y>0)_Y$ are probabilities of attempting to strike at least 1 WNP whale out of Y events. $E(y)_Y$ is the expected number of attempted-struck WNP whales out of Y total events. Y=Y** indicates that events are known to affect *non-PCFG* whales (otherwise Y = Y*, the number of events to gray whales in general). Cell entries are median and upper (95th percentile) probabilities.

	Model 1A	Model 1B	Model 2A	**Model 2B**	Model 3	Model 4
P_{WNP}	0.005 (0.008)	0.002 (0.008)	for Y = Y 0.003 (0.006) for Y = Y* 0.005 (0.007)	**for Y = Y** **0.002 (0.005)** **for Y = Y*** **0.002 (0.008)**	0.006 (0.025)	0.008 (0.035)
1 year						
$P(y>0)_{12**}$	0.054 (0.091)	0.029 (0.087)	0.054 (0.090)	**0.029 (0.087)**	NA	0.094 (0.349)
$P(y>0)_{16**}$	0.072 (0.120)	0.039 (0.114)	0.072 (0.119)	**0.038 (0.114)**	NA	0.124 (0.436)
$P(y>0)_{20}$	0.089 (0.147)	0.048 (0.141)	0.063 (0.106)	**0.034 (0.101)**	0.110 (0.397)	NA
$P(y>0)_{28}$	0.122 (0.200)	0.066 (0.192)	0.086 (0.145)	**0.047 (0.138)**	0.151 (0.507)	NA
$E(y)_{12**}$	0.06 (0.10)	0.03 (0.09)	0.06 (0.09)	**0.03 (0.09)**	NA	0.10 (0.42)
$E(y)_{16**}$	0.07 (0.13)	0.04 (0.12)	0.07 (0.13)	**0.04 (0.12)**	NA	0.13 (0.56)
$E(y)_{20}$	0.09 (0.16)	0.05 (0.15)	0.06 (0.11)	**0.03 (0.11)**	0.12 (0.50)	NA
$E(y)_{28}$	0.13 (0.22)	0.07 (0.21)	0.09 (0.16)	**0.05 (0.15)**	0.16 (0.70)	NA
5 year						
$P(y>0)_{60**}$	0.244 (0.380)	0.137 (0.366)	0.243 (0.377)	**0.136 (0.365)**	NA	0.391 (0.883)
$P(y>0)_{80**}$	0.311 (0.472)	0.178 (0.455)	0.310 (0.468)	**0.178 (0.454)**	NA	0.484 (0.943)
$P(y>0)_{80}$	0.311 (0.472)	0.178 (0.455)	0.228 (0.360)	**0.127 (0.346)**	0.373 (0.877)	NA
$P(y>0)_{140}$	0.479 (0.673)	0.291 (0.655)	0.364 (0.543)	**0.212 (0.524)**	0.558 (0.971)	NA
$E(y)_{60**}$	0.28 (0.48)	0.15 (0.45)	0.28 (0.47)	**0.15 (0.45)**	NA	0.49 (2.11)
$E(y)_{80**}$	0.37 (0.64)	0.20 (0.61)	0.37 (0.63)	**0.20 (0.60)**	NA	0.66 (2.82)
$E(y)_{80}$	0.37 (0.64)	0.20 (0.61)	0.26 (0.45)	**0.14 (0.42)**	0.47 (2.00)	NA
$E(y)_{140}$	0.65 (1.11)	0.34 (1.06)	0.45 (0.78)	**0.24 (0.74)**	0.82 (3.49)	NA

VISIT THE SCIENTIFIC PUBLICATIONS REPORT ARCHIVE

Table 3. Summary statistics for six models from four model sets. P_{WNP} is probability of taking (approaching) a WNP whale during a given take event. $P(z>0)_Z$ are probabilities of approaching at least 1 WNP whale out of Z events. $E(z)_Z$ is the expected number of approached WNP whales out of Z total events. Z=Z** indicates that events are known to affect *non-PCFG* whales (otherwise Z = Z*, the number of events to gray whales in general). Cell entries are median and upper (95th percentile) probabilities.

	Model 1A	Model 1B	Model 2A	**Model 2B**	Model 3	Model 4
P_{WNP}	0.005 (0.008)	0.002 (0.008)	for Z = Z 0.003 (0.006) for Z = Z* 0.005 (0.007)	**for Z = Z 0.002 (0.005) for Z = Z* 0.002 (0.008)**	0.006 (0.025)	0.008 (0.035)
1 year						
$P(z>0)_{60**}$	0.244 (0.380)	0.137 (0.366)	0.243 (0.377)	**0.136 (0.365)**	NA	0.391 (0.883)
$P(z>0)_{80**}$	0.311 (0.472)	0.178 (0.455)	0.310 (0.468)	**0.178 (0.455)**	NA	0.484 (0.943)
$P(z>0)_{100}$	0.373 (0.550)	0.218 (0.532)	0.276 (0.428)	**0.157 (0.412)**	0.442 (0.920)	NA
$P(z>0)_{140}$	0.479 (0.673)	0.291 (0.655)	0.364 (0.543)	**0.212 (0.524)**	0.558 (0.971)	NA
$E(z)_{60**}$	0.28 (0.48)	0.15 (0.45)	0.28 (0.47)	**0.15 (0.45)**	NA	0.49 (2.11)
$E(z)_{80**}$	0.37 (0.64)	0.20 (0.61)	0.37 (0.63)	**0.20 (0.60)**	NA	0.66 (2.82)
$E(z)_{100}$	0.47 (0.79)	0.25 (0.76)	0.32 (0.56)	**0.17 (0.53)**	0.58 (2.50)	NA
$E(z)_{140}$	0.65 (1.11)	0.34 (1.06)	0.45 (0.78)	**0.24 (0.74)**	0.81 (3.49)	NA
5 year						
$P(z>0)_{300**}$	0.753 (0.909)	0.521 (0.898)	0.752 (0.906)	**0.519 (0.897)**	NA	0.916 (1.000)
$P(z>0)_{400**}$	0.845 (0.959)	0.625 (0.952)	0.844 (0.958)	**0.624 (0.952)**	NA	0.963 (1.000)
$P(z>0)_{400}$	0.845 (0.959)	0.625 (0.952)	0.725 (0.893)	**0.494 (0.880)**	0.903 (1.000)	NA
$P(z>0)_{700}$	0.962 (0.996)	0.821 (0.995)	0.896 (0.980)	**0.697 (0.976)**	0.983 (1.000)	NA
$E(z)_{300**}$	1.40 (2.48)	0.74 (2.27)	1.39 (2.36)	**0.73 (2.26)**	NA	2.47 (10.56)
$E(z)_{400**}$	1.86 (3.18)	0.98 (3.03)	1.85 (3.15)	**0.98 (3.02)**	NA	3.29 (14.07)
$E(z)_{400}$	1.86 (3.18)	0.98 (3.03)	1.29 (2.23)	**0.68 (2.12)**	2.33 (9.98)	NA
$E(z)_{700}$	3.26 (5.56)	1.72 (5.30)	2.26 (3.90)	**1.19 (3.70)**	4.07 (17.46)	NA

VISIT THE SCIENTIFIC PUBLICATIONS REPORT ARCHIVE

Comparison to PBR

Table 4 provides 5-year estimates of PBR based on F_R = 0.1, 0.5, and 1.0. Uncertainty in the estimates (e.g., 95% CI) reflects uncertainty in the proportion of the WNP stock that migrates with the ENP stock. For F_R = 0.1, striking one WNP whale in the 5-year period would exceed PBR. For F_R = 0.5, one WNP strike could exceed PBR, depending on how many WNP individuals migrate with the ENP stock. Fewer WNP whales in U.S. waters would mean higher chance that one strike would exceed PBR, but it would also translate into lower probability of there being a WNP strike in the first place (i.e., lower than reflected in the Table 1 estimates). For F_R = 1, striking one WNP whale in the 5-year period would not exceed PBR.

Table 4. Estimates of PBR (5-year total) for the WNP gray whale stock under three different values of F_R. Uncertainty in the estimates reflects uncertainty in the proportion of the WNP that uses U.S. waters; the lower estimate corresponds to a little more than 0.15 of the WNP stock migrating in ENP areas, whereas the upper estimate corresponds to nearly all WNP animals migrating in ENP areas.

	F_R = 0.1	F_R = 0.5	F_R = 1.0
2.5%	0.10	0.50	0.99
median	0.33	1.67	3.35
97.5%	0.57	2.85	5.69

DISCUSSION

In general, we consider Model set 2 the most plausible of the model sets used, because it makes use of information from sightings in the MUA from the NWA coast area as well as relative abundance of the WNP vs. ENP. In contrast, Model set 1 ignores the MUA sightings information, and Models 3 and 4 ignore our knowledge of the WNP being small relative to the ENP. We also feel that, within Model sets 1 and 2, the B-versions of each model are more appropriate than A-versions, because the B models make fewer assumptions. The B models assume no prior knowledge about $P_{WNP|mig}$, except to specify a reasonable upper bound, whereas the A models assume that WNP and ENP migrants are equally available to the hunt on a per capita basis. Therefore, Models 2A and 2B, but especially 2B, may be considered the most useful estimates.

Models 3 and 4 are probably the least justifiable, since by ignoring information about the WNP population size they allow for upper parameter estimates that are likely implausible. For example, if we assume that WNP and ENP animals are equally available to the hunt and there are 16,000-22,000 ENP animals, then the upper estimate for Model 4 of P_{WNP} = 0.035 corresponds to a WNP population estimate of nearly 560-770 animals, which far exceeds existing estimates. Alternatively, WNP animals would need to be far more available to hunters on per capita basis than ENP animals for behavioral reasons, and there is no reason presently to expect this is the case.

Estimates from our analysis are considered precautionary since they assume that the Makah will achieve their proposed maximum strike limits. That being said, the results herein offer a conservative initial step in assessing the potential risk of WNP gray whales incurring mortality incidental to the proposed hunt on the ENP population by the Makah Indian Tribe.

VISIT THE SCIENTIFIC PUBLICATIONS REPORT ARCHIVE

REFERENCES

Bradford, A.L., Weller, D.W., Wade, P.R., Burdin, A.M. and Brownell, R.L., Jr. 2008. Population abundance and growth rate of western gray whales *Eschrichtius robustus*. Endangered Species Research. 6(1):1-14.

Burdin, A.M., Sychenko, O.A. and Sidorenko, M.M. 2012. Status of western gray whales off Sakhalin Island, Russia in 2011. Paper SC/64/BRG5 presented to the International Whaling Commission Scientific Committee. [Available from http://www.iwcoffice.org/]

Calambokidis J., Laake J.L., and Klimek A. 2012. Updated analysis of abundance and population structure of seasonal gray whales in the Pacific Northwest, 1998-2010. Paper SC/M12/AWMP2-REV presented to the International Whaling Commission Scientific Committee. [Available from http://www.iwcoffice.org/]

IUCN 2012. Report of the 11th Meeting of the Western Gray Whale Advisory Panel. Geneva, Switzerland. [Available from http://www.iucn.org/wgwap/publications_and_reports/]

IWC 2012. Report of the 2011 Scientific Committee from its annual meeting held from 30 May-11 June 2011 in Tromsø, Norway. Journal of Cetacean Research and Management 13(Supplement) 2012.

Laake, J., Punt, A., Hobbs, R., Ferguson, M., Rugh, D. and Breiwick, J. 2009. Re-analysis of gray whale southbound migration surveys 1967-2006. NOAA Technical Memorandum. NMFS-AFSC-203. 55pp.

Lang, A.R. 2010. The population genetics of gray whales (*Eschrichtius robustus*) in the North Pacific. Ph.D. dissertation, University of California, San Diego, CA 222 pp.

Lang, A.R., Weller, D.W., LeDuc, R., Burdin, A.M., Pease, V.L., Litovka, D., Burkanov, V. and Brownell, R.L., Jr. 2011. Genetic analysis of stock structure and movements of gray whales in the eastern and western North Pacific. Paper SC/63/BRG10 presented to the International Whaling Commission Scientific Committee. [Available from http://www.iwcoffice.org/]

Mate, B., Bradford, A.L., Tsidulko, G., Vertyankin, V. and Ilyashenko, V. 2011. Late-feeding season movements of a western North Pacific gray whale off Sakhalin Island, Russia and subsequent migration into the Eastern North Pacific. Paper SC/63/BRG23 presented to the International Whaling Commission Scientific Committee. [Available from http://www.iwcoffice.org/]

Moore, J.E. and Weller, D.W. 2012. Probability of taking a western North Pacific gray whale during the proposed Makah hunt. Paper SC/64/BRG9 presented to the International Whaling Commission Scientific Committee. [Available from http://www.iwcoffice.org/]

NMFS 2005. Revisions to the Guidelines for Assessing Marine Mammal Stocks. 24pp. Available at: *http://www.nmfs.noaa.gov/pr/pdfs/sars/gamms2005.pdf*

NMFS 2012. Draft 2012 U.S. Pacific Marine Mammal Stock Assessments. Federal Register 77:47043. 7 August 2012. Available at: http://www.nmfs.noaa.gov/pr/pdfs/sars/po2012_draft.pdf

NOAA 2008.Draft environmental impact statement for proposed authorization of the Makah whale hunt. United States Department of Commerce, NOAA, NMFS, Northwest Region.

Reeves, R.R., Smith, T.D. and Josephson, E.A. 2008. Observations of western gray whales by ship-based whalers in the 19th century. Journal of Cetacean Research and Management 10(3):247-256.

VISIT THE SCIENTIFIC PUBLICATIONS REPORT ARCHIVE

Tyurneva, O. Yu, Yakovlev, Yu M., Vertyankin, V.V. and Selin, N.I. 2010. The peculiarities of foraging migrations of the Korean-Okhotsk gray whale (Eschrichtius robustus) population in Russian waters of the Far Eastern seas. Russian Journal of Marine Biology. 36(2):117-124.

Urbán R., J., Weller, D., Tyurneva, O., Swartz, S., Bradford, A., Yakovlev, Y., Sychenko, O., Rosales N., H., Martínez A., S., Burdin, A. and Gómez-Gallardo U., A. 2012. Report on the photographic comparison of the western and Mexican gray whale catalogues. Paper SC/64/BRG13 presented to the International Whaling Commission Scientific Committee [Available from http://www.iwcoffice.org/]

Weller, D.W., Burdin, A.M., Ivashchenko, Y.V., Tsidulko, G.A. and Brownell, R.L., Jr. 2003. Summer sightings of western gray whales in the Okhotsk and western Bering Seas. Paper SC/55/BRG9 submitted to the International Whaling Commission Scientific Committee. [Available from http://www.iwcoffice.org/]

Weller, D.W., Würsig, B., Bradford, A.L., Burdin, A.M., Blokhin, S.A., Minakuchi, H. and Brownell, R. L. Jr. 1999. Gray whales (*Eschrichtius robustus*) off Sakhalin Island, Russia: seasonal and annual patterns of occurrence. Marine Mammal Science, 15: 1208-1227.

Weller, D.W., Klimek, A., Bradford, A.L., Calambokidis, J., Lang, A.R., Gisborne, B., Burdin, A.M., Szaniszlo, W., Urbán, J., Gomez-Gallardo Unzueta, A., Swartz, S. and Brownell, R.L., Jr. 2012. Movements of gray whales between the western and eastern North Pacific. Endangered Species Research 18:193-199

VISIT THE SCIENTIFIC PUBLICATIONS REPORT ARCHIVE

Assessing the Risk of Ships Striking Large Whales in Marine Spatial Planning

J. V. Redfern[1*], M. F. McKenna[2], T. J. Moore[1], J. Calambokidis[3], M. L. DeAngelis[4], E. A. Becker[5], J. Barlow[1], K. A. Forney[5], P. C. Fiedler[1], S. J. Chivers[1]

(1) Protected Resources Division, Southwest Fisheries Science Center, National Marine Fisheries Service, National Oceanic and Atmospheric Administration, 8901 La Jolla Shores Drive, La Jolla, CA 92037
(2) Marine Mammal Commission, 4340 East-West Highway, Suite 700, Bethesda, Maryland 20814
(3) Cascadia Research, 218 1/2 W 4th Ave., Olympia, WA 98501
(4) Protected Resources Division, Southwest Regional Office, National Marine Fisheries Service, National Oceanic and Atmospheric Administration, 501 W. Ocean Blvd. Suite 4200, Long Beach, CA 90802
(5) Protected Resources Division, Southwest Fisheries Science Center, National Marine Fisheries Service, National Oceanic and Atmospheric Administration, 110 Shaffer Rd, Santa Cruz, CA 95060

Keywords: risk analysis, habitat modeling, generalized additive models, commercial shipping

* email jessica.redfern@noaa.gov

VISIT THE SCIENTIFIC PUBLICATIONS REPORT ARCHIVE

Abstract

Marine spatial planning provides a comprehensive framework for managing multiple uses of the marine environment and has the potential to minimize environmental impacts and reduce conflicts among users. Spatially explicit assessments of the risks to key marine species from human activities are a requirement of marine spatial planning. We assessed the risk of ships striking humpback (*Megaptera novaeangliae*), blue (*Balaenoptera musculus*), and fin (*B. physalus*) whales in alternative shipping routes derived from patterns of shipping traffic off Southern California (U.S.A.). Specifically, we developed whale-habitat models and assumed ship-strike risk for the alternative shipping routes was proportional to the number of whales predicted by the models to occur within each route. This definition of risk assumes all ships travel within a single route. We also calculated risk assuming ships travel via multiple routes. We estimated the potential for conflict between shipping and other uses (military training and fishing) due to overlap with the routes. We also estimated the overlap between shipping routes and protected areas. The route with the lowest risk for humpback whales had the highest risk for fin whales and vice versa. Risk to both species may be ameliorated by creating a new route south of the northern Channel Islands and spreading traffic between this new route and the existing route in the Santa Barbara Channel. Creating a longer route may reduce the overlap between shipping and other uses by concentrating shipping traffic. Blue whales are distributed more evenly across our study area than humpback and fin whales; thus, risk could not be ameliorated by concentrating shipping traffic in any of the routes we considered. Reducing ship-strike risk for blue whales may be necessary because our assessment of the potential number of strikes suggests that they are likely to exceed allowable levels of anthropogenic impacts established under U.S. laws.

VISIT THE SCIENTIFIC PUBLICATIONS REPORT ARCHIVE

Introduction

Marine spatial planning (MSP) provides a comprehensive framework for managing multiple uses of the marine environment (e.g., shipping, military training, and fishing) and has the potential to minimize environmental impacts and reduce conflicts among users (Crowder et al. 2006). MSP must be based on ecological principles to sustain ecosystem integrity. For example, one outcome of decision making should be healthy populations of top predators and prey species that affect the structure and stability of food webs and species that have strong effects on community structure and function (Foley et al. 2010). Spatially explicit risk assessments are a basic requirement of MSP because they link the distribution of these key species to the potential effects and distribution of anthropogenic activities (Stelzenmüller et al. 2010; Grech et al. 2011).

An example of the connections between users of the marine environment and the possibility for conflict recently occurred in Southern California (U.S.A.) (Fig. 1a, b) when the California Air Resources Board implemented the Ocean-Going Vessel Fuel Rule (hereafter, fuel rule). The fuel rule was intended to reduce emissions of particulate matter, sulfur oxides, and nitrogen oxides by requiring large, commercial ships to use cleaner-burning fuels when traveling within approximately 44 km (24 nautical miles) of the mainland coast (Soriano et al. 2008). Before implementation of the rule, a majority of ships traveled through the traffic separation scheme (TSS) adopted by the International Maritime Organization in the Santa Barbara Channel. Following implementation, a higher proportion of ships began traveling south of the northern Channel Islands (McKenna 2011) to reduce the time spent using more expensive, cleaner fuels.

This shift resulted in increased shipping traffic in military ranges and raised concerns for maritime safety because the movement of ships outside a TSS is less predictable and thus increases the potential for collisions and oil spills. Thus, the U.S. Coast Guard (2010) initiated a

VISIT THE SCIENTIFIC PUBLICATIONS REPORT ARCHIVE

study of the routes to the 2 largest ports in Southern California (Los Angeles and Long Beach) (Fig. 1c). Public comments submitted as part of this study included 2 primary concerns. The U.S. Navy and Air Force said any disruption of their military activities from increased shipping traffic could add to operational costs and limit capacity to support national security. Several non-profit groups, the U.S. National Marine Fisheries Service, and the Channel Islands National Marine Sanctuary requested that the Coast Guard consider the risk of ships striking large whales.

Large whales are vulnerable to collisions with all vessel types, sizes, and classes throughout the world's oceans (Laist et al. 2001). Waters off Southern California include seasonal feeding areas for humpback (*Megaptera novaeangliae*) and blue (*Balaenoptera musculus*) whales (Calambokidis & Barlow 2004; Calambokidis et al. 2009), and aggregations of fin whales (*B. physalus*) have been observed year-round (Forney et al. 1995). All 3 species are listed as endangered under the U.S. Endangered Species Act. The U.S. Marine Mammal Protection Act requires calculation of potential biological removal, defined as "the maximum number of animals that may be removed annually by anthropogenic causes while allowing the population to reach or maintain its optimum sustainable population." The phrase *optimum sustainable population* is defined as "the number of animals which will result in the maximum productivity of the population or the species, keeping in mind the carrying capacity of the habitat and the health of the ecosystem of which they form a constituent element" (16 U.S.C. 1362[3][9]). For the population of blue whales along the U.S. West Coast, the potential biological removal is 3 individuals (Carretta et al. 2011). Ship strikes of blue whales have been documented for almost 2 decades along the California coast, but the issue received increased attention in 2007 when at least 4 blue whales were killed by ship strikes off Southern California (Berman-Kowalewski et al. 2010).

VISIT THE SCIENTIFIC PUBLICATIONS REPORT ARCHIVE

We conducted a spatially explicit assessment of the risk of ships striking (hereafter, ship-strike risk) humpback, blue, and fin whales off the coast of Southern California. Specifically, we modeled the number of whales as a function of habitat variables and assumed ship-strike risk for alternative shipping routes was proportional to the number of whales predicted by the models to occur within each route. The proportion of whales within a shipping route that will be struck is a function of whale densities, volume of shipping traffic, ship speed, and whale behavior. Information is lacking on the functional form of these relations and other factors that may affect ship-strike risk. Consequently, we quantified the co-occurrence of whales and shipping traffic as has been done in recent ship-strike studies (Vanderlaan et al. 2009; Williams & O'Hara 2010) and studies used to modify the TSS to the port of Boston through Stellwagen Bank National Marine Sanctuary to reduce ship-strike risk for right whales (*Eubalena glacialis*) (Merrick 2005). We assumed all ships traveled within a single route and approximated the multiroute traffic patterns observed off Southern California after implementation of the fuel rule. If whale distributions are the only criteria used to select optimal shipping routes, conflicts may arise between shipping and other uses (Fig. 1c, d). Therefore, we also estimated the potential for conflict due to overlap between the routes and areas used for other purposes (e.g., military training, fishing, and protection of resources).

Methods

Data Collection

We used whale sightings and oceanographic data collected by the National Marine Fisheries Service's Southwest Fisheries Science Center from August through November in 1991, 1993, 1996, 2001, 2005, 2008, and 2009. Surveys conducted from 1991 to 2008 covered broad

VISIT THE SCIENTIFIC PUBLICATIONS REPORT ARCHIVE

regions of the U.S. West Coast. The 2009 survey focused primarily on Southern California and represents approximately 40% of the total effort and a high proportion of the whale sightings (Supporting Information). On all surveys, line-transect methods were used to collect marine mammal data during daylight hours. We used approximately 9300 km of survey effort (Fig. 1b) collected in Beaufort sea states of five or lower. Survey effort consisted of 2 observers using pedestal-mounted 25x150 binoculars to search for marine mammals from the flying bridge of the ship; a third observer searched by eye or with 7x handheld binoculars and recorded both sightings and survey conditions.

When marine mammals were detected, the vessel approached the group as needed to identify the species and estimate group size. Observers independently recorded their best, high, and low estimates of group size for each sighting. For mixed species sightings, observers also estimated the percentage of each species in the group. To obtain a single estimate of group size for each sighting, we averaged the best estimate from each observer or the best estimate multiplied by the percentage of each species. If no observers gave a best estimate, we averaged the low estimates.

Oceanographic sampling was systematically conducted during each survey. A thermosalinograph measured sea surface temperature and salinity every 2 minutes or more frequently. Surface chlorophyll concentration and mixed-layer depth were measured at approximately 55-km or shorter intervals. We defined mixed-layer depth as the depth at which the temperature was 0.5˚ C less than sea surface temperature. We obtained mixed-layer depth estimates from expendable bathythermograph drops and conductivity, temperature, and depth casts.

VISIT THE SCIENTIFIC PUBLICATIONS REPORT ARCHIVE

Whale Models

The shape of the study area (Fig. 1b) was determined by availability of habitat data. We divided transects into continuous-effort segments of approximately 5 km as described by Becker et al. (2010). For each species, we used generalized additive models (GAMs) to relate the number of individuals in each segment to the following habitat variables: sea surface temperature and salinity, log-transformed surface chlorophyll concentrations, mixed-layer depth, and distance to the 200-m isobath. This isobath represents the shelf break for many areas of the California coast and is an important habitat feature for many species of large whales (Fiedler et al. 1998; Becker et al. 2010;). Relatively strong correlations were observed between surface chlorophyll concentration and sea surface temperature (-0.71), mixed-layer depth and sea surface temperature (-0.44), and mixed-layer depth and the distance to the 200-m isobath (0.55).

The distance traveled on effort in each segment was an offset in the models because the amount of effort varied among segments. Survey year was a linear term in the model for each species to account for long-term changes in whale abundance (Calambokidis & Barlow 2004; Moore & Barlow 2011). We used kriging to interpolate the oceanographic variables throughout the study area. Specifically, variograms were fit to the data collected from 1991 to 2008 along broad regions of the U.S. West Coast. We did not include 2009 data in the variograms because this survey occurred in a smaller area and sampling was conducted at a finer resolution. We used bilinear interpolation to extract values from the kriged grids at the midpoint of the transect segments. The 200-m isobath was derived from ETOPO1 (Amante & Eakins 2009), a 1 arc-minute global-relief model. We used negative values of the distance to the 200-m isobath in waters shallower than 200 m to differentiate shelf from slope waters.

VISIT THE SCIENTIFIC PUBLICATIONS REPORT ARCHIVE

We fit Poisson GAMs, in which overdispersion was corrected with a quasi-likelihood model, using the software package S+ (Version 8.1 for Windows, Tibco Software, Somerville, Massachusetts). The variables included in each model and the degrees of freedom for cubic smoothing splines were selected by an automated forward-backward stepwise approach and Akaike's information criterion (AIC) (Becker et al. 2010). Each model was fit 3 times, starting with a null model that included only the intercept. We used the dispersion parameter from the null model to calculate AIC values in the algorithm step.gam, which tested all predictor variables for inclusion in the second model as cubic smoothing splines with 2-3 degrees of freedom. For the third model, we used the dispersion parameter from the second model to calculate the AIC values in the algorithm step.gam, which tested all predictor variables for inclusion as linear terms or cubic smoothing splines with 2-3 degrees of freedom.

To ensure all potentially important variables were included in the final models, we evaluated the following for the 5 candidate models with the lowest AIC values in the second call to step.gam: $\Delta_i = AIC_{candidate} - AIC_{best}$, Akaike weights, cumulative Akaike weights, and evidence ratios (Symonds & Moussalli 2011). All variables and the highest degrees of freedom for each variable in any candidate model with Δ_i <2 were included in the final model (Becker et al. 2012). We used the percentage of explained deviance to assess model fit and annual ratios of observed to predicted numbers of whales to assess the accuracy of the predictions.

We used the models to predict the number of whales in each cell of a 2 x 2 km grid of the study area. Specifically, we made predictions for each year of survey data on the basis of the kriged oceanographic variables extracted at the center of each cell by bilinear interpolation and the distance to the 200-m isobath calculated at the center of each cell. We calculated whale density in each cell by dividing the predicted number of whales by 2*effort*ESW*g(0), where

VISIT THE SCIENTIFIC PUBLICATIONS REPORT ARCHIVE

effort was assumed to be 1 km because effort was included as an offset in the model; the effective strip width (ESW) was 1.715 for fin and blue whales and 2.894 for humpback whales (Barlow 2003); and the trackline detection probability, g(0), was 0.90 for all species (Barlow 2003). We summarized whale density throughout the study area by calculating the weighted average of the annual predictions, where the weights were the proportion of survey effort in the study area for each year. The average predictions do not account for within-year variation in species distributions; rather, they represent expected long-term patterns in humpback, blue, and fin whale distributions between August and November.

Spatial autocorrelation in species distributions can limit the interpretation of habitat relationships and restrict the transferability of habitat models in space and time (Dormann 2007). For each species, we developed Moran's I correlograms, with lags from 0-50 km in approximately 5-km increments, for the number of whales observed in the segments to test for spatial autocorrelation. Weights within each lag were defined by the inverse distance between points. For each lag, 95% confidence intervals were derived from 500 simulations in which the number of whales was randomly permuted. Spatial autocorrelation at individual lags was assumed to be significant if the observed Moran's I value was not included in the confidence interval.

Risk

We used Automatic Identification System (AIS) data collected between 15 September and 30 November in 2008 and 2009 (McKenna 2011) to analyze traffic patterns for commercial ships that were at least 100 m in length. Specifically, we created linear ship transits by joining successive position reports with the same ship identifier that occurred no more than 1 hour apart

VISIT THE SCIENTIFIC PUBLICATIONS REPORT ARCHIVE

and had less than a 30-degree difference between headings. These criteria minimized inaccuracies in the transits caused by uncertainty in ship locations. The transit analyses do not account for seasonal variations in shipping traffic; rather, they represent traffic patterns observed during a period that coincides with the whale surveys.

The 4 alternative shipping routes we considered (Fig. 1e) were derived from the 2008 and 2009 ship transits. The Channel route is a TSS adopted by the International Maritime Organization. The Central route spans our study area in a region of ship traffic south of the northern Channel Islands. The Central Fan represents the option of establishing only the eastern portion of the Central route; consequently, the fan represents a range of possible approaches to this route. We derived the boundaries of the fan from the 2009 ship transits. The location of the Southern route was constrained by the protected areas around Santa Barbara, Santa Catalina, and San Nicolas Islands. The lengths of the Channel, Central, and Southern routes are similar. All shipping routes were composed of an inbound lane, an outbound lane, and a middle traffic separation zone, following conventions for the TSS in the Santa Barbara Channel. For all routes, we assumed that no ships traveled in the traffic-separation zone.

We overlaid the number of whales predicted by the models in 2 x 2 km grid cells on a map of each shipping route. The predicted number of whales within the inbound and outbound lanes was summed to obtain the total number of whales within each route. We assumed all traffic occurred within a route and that ship density was one for all routes except the Central Fan route. To account for the lower ship density expected in the fan portion of the Central Fan route, we calculated ship density as the ratio of the area in the Central route that occurred in the fan to the area of the fan. We multiplied the predicted number of whales within each route by ship density to estimate ship-strike risk. Thus, ship-strike risk is a measure of the co-occurrence of

VISIT THE SCIENTIFIC PUBLICATIONS REPORT ARCHIVE

whales and shipping traffic. We summarized the results by calculating the weighted average and standard error of the annual risk estimates, where the weights were the proportion of survey effort in the study area for each year. We defined the relative risk for each route as the difference between the average route risk and the average Channel route risk divided by the average Channel route risk.

Assuming all shipping traffic occurs in each route is helpful for identifying the route that has the smallest overlap with whale distributions. However, ship transits derived from the 2008 AIS data show that approximately 77% of shipping traffic occurred in the Channel route, approximately 12% of traffic occurred in the Central Fan route, and the remaining 11% was broadly distributed. Following implementation of the fuel rule in 2009, approximately 29% of shipping traffic occurred in the Channel route, 39% of traffic occurred in the Central Fan route, and the remaining traffic was broadly distributed south of the northern Channel Islands. Consequently, we also evaluated risk assuming traffic occurred in both the Channel and Central Fan routes, which captured the majority of the observed traffic in both years. This assumption resulted in Channel traffic estimates of 87% and Central Fan traffic estimates of 13% in 2008. In 2009 the Channel estimate was 43% and the Central Fan estimate was 57%.

Habitat-modeling studies suggest annual predictions of species distributions may contain substantial error, but average predictions can provide accurate summaries of expected long-term patterns in species distributions (e.g., Barlow et al. 2009). Consequently, we calculated the risk associated with a predominantly Channel traffic pattern (approximated from AIS data collected in 2008 before implementation of the fuel rule) and risk associated with a mixed traffic pattern (approximated from AIS data collected in 2009 after implementation of the fuel rule) as the sum of the traffic percentage for each route multiplied by the average of the annual risk estimates

VISIT THE SCIENTIFIC PUBLICATIONS REPORT ARCHIVE

calculated assuming all traffic occurs in the route. We also used the annual risk estimates to calculate the standard error of the risk associated with the multiroute traffic patterns. This approach allowed us to directly compare the risk estimates for the traffic patterns to the risk estimates that assume all traffic occurs within a single route.

Route-Use Overlap

The primary human uses of Southern California waters are shipping, military training, and fishing (Fig. 1c). We obtained dominant use areas for commercial fishing from the California Ocean Uses Atlas Project (NMPAC & MCBI 2010). Protected areas off Southern California (NMPAC 2011; CDFG 2012) have been designated by both state and federal governments for a suite of reasons ranging from water quality to protection of marine life (Fig. 1d). Waters off Southern California also contain the federally managed Channel Islands National Marine Sanctuary (Fig. 1d). Automatic Identification System data show that ships transit through a majority of these areas (McKenna 2011). Shipping traffic in the sanctuary is predominantly confined to the TSS, which overlaps with sanctuary boundaries. For each of these uses, we calculated the area that occurs in the inbound and outbound lanes of the shipping routes.

Results

The final models for each species (Table 1) differed in the variables selected or the shape of the relations (Supporting Information) and thus predicted distinct high-density areas for each species (Fig. 2). The habitat relations for all species were similar to those observed during fine-scale surveys off Southern California (Fiedler et al. 1998) and along the entire U.S. West Coast (Becker et al. 2010). Humpback whale habitat occurred in the northernmost portion of our study

VISIT THE SCIENTIFIC PUBLICATIONS REPORT ARCHIVE

area (Fig. 2a), in productive coastal waters characterized by cold temperatures, low salinities, and high chlorophyll concentrations (Supporting Information). The habitat model explained 31.2% of the deviance. Although predictions of humpback whale numbers across all years were accurate, annual ratios of observed to predicted number of whales indicated the habitat model did not accurately explain the number of humpback whales in individual years (Supporting Information). Significant, positive spatial autocorrelation (Moran's $I = 0.010$ to 0.043) was observed for humpback whales across the distances considered (0-50 km).

Blue and fin whales were more broadly distributed (Fig. 2b, c), and the habitat models for these species explained lower percentages of deviance (14.9% for blue whales and 17% for fin whales) compared with humpback whales. However, ratios of observed to predicted number of whales for both species indicated greater accuracy in the predictions for individual years than the humpback whale model (Supporting Information). High densities of blue whales occurred along the 200-m isobath in waters that had intermediate mixed-layer depths and high concentrations of surface chlorophyll (Supporting Information). This habitat occurred close to shore and extended somewhat into the Santa Barbara Channel in the north. It also occurred in offshore waters farther south (Fig. 2b). Blue whales showed significant, positive spatial autocorrelation at 5 km (Moran's $I = 0.066$). Fin whale habitat (Fig. 2c) occurred in offshore waters, which were characterized by cold surface temperatures, intermediate mixed-layer depths, and intermediate concentrations of surface chlorophyll (Supporting Information). Fin whales showed significant, positive spatial autocorrelation at 45 km (Moran's $I = 0.016$).

Ship-strike risk was highest for humpback whales under the assumption that all traffic occurred in the Channel route (risk = 3.58) and lowest under the assumption that all traffic occurred in the Southern route (risk = 0.93) (Fig. 3 & Table 2). The opposite pattern was

VISIT THE SCIENTIFIC PUBLICATIONS REPORT ARCHIVE

observed for fin whales; risk was 6.39 for the Channel route and 13.70 for the Southern route (Fig. 3 & Table 2). For both species, risk assuming some distribution of traffic among routes occurred between these 2 extremes. Following implementation of the fuel rule (approximated from the mixed traffic pattern observed in 2009), risk decreased from 3.32 to 2.41 for humpback whales and increased from 6.85 to 8.41 for fin whales (Table 2). The change in risk occurred because a higher proportion of ships began traveling south of the northern Channel Islands instead of using the TSS in the Santa Barbara Channel. Predictions of high densities of blue whales spanned the study area (Fig. 2b) and resulted in similar risk estimates among all routes and little change in risk following implementation of the fuel rule (Fig. 3 & Table 2). The variance in risk was high for all species (Table 2) because of interannual variability in distribution and availability of habitat.

We calculated the potential for conflict due to overlap between the shipping routes and areas used for other purposes. The Channel route had the least overlap with military ranges, but it was the only route that overlapped with the National Marine Sanctuary and other marine protected areas (Table 2). Fishing areas had the highest overlap with the Channel route; however, better fishing data are needed to determine how much fishing actually occurs within the TSS. The largest overlap was between the Central Fan route and military ranges because of the large area traversed by ships before entering the route.

Discussion

An average of 1 humpback whale, 1.8 blue whale, and 1.2 fin whale ship strikes were documented per year along the California coast from 2005 to 2010 (NMFS 2011). The documented number of strikes is an underestimate of the actual number of strikes because ship

VISIT THE SCIENTIFIC PUBLICATIONS REPORT ARCHIVE

strikes have a low probability of detection (Laist et al. 2001). For example, Kraus et al. (2005) estimated a carcass-detection rate of 17% for right whales. The carcass-detection rate for humpback, blue, and fin whales could be <17% because right whales tend to float after death. If the carcass-detection rate is lower for these species, the actual number of strikes would be higher. To correct the observed number of ship strikes, we assumed a 17% carcass-detection rate and estimated that 5.9 humpback whales, 10.6 blue whales, and 7.1 fin whales were struck by ships each year. Potential biological removals, calculated on the basis of the definition in the U.S. Marine Mammal Protection Act, are 11.3 humpback whales and 16 fin whales for the U.S. West Coast population (Carretta et al. 2011). The estimated number of ship strikes for these species is below their potential biological removals and thus, suggests the number of strikes may be sustainable. Even conservative estimates of the number of blue whale ship strikes, however, are higher than the potential biological removal of 3 individuals. Consequently, blue whale ship strikes likely exceed allowable levels established under U.S. laws.

Although these calculations only include ship strikes and a full assessment of the status of these species must also include fisheries entanglements and other anthropogenic effects, the potential population-level consequences of these removals are corroborated by observed trends in abundance. Increases in abundance over time have been observed for both humpback (Calambokidis & Barlow 2004) and fin whales (Moore & Barlow 2011) along the California coast. In contrast, there is no evidence that the blue whale population in the North Pacific is growing. There is evidence that blue whale occurrence off California has declined, but these declines are likely caused by a northward shift in their feeding areas (Calambokidis et al. 2009). Given the likelihood that blue whale ship strikes exceed allowable levels established under U.S. laws, further research is needed to determine whether ship strikes could be limiting population

VISIT THE SCIENTIFIC PUBLICATIONS REPORT ARCHIVE

growth for blue whales and how to reduce ship-strike risk. Blue whales were distributed more evenly than humpback and fin whales off Southern California. Consequently, shifting traffic among the routes considered in our analyses did not reduce risk. Possibilities for reducing risk include fine-scale alterations of the existing TSS (e.g., narrowing the Channel route to minimize overlap with the 200-m isobath) and alternative management strategies, such as the seasonal management areas that have been used on the U.S. East Coast to reduce ship-strike risk for right whales (Lagueux et al. 2011).

For humpback and fin whales, these analyses represent a powerful tool for balancing user-user and user-environment conflicts when evaluating optimal shipping routes. Our results showed that the Central Fan route (Fig. 1e) had the highest spatial overlap with military ranges (Table 2). The distribution of southern shipping traffic following implementation of the fuel rule was even broader than this route (McKenna 2011) and resulted in a magnified potential for user-user conflict. User-environment conflicts were also magnified because ship-strike risk for fin whales is not uniform throughout the region of increased southern shipping traffic (e.g., the Southern route has a higher risk than the Central route [Table 2]). The general increase in ship-strike risk for fin whales associated with implementation of the fuel rule is consistent with fin whale stranding records. The number of documented fin whale ship strikes in 2009 was the second largest in 20 years of stranding records (NMFS 2011).

One possible way to reduce both of these conflicts is to designate a new TSS at an optimal location south of the northern Channel Islands and determine whether this new TSS should replace or be established in conjunction with the existing TSS in the Santa Barbara Channel. Our analyses of 4 alternative shipping routes show a contrast in ship-strike risk for humpback and fin whales (Fig. 3) because they have opposing areas of higher densities off

VISIT THE SCIENTIFIC PUBLICATIONS REPORT ARCHIVE

Southern California (Fig. 2a, c). Specifically, selection of the route that has the lowest risk for one species (i.e., the Southern route for humpback whales or the Channel route for fin whales [Table 2]) resulted in maximizing risk for the other species. Having all shipping traffic occur in either the Central or Central Fan route reduced risk for fin whales (10.7 and 9.9, respectively) relative to having all traffic occur in the Southern route (13.7). It also provided a decreased risk for humpback whales that was only slightly less than the decrease achieved in the Southern route (Fig. 3).

The changes in risk observed after implementation of the fuel rule, however, suggest that distributing traffic between the Channel route and either the Central Fan or Central route may balance the risks for humpback and fin whales. Specifically, our assessment of risk following implementation of the fuel rule, assuming 43% of traffic occurred in the Channel route and 57% occurred in the Central Fan route, resulted in intermediate changes in risk for both species (Fig. 3). The decrease in risk for humpback whales was -0.33 (range: -0.08 to -0.74) following implementation of the fuel rule and the increase in risk for fin whales was 0.32 (range: 0.07 to 1.14). Interannual variability in this region was too high to allow us to differentiate risk between the Central and Central Fan routes for either species. However, there were clear differences in the amount of overlap between these routes and other users. The Central Fan route has a shorter designated route than the Central route, which allows ships to choose their approach to the route and results in higher overlap with military ranges. Consequently, it may be useful to consider other users' needs when determining the length of the route in this area. For example, it may be more important to exclude shipping from certain areas within the military ranges. More data are needed to better understand the actual allocation of fishing effort and its overlap with the shipping routes.

VISIT THE SCIENTIFIC PUBLICATIONS REPORT ARCHIVE

We identified spatial autocorrelation at varying distances in the observations of all 3 species across the 7 years of surveys in our study area. The whale-habitat models are expected to reflect this autocorrelation. Although spatial autocorrelation does not necessarily generate bias in ecology analyses (Diniz-Filho et al. 2003), it can limit the interpretation of species-habitat relations and restrict the transferability of habitat models in space and time (Dormann 2007). Consequently, our models should not be used to make predictions outside the study area, where spatial autocorrelation may differ, or to infer mechanistic relations between whale distributions and individual habitat variables. It is also possible that spatial autocorrelation may differ in the future (e.g., in association with longer-term oceanographic variability); therefore, these models and the risk assessment should be updated periodically.

The uncertainty in our risk estimates was due primarily to interannual variability in species distributions and can be reduced by extending the time series of line-transect data and improving the habitat variables through finer-resolution sampling and incorporation of prey data. Seasonality in the risk estimates should also be assessed because fin whales are present off Southern California all year and some blue and humpback whales may have arrived before or remained after the period in which our data were collected. The risk estimates could also be expanded to incorporate the amount of time whales spend at the surface, how encounters with ships affect whale behavior, and effects of ship speed and traffic volume. Other potential threats to large whales in the California Current include noise from commercial shipping, entanglements in fishing gear, ocean-based pollution, and climate change (Halpern et al. 2009). These threats can be integrated in analyses of cumulative effects to assess consequences for the population viability of large whales.

VISIT THE SCIENTIFIC PUBLICATIONS REPORT ARCHIVE

Acknowledgments

This study would not have been possible without the tireless efforts of the crew and scientists aboard the *David Starr Jordan*, the *McArthur*, and the *McArthur II*. We also wish to thank E. Fleishman, H. Marsh, anonymous reviewers, C. Redfern, J. Carretta, and S. Mesnick for insightful comments on the manuscript.

Supporting Information

Sample sizes and ratios of the number of whales seen each year to the number predicted by our habitat models (Appendix S1) and functional forms for variables included in the generalized additive models (Appendix S2) are available online. The authors are solely responsible for the content and functionality of these materials. Queries (other than absence of the material) should be directed to the corresponding author.

Literature Cited

Amante, C., and B. W. Eakins. 2009. ETOPO1 1 arc-minute global relief model: procedures, data sources and analysis. Technical memorandum NESDIS NGDC-24. National Geophysical Data Center, Boulder, Colorado.

Barlow, J. 2003. Preliminary estimates of the abundance of cetaceans along the U.S. west coast: 1991-2001. Administrative report LJ-03-03. U.S. National Marine Fisheries Service, Southwest Fisheries Science Center, La Jolla, California.

Barlow, J., M. C. Ferguson, E. A. Becker, J. V. Redfern, K. A. Forney, I. L. Vilchis, P. C. Fiedler, T. Gerrodette, and L. T. Ballance. 2009. Predictive modeling of cetacean densities in the eastern Pacific Ocean. Technical memorandum NMFS-SWFSC-444. U.S.

VISIT THE SCIENTIFIC PUBLICATIONS REPORT ARCHIVE

National Marine Fisheries Service, Southwest Fisheries Science Center, La Jolla, California.

Becker, E. A., D. G. Foley, K. A. Forney, J. Barlow, J. V. Redfern, and C. L. Gentemann. 2012. Forecasting cetacean abundance patterns to enhance management decisions. Endangered Species Research **16**:97-112.

Becker, E. A., K. A. Forney, M. C. Ferguson, D. G. Foley, R. C. Smith, J. Barlow, and J. V. Redfern. 2010. Comparing California Current cetacean-habitat models developed using in situ and remotely sensed sea surface temperature data. Marine Ecology Progress Series **413**:163-183.

Berman-Kowalewski, M., et al. 2010. Association between blue whale (*Balaenoptera musculus*) mortality and ship strikes along the California coast. Aquatic Mammals **36**:59-66.

Calambokidis, J., and J. Barlow. 2004. Abundance of blue and humpback whales in the eastern North Pacific estimated by capture-recapture and line-transect methods. Marine Mammal Science **20**:63-85.

Calambokidis, J., J. Barlow, J. K. B. Ford, T. E. Chandler, and A. B. Douglas. 2009. Insights into the population structure of blue whales in the Eastern North Pacific from recent sightings and photographic identification. Marine Mammal Science **25**:816-832.

CDFG (California Department of Fish and Game). 2012. Marine protected areas spatial data. CDFG, Monterey, California. Available from http://www.dfg.ca.gov/marine/gis/downloads.asp (accessed January 2012).

Carretta, J. V., et al. 2011. U.S. Pacific marine mammal stock assessments: 2010. Technical memorandum, NMFS-SWFSC-476. U.S. National Marine Fisheries Service, Southwest Fisheries Science Center, La Jolla, California.

VISIT THE SCIENTIFIC PUBLICATIONS REPORT ARCHIVE

Crowder, L. B., et al. 2006. Resolving mismatches in U.S. ocean governance. Science **313**:617-618.

Diniz-Filho, J. A. F., L. M. Bini, and B. A. Hawkins. 2003. Spatial autocorrelation and red herrings in geographical ecology. Global Ecology and Biogeography **12**:53-64.

Dormann, C. F. 2007. Effects of incorporating spatial autocorrelation into the analysis of species distribution data. Global Ecology and Biogeography **16**:129-138.

Fiedler, P. C., S. B. Reilly, R. P. Hewitt, D. Demer, V. A. Philbrick, S. Smith, W. Armstrong, D. A. Croll, B. R. Tershy, and B. R. Mate. 1998. Blue whale habitat and prey in the California Channel Islands. Deep Sea Research Part II: Topical Studies in Oceanography **45**:1781-1801.

Foley, M. M., et al. 2010. Guiding ecological principles for marine spatial planning. Marine Policy **34**:955-966.

Forney, K. A., J. Barlow, and J. V. Carretta. 1995. The abundance of cetaceans in California waters. Part II: aerial surveys in winter and spring of 1991 and 1992. Fishery Bulletin **93**:15-26.

Grech, A., R. Coles, and H. Marsh. 2011. A broad-scale assessment of the risk to coastal seagrasses from cumulative threats. Marine Policy **35**:560 - 567.

Halpern, B. S., C. V. Kappel, K. A. Selkoe, F. Micheli, C. M. Ebert, C. Kontgis, C. M. Crain, R. G. Martone, C. Shearer, and S. J. Teck. 2009. Mapping cumulative human impacts to California Current marine ecosystems. Conservation Letters **2**:138–148.

Kraus, S. D., et al. 2005. North Atlantic right whales in crisis. Science **309**:561–562.

VISIT THE SCIENTIFIC PUBLICATIONS REPORT ARCHIVE

Lagueux, K. M., M. A. Zani, A. R. Knowlton, and S. D. Kraus. 2011. Response by vessel operators to protection measures for right whales *Eubalaena glacialis* in the southeast US calving ground. Endangered Species Research **14**:69-77.

Laist, D. W., A. R. Knowlton, J. G. Mead, A. S. Collet, and M. Pod. 2001. Collisions between ships and whales. Marine Mammal Science **17**:35–75.

McKenna, M. F. 2011. Blue whale response to underwater noise from commercial ships. Ph.D. dissertation. Biological Oceanography, University of California, San Diego.

Merrick, R. L. 2005. Seasonal management areas to reduce ship strikes of northern right whales in the Gulf of Maine. Reference document 05-19. Northeast Fisheries Science Center ,Woods Hole, Massachusets.

Moore, J. E., and J. Barlow. 2011. Bayesian state-space model of fin whale abundance trends from a 1991–2008 time series of line-transect surveys in the California Current. Journal of Applied Ecology **48**:1195–1205.NMFS (National Marine Fisheries Service). 2011. California marine mammal stranding database. NMFS, Long Beach, California.

NMPAC (National Marine Protected Areas Center) and MCBI (Marine Conservation Biology Institute). 2010. California ocean uses atlas. NMPAC, Monterey, California. Available from http://www.mpa.gov/dataanalysis/atlas_ca (accessed February 2011).

National Marine Protected Areas Center (MPAC). 2011. MPA inventory database (March, version 2). MPAC, Monterey, California. Available from http://www.mpa.gov/dataanalysis/mpainventory (accessed January 2012).

Soriano, B., et al. 2008. Fuel sulfur and other operational requirements for ocean-going vessels within California waters and 24 nautical miles of the California Baseline. California Environmental Protection Agency, Air Resources Board, Sacramento, California.

VISIT THE SCIENTIFIC PUBLICATIONS REPORT ARCHIVE

Available from http://www.arb.ca.gov/regact/2008/fuelogv08/ISORfuelogv08.pdf (accessed December 2012).

Stelzenmüller, V., J. Ellis, and R. S.I. 2010. Towards a spatially explicit risk assessment for marine management: assessing the vulnerability of fish to aggregate extraction. Biological Conservation **143**:230-238.

Symonds, M. R. E., and A. Moussalli. 2011. A brief guide to model selection, multimodel inference and model averaging in behavioural ecology using Akaike's information criterion. Behavioral Ecology and Sociobiology **65**:13-21.

U.S. Coast Guard (USCG). 2010. Port Access Route Study: In the Approaches to Los Angeles-Long Beach and in the Santa Barbara Channel. USCG, Washington, D.C. Available from https://federalregister.gov/a/2010-7815 (accessed December 2012).

Vanderlaan, A. S. M., J. J. Corbett, S. L. Green, J. A. Callahan, C. Wang, R. D. Kenney, C. T. Taggart, and J. Firestone. 2009. Probability and mitigation of vessel encounters with North Atlantic right whales. Endangered Species Research **6**:273-285.

Williams, R., and P. O'Hara. 2010. Modelling ship strike risk to fin, humpback and killer whales in British Columbia, Canada. Journal of Cetacean Research and Management **11**:1-8.

VISIT THE SCIENTIFIC PUBLICATIONS REPORT ARCHIVE

Table 1. Summary of generalized additive models relating the number of humpback, blue, and fin whales to year, distance to the 200-m isobath in kilometers (isobath), and oceanographic variables*

Species and candidate model	df	Explained deviance	AIC	Δ_i	Akaike weight	Cumulative Akaike weight	Evidence ratio
Humpback whale							
s(LNSC,2)	2.93	0.287	451.14	0	0.277	0.277	
s(LNSC,3)	3.89	0.297	451.24	0.09	0.264	0.541	1.05
SST+s(LNSC,2)	3.93	0.297	451.28	0.14	0.259	0.800	1.07
SSS+s(LNSC,2)	3.93	0.295	452.37	1.22	0.150	0.950	1.84
isobath+s(LNSC,2)	3.93	0.289	456.07	4.93	0.024	0.974	11.76
Blue whale							
isobath+s(MLD,3)+s(LNSC,3)	7.88	0.139	1005.37	0	0.392	0.392	
s(isobath,3)+s(MLD,3)+s(LNSC,3)	9.86	0.149	1006.14	0.76	0.268	0.660	1.46
s(isobath,2)+s(MLD,3)+s(LNSC,3)	8.86	0.143	1006.62	1.24	0.210	0.870	1.86
isobath+SSS+s(MLD,3)+s(LNSC,3)	8.88	0.140	1010.10	4.73	0.037	0.907	10.62
s(isobath,2)+SSS+s(MLD,3)+ s(LNSC,3)	9.85	0.144	1010.93	5.55	0.024	0.932	16.05
Fin whale							
SST+s(MLD,3)+s(LNSC,3)	7.87	0.170	1656.59	0	0.99	0.99	
s(SST,2)+s(MLD,3)+s(LNSC,3)	8.88	0.171	1666.90	10.31	0.01	0.99	173.41
SST+SSS+s(MLD,3)+s(LNSC,3)	8.87	0.170	1668.20	11.61	0.00	1.00	331.89
isobath+SST+s(MLD,3)+s(LNSC,3)	8.87	0.170	1668.89	12.31	0.00	1.00	470.75
SST+s(MLD,3)+s(LNSC,2)	6.88	0.155	1670.63	14.04	0.00	1.00	1119.67

*Abbreviations: SST, sea surface temperature (°C); SSS, sea surface salinity (PSU); MLD, mixed-layer depth (m); LNSC, logarithm of surface chlorophyll concentration; AIC, Akaike's information criterion; df, degrees of freedom; $\Delta_i = AIC_{candidate} - AIC_{best}$. Terms are represented as smoothing spline functions with associated df (e.g., s[SST,2]) or linear terms (e.g., SST). All candidate models include a linear year term and are corrected for effort with an offset; the year and offset terms are not shown in the table. The 5 candidate models with the lowest AIC values are presented for each species. The final model for each species includes all variables and the highest df for the smoothing spline for each variable found in any candidate model with $\Delta_i < 2$.

VISIT THE SCIENTIFIC PUBLICATIONS REPORT ARCHIVE

Table 2. Ship-strike risk[a] to whales off Southern California calculated from annual predictions of the number of whales in each route and potential conflicts between use of alternative shipping routes (Fig. 1e) and other primary types of uses.[b]

Shipping routes[c]	Humpback whales (SE)	Blue whales (SE)	Fin Whales (SE)	Military (km^2)	Fishing (km^2)	Sanctuary (km^2)	Other protected areas (km^2)
Channel route	3.58 (1.32)	5.91 (1.05)	6.39 (1.78)	289.84	61.77	185.94	38.30
Central Fan route	1.52 (0.43)	5.32 (1.11)	9.93 (1.86)	650.23	0.77	0	0
Central route	1.31 (0.40)	5.09 (1.16)	10.66 (2.13)	2563.28	0.77	0	0
Southern route	0.93 (0.24)	5.57 (1.52)	13.70 (2.89)	876.26	3.75	0	0
Predominantly channel	3.32 (1.20)	5.84 (1.02)	6.85 (1.67)				
Mixed traffic	2.41 (0.80)	5.58 (1.00)	8.41 (1.56)				

[a]We assumed risk was proportional to the mean predicted number of whales in each route. Risk was calculated assuming all traffic occurs within a route and by approximating traffic patterns observed before and after implementation of a rule intended to reduce air pollution by requiring ships to use cleaner-burning fuels when traveling close to the mainland coast.

[b] Estimated as the overlap between each route and areas used for other purposes.

[c] The predominantly Channel traffic pattern observed in 2008 was approximated on the basis that 87% of traffic occurred in the Channel route and 13% of traffic occurred in the Central Fan route. The mixed traffic pattern observed in 2009 was approximated on the basis that 43% of traffic occurred in the Channel route and 57% of traffic occurred in the Central Fan route.

VISIT THE SCIENTIFIC PUBLICATIONS REPORT ARCHIVE

Figure 1. (a) Location of the Southern California study area (outlined in black) on the southwestern coast of the United States, (b) transects surveyed on cruises conducted primarily between August and November in 1991, 1993, 1996, 2001, 2005, 2008, and 2009 (c) primary human uses of the study area (shipping is represented by the 2 largest ports [black squares] and the traffic separation scheme) (d) Channel Islands National Marine Sanctuary and protected areas, and (e) alternative shipping routes considered in our analyses (Central Fan represents the option of establishing only the eastern portion of the Central route; thus, the fan [stippled] represents a range of possible approaches to this route).

Figure 2. Mean (SE) predicted densities of (a) humpback, (b) blue, and (c) fin whales for the subset of the study area that overlapped with the shipping routes (black lines) (black dots, sightings).

Figure 3. Relative ship-strike risk for 3 whale species. We calculated risk assuming all shipping traffic occurs in the Channel route (traffic separation scheme adopted by the International Maritime Organization). We compared this risk to risk calculated assuming all traffic occurs in alternative routes (Fig. 1e). Also compared are relative ship-strike risk for the predominantly Channel traffic pattern observed in 2008 and the mixed traffic pattern observed in 2009. Negative values imply risk is higher in the Channel route than the alternative route, whereas positive values suggest the alternative route has higher risk than the Channel route.

VISIT THE SCIENTIFIC PUBLICATIONS REPORT ARCHIVE

Figure 1.

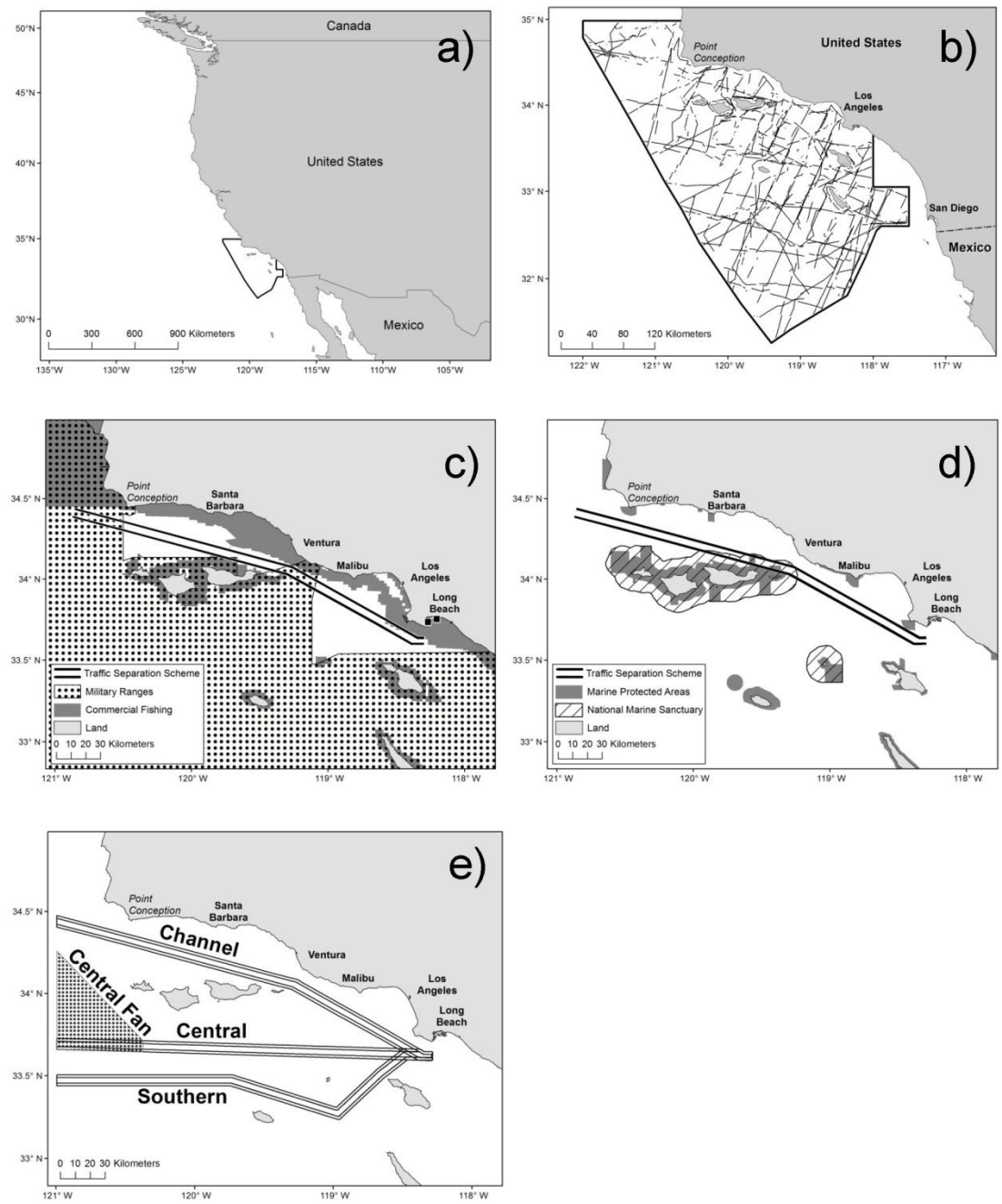

VISIT THE SCIENTIFIC PUBLICATIONS REPORT ARCHIVE

Figure 2.

a) Humpback whales

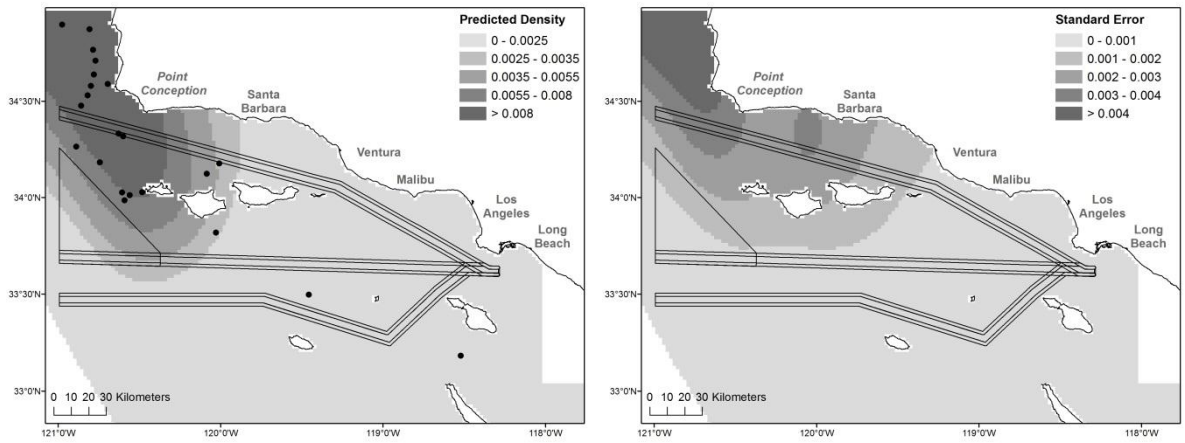

b) Blue whales

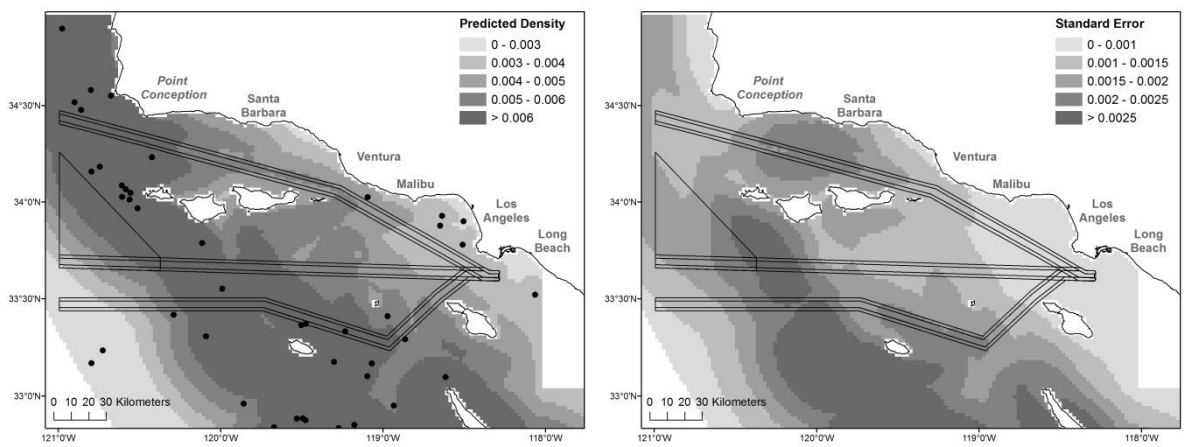

c) Fin whales

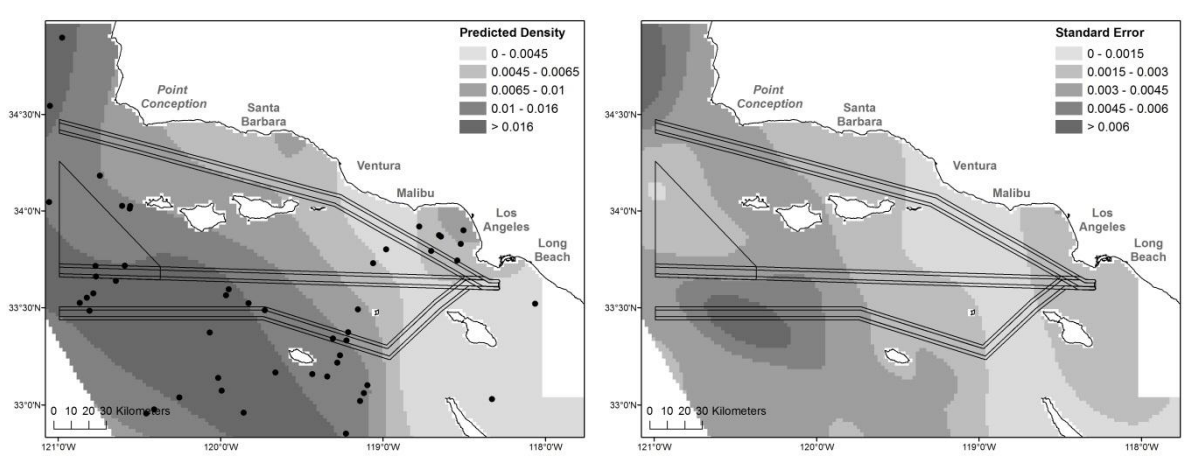

VISIT THE SCIENTIFIC PUBLICATIONS REPORT ARCHIVE

Figure 3.

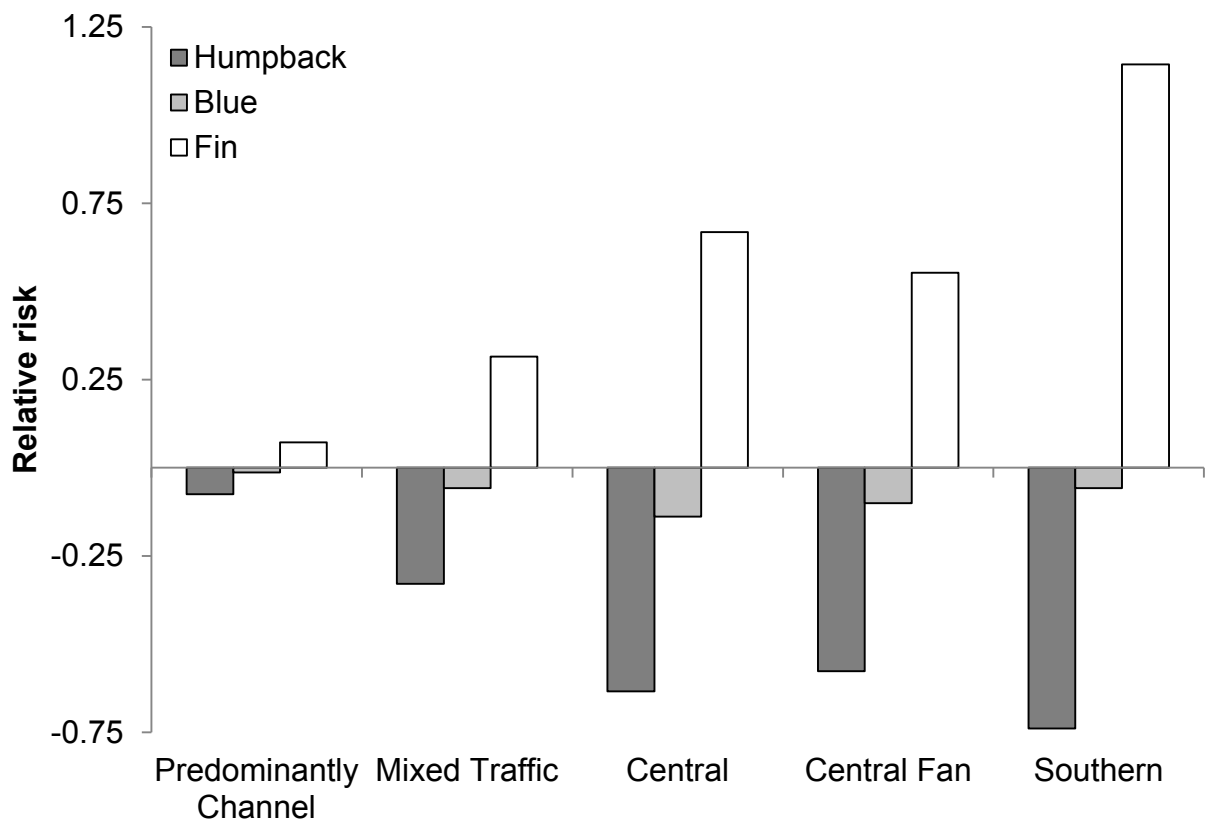

VISIT THE SCIENTIFIC PUBLICATIONS REPORT ARCHIVE

Appendix S2. Functional forms for variables included in the generalized additive models relating the number of a) humpback, b) blue, and c) fin whales to year, distance to the 200-m isobath in kilometers (Isobath), and oceanographic variables (sea surface temperature in degrees C = SST, sea surface salinity in PSU = SSS, mixed layer depth in meters = MLD, and the logarithm of surface chlorophyll concentration = LNSC). Data points for each variable are shown as tick marks on the x-axes. The y-axes, representing the smoothing spline function and associated upper and lower curves at twice the standard error, are labeled to indicate the degrees of freedom for the spline (linear terms are represented by a single degree of freedom). The y-axes for the variables selected in the model for each species have the same scale, although the scales differ among species.

a) Humpback Whales

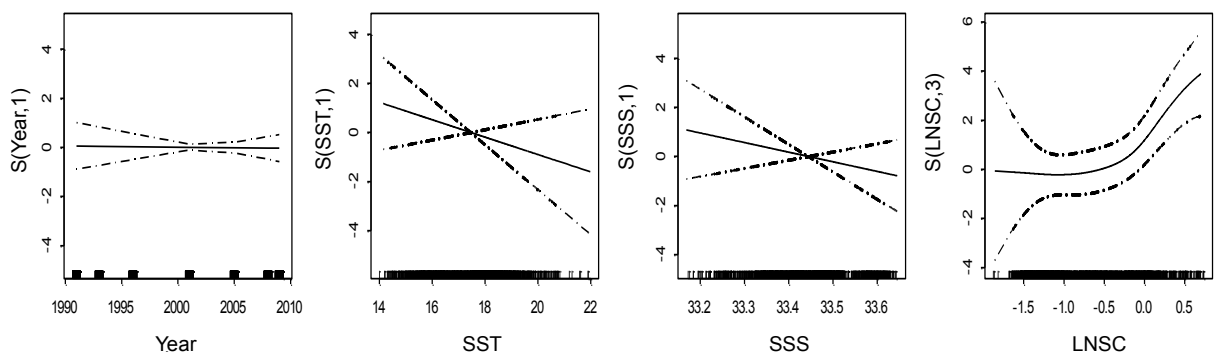

b) Blue Whales

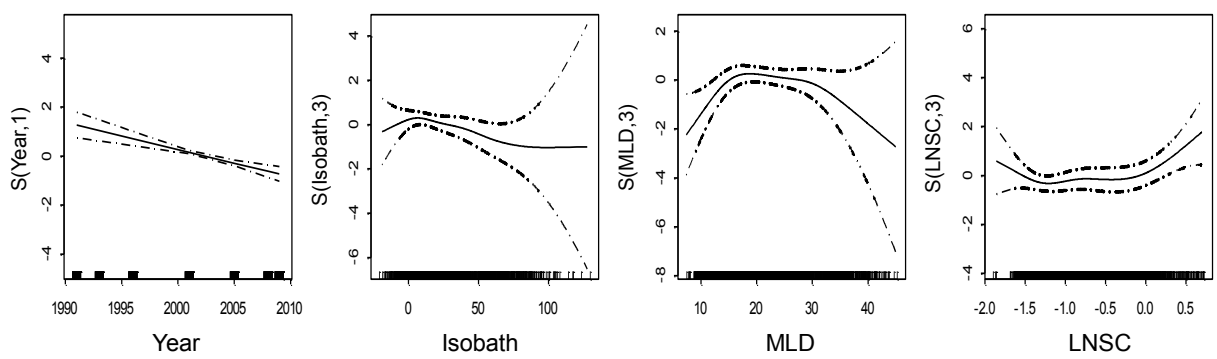

c) Fin Whales

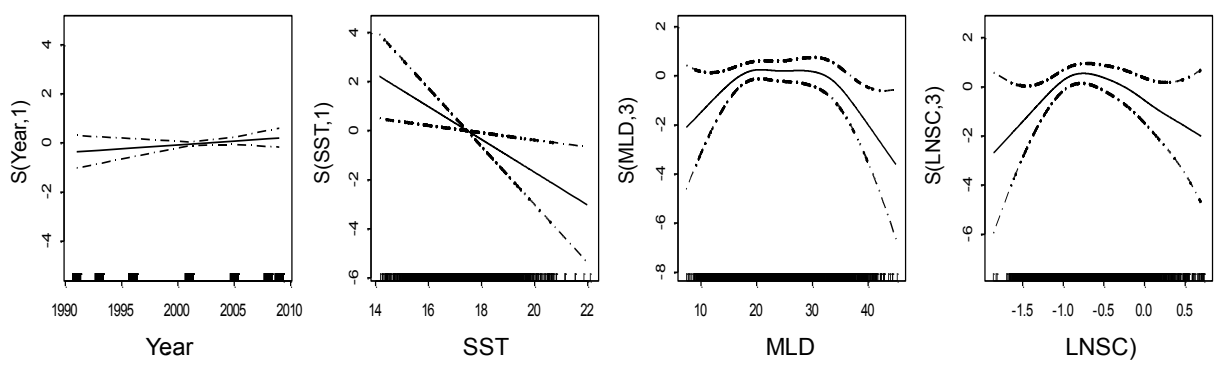

VISIT THE SCIENTIFIC PUBLICATIONS REPORT ARCHIVE